

Spring 2012

Design and Use of an Alternative Fuel Testing Apparatus and Assessment of the Feasibility of Biodiesel

Matthew Tanner

Follow this and additional works at: https://digitalcommons.bucknell.edu/masters_theses



Part of the [Mechanical Engineering Commons](#)

Recommended Citation

Tanner, Matthew, "Design and Use of an Alternative Fuel Testing Apparatus and Assessment of the Feasibility of Biodiesel" (2012). *Master's Theses*. 87.

https://digitalcommons.bucknell.edu/masters_theses/87

This Masters Thesis is brought to you for free and open access by the Student Theses at Bucknell Digital Commons. It has been accepted for inclusion in Master's Theses by an authorized administrator of Bucknell Digital Commons. For more information, please contact dcadmin@bucknell.edu.

I, Matthew A. Tanner, do grant permission for my thesis to be copied.

DESIGN AND USE OF AN ALTERNATIVE FUEL TESTING APPARATUS AND
ASSESSMENT OF THE FEASIBILITY OF BIODIESEL

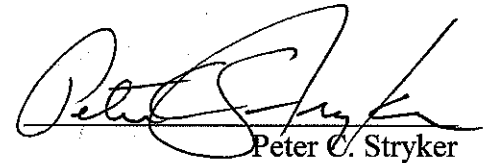
by

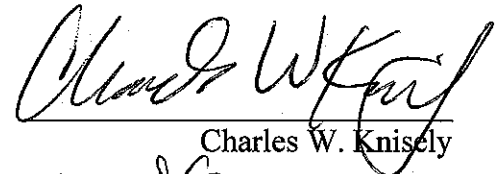
Matthew Tanner

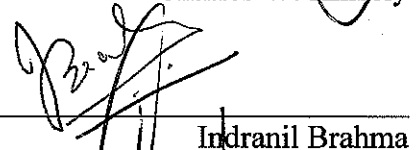
A Thesis in Mechanical Engineering


Presented to the Faculty of
Bucknell University
In Partial Fulfillment of the Requirements for the Degree of
Master of Science in Mechanical Engineering

Approved:


Peter C. Stryker


Charles W. Knisely


Indranil Brahma


Christopher J. Mordaunt

September 2011

ACKNOWLEDGEMENTS

Most importantly, I would like to thank my family for their unconditional support and guidance. I could never repay or thank my parents enough for being such a positive influence on my life and always being there for me. I owe a special thanks to my brother Troy for not only being a life-long companion and a motivator but also for teaching me the importance of communication and team work. This major accomplishment in my life is a reflection of the sacrifices and efforts made by my family.

I would also like to thank Professor Peter Stryker for giving me the opportunity to complete this project and providing guidance along the way. Completion would not have been possible without his support and the support and knowledge of Professor Indranil Brahma and Professor Christopher Mordaunt. I also thank fellow graduate student Wade Pierce for his help and willingness to lend a hand despite his own problems and busy schedule. Wade was like a brother to me throughout this project and our friendship is invaluable to me. Thanks to Tim Baker and Dan Johnson for sharing their wisdom and expertise in the machine shop. I greatly value the things they have taught me and the friendship we have developed. Also, thanks to Wade Hutchinson for helping me with data acquisition and LabVIEW programming, and Tom Thul for his help and advice with electrical systems.

TABLE OF CONTENTS

LIST OF FIGURES	viii
LIST OF TABLES	xii
ABSTRACT	xiv
CHAPTER 1 Introduction.....	1
1.1 Internal Combustion Engine	1
1.2 Environmental Issues	3
1.3 Fuel Consumption Reduction Solutions	6
1.4 Thesis Objectives	8
1.5 Testing Method	8
1.6 Design of Experiment	9
Chapter 2 Literature Review	10
2.1 Biodiesel Definition	10
2.2 Biodiesel Production	12
2.3 Biodiesel Sustainability	14
2.4 Published Testing and Results	15
2.5 Physical Property Effects	16

2.6 Chemical Property Effects	20
2.7 Testing Methods.....	24
Chapter 3 Test Cell Design	27
3.1 Design Criteria	27
3.2 Design Constraints	28
3.3 Previous Work and Modifications	28
3.4 Engine Selection	29
3.5 Engine Implementation.....	30
3.6 Intake System.....	32
3.7 Exhaust System.....	33
3.8 Speed Reduction System.....	34
3.9 Engine Mount.....	39
3.10 Fuel Delivery System.....	41
3.11 Speed Control System.....	42
3.12 Engine Starting System.....	43
3.13 Emissions Analysis Equipment.....	44
3.7 Data Acquisition	47

Chapter 4 Testing and Design Verification	50
4.1 Test Plan.....	50
4.2 Operation Procedures	53
4.3 Measurement Calibrations	53
4.4 Design Verification.....	57
4.5 Accuracy and Repeatability	57
Chapter 5 Experimental Results.....	63
5.1 Fuel Properties	63
5.2 Experimental Testing Data	70
5.3 Calculated Data.....	73
5.3.1 Power	73
5.3.2 Brake Mean Effective Pressure (BMEP)	75
5.3.3 Brake Specific Fuel Consumption	76
5.3.4 Thermal Efficiency	77
5.3.5 Air Mass Flow Rate	78
5.3.6 Air/Fuel Ratio	80
5.3.7 Corrected NOx.....	81

5.3.8 Exhaust Energy	83
5.3.9 Heat Rejection.....	84
Chapter 6 Discussion and Conclusion	86
6.1 Discussion of Fuel Properties	86
6.2 Discussion of Engine Performance Parameters	87
6.2.1 Discussion of Brake Mean Effective Pressure Results	87
6.2.2 Discussion of Brake Specific Fuel Consumption Results.....	89
6.2.3 Discussion of Thermal Efficiency Results.....	91
6.2.4 Discussion of Air/Fuel Ratio	93
6.2.5 Discussion of Heat Losses	95
6.3 Discussion of Emissions Results	97
6.3.1 Discussion of Unburned Hydrocarbon Emissions	97
6.3.2 Discussion of Carbon Monoxide Emissions	99
6.3.3 Discussion of Carbon Dioxide Emissions.....	101
6.3.4 Discussion of NO _x Emissions	103
6.4 Conclusions.....	106
6.5 Recommendations for Future Work.....	107

References.....	110
Appendix A: Emissions Equipment Operation Procedure.....	115
Appendix B: Data File Preparation Procedure.....	121
Appendix C: Dynamometer Startup and Operation Procedure.....	123
Appendix D: Data File Analysis Procedure.....	131
Appendix E: Fuel Changing Procedure	140
Appendix F: Partial Pressure Calculation.....	143
Appendix G: NOx Correction Factor Calculation	146
Appendix H: Engineering Drawings.....	148

LIST OF FIGURES

Figure 2-1: Transesterification of triglycerides to fatty acid methyl esters	12
Figure 2-2: Schematic of typical biodiesel production process	14
Figure 2-3: Emissions reduction from biodiesel blending	16
Figure 2-4 Dynamometer Schematic.	25
Figure 3-1: Dynamometer Control Box	29
Figure 3-2: Briggs and Stratton 10 HP Configured to the Test Bench	30
Figure 3-3: Intake and Exhaust System Design.....	34
Figure 3-4: Torque Verification Plot	35
Figure 3-5: Speed Reduction System.....	36
Figure 3-6: Jack Shaft Assembly	38
Figure 3-7: Belt Reduction Pulley Selection Chart.....	39
Figure 3-8: Anchor Industries #2265 Engine Mount.....	40
Figure 3-9: Yanmar Engine Mount.....	40
Figure 3-10: Yanmar fuel delivery system schematic	42
Figure 3-11: Emissions Analyzer Plumbing Schematic	45
Figure 3-12: Emissions gas bottle cart.....	46
Figure 3-13: User interface of custom LabVIEW® program	47
Figure 3-14: Sartorius PMA 7200-X Explosion Proof Paint Scale	49

Figure 5-1: Biodiesel Property Sheet.....	64
Figure 6-1: Yanmar Biodiesel Blending: Brake Specific Fuel Consumption.....	91
Figure 6-2: Yanmar Biodiesel Blending: Thermal Efficiency Results Plot	93
Figure 6-3: Yanmar Biodiesel Blending: Air/Fuel Ratio Results Plot	94
Figure 6-4: Yanmar Biodiesel Blending: Energy Lost to Exhaust	96
Figure 6-5: Yanmar Biodiesel Blending: Heat Rejection.....	97
Figure 6-6: Yanmar Biodiesel Blending: Hydrocarbon Emissions Plot.....	99
Figure 6-7: Yanmar Biodiesel Blending: Carbon Monoxide Emissions Plot.....	100
Figure 6-8: Yanmar Biodiesel Blending: Exhaust Gas Temperatures Plot	101
Figure 6-9: Yanmar Biodiesel Blending: Carbon Dioxide Emissions Plot	103
Figure 6-10: Yanmar Biodiesel Blending: Corrected NO _x Emissions Plot	106
Figure A-1: Equipment Schematic Overview.....	115
Figure A-2: Horiba PG-250 Rear Panel Schematic	116
Figure A-3: Heated Filter Element	117
Figure A-4: Horiba Sample Filter	117
Figure C-1: Test Cell Schematic.....	123
Figure C-2: Dynamometer Control Box	124
Figure C-3: Exhaust System Switch	125
Figure C-4: Fuel Tank and Shutoff Valve	126

Figure C-5: Emissions Sample Port Cap	127
Figure C-6: Emissions Heated Sample Line	128
Figure C-7: LabVIEW® User Note Input.....	129
Figure D-1: Fueling Calculation.....	132
Figure D-2: Average Fueling Calculation.....	133
Figure D-3: Summary Data Sheet.....	134
Figure D-4: Summary Formatting: Insert 12 Columns.....	134
Figure D-5: Summary Formatting: Column Titles	134
Figure H-1: Bearing Installation Drivers.....	148
Figure H-2: Belt Guard	149
Figure H-3: Compression Tester.....	150
Figure H-4: Exhaust Clamp	151
Figure H-5: Exhaust Flange	152
Figure H-6: Exhaust Flange Yanmar Side	153
Figure H-7: Flywheel Holder.....	154
Figure H-8: Flywheel Puller	155
Figure H-9: Hone Top Plate.....	156
Figure H-10: Intake Filter Adapter	157
Figure H-11: Intake Manifold Adapter	158
Figure H-12: Jackshaft Adjuster	159

Figure H-13: Jackshaft Base Plate	160
Figure H-14: Jackshaft Post	161
Figure H-15: Oil Plug	162
Figure H-16: Positive Piston Stop.....	163
Figure H-17: Scatter Shield	164
Figure H-18: Shaft Alignment Bar	165
Figure H-19: Shaft Alignment Coupler	166
Figure H-20: Yanmar Engine Mount.....	167

LIST OF TABLES

Table 2-1: Fatty Acid Composition of Plant Oils and Beef Tallow.	12
Table 3-1: Yanmar L100EE Specifications.....	31
Table 4-1: Fuel Blending Data.....	51
Table 4-2: Fuel Blend and Engine Operating Point Test Plan.....	52
Table 4-3: Emissions Sample Measurement Delay	52
Table 4-4: Horiba Span Gas Concentrations	56
Table 4-5: Test Point Deviations of Speed and Torque from B80 Test May 25, 2011	59
Table 4-6: Speed and Torque Deviation of B80 Tests on May 12 and May 25	59
Table 4-7: Deviation of Airflow and Brake Specific Fuel Consumption: B80 Testing on 5-12 and 5-25	60
Table 4-8: Deviation of Thermal Efficiency and NO _x Measurements: B80 Testing on 5-12 and 5-25	60
Table 4-9: Deviation of Oxygen and Carbon Dioxide Measurements: B80 Testing on 5-12 and 5-25	61
Table 4-10: Deviation of Unburned Hydrocarbons and Carbon Monoxide Measurements: B80 Testing on 5-12 and 5-25.....	61
Table 4-11: Deviations of Carbon Monoxide (CO) and Unburned Hydrocarbons (UHC) Measurements Between Tests of B2, B20, B40, and B80.	62
Table 5-1: Fuel Blend Chemical Composition.....	66
Table 5-2: Mass and Molar Values of Water and Fuel from Bomb Calorimeter Testing	68
Table 5-3: Experimental Net and Lower Heating Values for Biodiesel Blends.....	68

Table 5-4: Kinematic Viscosity Test Results for Biodiesel Blends.....	69
Table 5-5: B2 Experimental Data	70
Table 5-6: B20 Experimental Data	71
Table 5-7: B40 Experimental Data	71
Table 5-8: B60 Experimental Data	72
Table 5-9: B80 Experimental Data	72
Table 5-10: B100 Experimental Data	73
Table 5-11: Calculated Power Values (Horsepower)	74
Table 5-12: Calculated Power Values (kilowatts)	75
Table 5-13: Calculated BMEP Values (kPa)	76
Table 5-14: Calculated BSFC Values (g/kW-hr).....	77
Table 5-15: Calculated Thermal Efficiency Values (%).....	78
Table 5-16: Calculated Air Density Values (g/ft ³)	80
Table 5-17: Calculated Values of Air Mass Flow Rate (g/s).....	80
Table 5-18: Calculated Values of Air/Fuel Ratio	81
Table 5-19: NO _x Correction Factors and Ambient Weather Conditions	82
Table 5-20: Corrected NO _x Emissions (ppm)	82
Table 5-21: Calculated Values of Energy Lost to Exhaust Gas (% of total energy)	83
Table 5-22: Energy Lost to Heat Rejection (% of total).....	85
Table 6-1: Deviation of Calculated BMEP Values.....	89

ABSTRACT

Petroleum supply and environmental pollution issues constantly increase interest in renewable low polluting alternative fuels. Published test results show decreased pollution with similar power output and fuel consumption from Internal Combustion Engines (ICE) burning alternative fuels. More specifically, diesel engines burning biodiesel derived from plant oils and animal fats not only reduce harmful exhaust emissions but are renewable and environmentally friendly. To validate these claims and assess the feasibility of alternative fuels, independent engine dynamometer and emissions testing was performed. A testing apparatus capable of making relevant measurements was designed, built, and used to test and determine the feasibility of biodiesel. The apparatus marks the addition of a valuable testing tool to the University and provides a foundation for future experiments. This thesis will discuss the background of biodiesel, testing methods, design and function of the testing apparatus, experimental results, relevant calculations, and conclusions.

CHAPTER 1 INTRODUCTION

Petroleum has become a very important part of everyday life. We use it to fuel our vehicles, power industries, and heat our homes. In 2009 the US consumed 19 million barrels of petroleum per day and consumption is forecasted to increase to 21.09 million barrels per day by 2035 [1]. Of all the petroleum used in the United States our transportation needs account for 71% of the total consumption [1]. Ninety five percent of the energy used for transportation each year comes from petroleum, while only 3% is supplied by renewable energy [1]. Two problems result from this trend: The amount of pollution and carbon dioxide produced is destroying our environment; and, since the supply of petroleum is finite, it will run out. As energy demand and population growth continually increase, the petroleum supply and condition of our environment continually degrade. The need for alternative renewable fuels is equaled only by the need for more efficient, less polluting vehicles.

1.1 Internal Combustion Engine

The Internal Combustion Engine (ICE) powers the majority of vehicles on the road today. This includes all vehicles from motorcycles and small passenger cars to heavy commercial trucks. The ICE is classified by ignition type. The two most common types are gasoline-burning Spark Ignition engines (SI) and diesel-burning Compression Ignition engines (CI). While similar in many respects, each type has advantages and

disadvantages. Diesel engines are more efficient and offer more torque than SI engines, where torque is the measure of an engine's ability to do work [2]. The increased torque and efficiency are a result of higher compression ratios and reduced pumping work. The power output of a diesel engine is controlled by the amount of fuel injected, as opposed to a SI engine which controls the amount of airflow (and consequently fuel flow) with a throttle. Under light loading conditions the use of a throttle requires combustion air be pulled past the throttle. This requires additional work and reduces the efficiency of the engine. Because CI engines regulate the amount of fuel delivered to the combustion chamber, air is usually in excess. This causes a lean burning condition and provides more complete combustion of the fuel. At full power, gasoline engines typically operate at a slightly rich condition. This maximizes power but decreases efficiency and increases the amount of unburned fuel in the exhaust [3].

To handle the increased compression ratios, CI engines are much more robust in design. This makes the engines more durable, but comes with an increased production cost and added weight. The importance of fuel filter service and increased engine oil capacity makes the regular maintenance of a CI more costly, but when properly maintained, a CI engine will last three times as long before an overhaul is needed. Historically, the SI engine is more common in passenger cars because it is relatively light in weight, low in cost, and provides better acceleration because of higher peak engine speed and horsepower [4]. The CI engine is more common in heavy-duty applications because of

high fuel efficiency, high torque output, and extended life span [4]. With regulations constantly demanding increased fuel efficiency and decreased exhaust emissions, the CI platform becomes more attractive for all applications.

1.2 Environmental Issues

Aside from supply issues, environmental concerns associated with fossil fuels are also a problem. The products of hydrocarbon combustion are carbon dioxide, water, and nitrogen ideally. In reality, burning of any fuel releases many harmful emissions, decreasing the quality of the air we breathe, the water we drink, and the integrity of our environment. The connection between air pollution and automobile use has been well known since the 1940's [3]. It was first noticed in California where oxides of nitrogen reacted with hydrocarbons in the presence of sunlight to form smog. This event influenced the application of emissions standards for automobiles. While emissions standards have reduced the amount of pollution from automobiles the problem still exists. Although advancements have been made in engine design to optimize combustion, the process is never perfect. As a result, the typical pollutants found in automotive exhaust are Carbon Monoxide (CO), Oxides of Nitrogen (NO_x), Unburned Hydrocarbons (UHC), and Particulate Matter (PM) [3]. Another product of concern but not typically considered a pollutant is Carbon Dioxide (CO₂).

Carbon monoxide is colorless, odorless, extremely lethal gas, and is produced by a lack of oxygen during combustion. Because spark ignition engines typically operate at a slightly fuel rich condition for maximum power, carbon monoxide is typically a product of gasoline combustion. Compression ignition engines typically operate at a fuel lean condition so carbon monoxide is not a major product of diesel combustion [5]. The implications of carbon monoxide are more of a problem in small, dense areas. Concentrations of a few thousand parts per million of this gas can be life threatening [6].

Secondary reactions during combustion produce oxides of nitrogen or "NO_x." NO_x includes nitric oxide (NO), nitrogen dioxide (NO₂), and nitrous oxide (N₂O). These oxides are formed from atmospheric oxygen and nitrogen through a series of reactions at temperatures above 1600°C. Nitric oxide which is naturally converted to NO₂ in the atmosphere is odorless, colorless, and relatively non-toxic. NO₂, however, is toxic and dangerous to human health in low concentrations. This pungent reddish-brown pollutant attacks the hemoglobin and affects the oxygen transport in the blood. Damage to the human respiratory system is common in highly polluted areas. NO_x is also involved in the formation of acid rain, smog, and the depletion of the ozone layer by reacting with Hydrocarbons in the atmosphere [6].

Unburned Hydrocarbons (UHC) emissions include a wide variety of compounds. The UHC compounds in exhaust are mostly unburned fuel and partially oxidized fuel. UHC

emissions are formed several different ways but largely by fuel rich combustion. Since diesel engines typically run at lean conditions, UHC emissions are less severe compared to a spark ignition engines. Many of the HC compounds formed irritate the respiratory system and are reactants in photochemical smog [6].

Particulate Matter (PM) is an emission primarily associated with compression ignition engines. It contains many different compounds and is composed of extremely small particles and liquid droplets. The particles range in size, but the majority are in the range of 15-30 nanometers [3]. The Environmental Protection Agency (EPA) considers the size of the particles to be directly related to their potential for causing health problems [7]. It is believed that nano-sized particles can enter deep into the lungs. Health effects from exposure to high concentrations of PM include respiratory irritation, lung cancer, and premature death from cardiovascular, cardiopulmonary, or respiratory causes [7].

Carbon dioxide is an inevitable product of hydrocarbon combustion. Although it is not typically included as a pollutant (because of its non-toxic nature), it is considered a greenhouse gas responsible for global warming and has become a concern. The production is directly related to fuel consumption and is primarily regulated in this way. Currently vehicles each produce about 6 to 9 tons of CO₂ per year for a total of 1.7 billion tons of CO₂ yearly. The rapid production of this greenhouse gas is contributing to global climate change at a faster rate now than ever [8].

1.3 Fuel Consumption Reduction Solutions

It seems that decreasing petroleum consumption is the solution to our problems. This can be achieved by increasing the efficiency of engines and implementing non fossil fuel based alternative fuels. Alternative fuels can be used in spark ignition and compression ignition engines to reduce petroleum consumption and emissions. These fuels are derived from sources other than petroleum including renewable fuels made from plants, algae, and animal fats. Carbon dioxide is naturally absorbed by plants during photosynthesis. Using plants to make fuel helps offset the carbon dioxide produced when burning fuel and reduce the global warming effect. Many alternative fuels also burn cleaner than petroleum products, further reducing the negative effects on the environment.

Some alternative power sources could also be used to reduce petroleum consumption and environmental pollution. Electric vehicles produce zero emissions and offer smooth quiet operation. The zero emissions claim requires that the electricity used to power the vehicles comes from a non-polluting power plant, such as nuclear, wind, hydro, or solar. The problem with this type of vehicle is the cost and performance of the batteries used to store the energy. Batteries are expensive, have low energy density, and require a significant amount of time to recharge. Typical maximum range for an electric car is claimed to be about 200 miles under ideal conditions before a several hour recharge is needed. Maximum range under normal driving conditions is yet to be established. The

cost and short lifetime of the battery packs make the electric car expensive to own and maintain [9].

Much like electric vehicles, hydrogen fuel cell vehicles utilize an efficient electric motor, but do not require expensive bulky batteries. The electricity used to power the motors is instead produced using a chemical process requiring hydrogen and oxygen. The hydrogen required can either be stored in a high pressure tank or reformed from hydrogen rich fuels such as methanol, natural gas, and gasoline. Fuel cell vehicles produce no emissions when using pure hydrogen and very low emissions when using hydrogen rich fuels. The largest downside of this technology is the cost, safety, and pollution issues associated with producing and storing hydrogen [10].

The Hybrid Electric Vehicle (HEV) utilizes power from an electric motor and an internal combustion engine to drive the vehicle. Efficiency is increased by selectively using each power source in its most efficient loading condition. HEV's typically use an ICE utilizing the Miller Cycle. The Miller Cycle features an expansion stroke that is greater than the compression stroke, which increases efficiency. Also, energy is conserved with a regenerative braking system, which captures kinetic energy typically lost when slowing the vehicle [11].

1.4 Thesis Objectives

Alternative fuels have the potential to reduce fossil fuel dependence and are believed to have better burning characteristics compared to fossil fuels. The objective of this thesis is to create a test bed for determining and comparing the performance and emissions characteristics of standard and alternative fuels burned in CI engines. This thesis will discuss design and construction of the apparatus which includes modification of an existing dynamometer, the selection and addition of a CI engine, data acquisition equipment, and emissions analysis equipment. This apparatus will be used for standardized testing and comparison of alternative fuels and, if feasible, allow for engine modifications to optimize the performance and emissions characteristics of fuels.

1.5 Testing Method

As demand and interest in alternative fuels heightens, the development of new fuels and additives also increases. It is important to test the performance of these fuels in an actual engine to determine if the fuel is a feasible alternative. A dynamometer is necessary to perform consistent and accurate testing and make comparisons between tests. A dynamometer allows for safe, controlled, and consistent testing in a stationary location where data acquisition equipment can be easily configured. To determine feasibility, comparisons must be made between power, thermal efficiency, specific fuel consumption, and exhaust emissions. To obtain these parameters, measurements of

engine speed, engine torque, fuel flow, air flow, temperature, and exhaust composition must be made.

1.6 Design of Experiment

The purpose of this experiment is to examine the feasibility of renewable alternative fuels in reducing emissions and fossil fuel dependence, in particular biodiesel and biodiesel blends. Baseline testing with standard diesel fuel will set the benchmark for comparisons to be made. Testing is performed with a dynamometer and a direct injection single cylinder diesel engine. The testing is performed at a range of engine speeds and the torque that provides the best fuel efficiency. The fuels tested will be standard diesel fuel, pure biodiesel derived from soybean oil, and blends of the two. The goal is to study the performance characteristics of each fuel and determine the best fuel to maximize efficiency and minimize harmful exhaust emissions. Fuel properties such as cetane number, kinematic viscosity, energy content, and oxygen content will be used to justify the performance and emissions results.

CHAPTER 2 LITERATURE REVIEW

This chapter will present an overview of the research performed to define biodiesel as a promising alternative fuel. A review of biodiesel including benefits, properties, chemistry, production processes, and combustion characteristics will be presented in addition to testing methods and testing results.

2.1 Biodiesel Definition

Raw vegetable oil can be used as an alternative to standard diesel fuel but the high viscosity and low volatility of the oil can cause serious engine problems over time, and is thus not considered a viable fuel. A better and viable alternative to standard diesel is the modified version of raw vegetable oil or animal fat commonly known as Biodiesel. Biodiesel has similar properties to fossil diesel fuel and can be used in conventional diesel engines without modifications. Biodiesel is a fuel composed of fatty acid methyl esters derived from plant oil or animal fats. It can be easily produced from waste deep fryer oil, animal fats, and oil seeds such as soybean, canola, and palm seed. Transesterification of the oil breaks the oil molecule into an ester and glycerol. After removing the glycerol, the remaining ester is known as biodiesel. Biodiesel is renewable, non-toxic, and biodegradable. The calorific value of biodiesel is less than that of diesel because of oxygen atoms attached to the fuel molecule. Biodiesel has a higher cetane number than standard diesel and also lower sulfur, aromatics, and volatility [12].

The process for producing biodiesel is relatively simple and can be performed on a small personal use scale to a large industrial scale. Most all vegetable oils and animal fats are composed of long chain triglycerides and can be used to produce biodiesel. Triglycerides are compounds of glycerol and varying amounts of fatty acids. The major fatty acids have a chain length of 16 to 18 carbons, much like the straight chain hydrocarbons of fossil diesel fuel, which have a length of about 16 carbons. For this reason methyl esters produced from the fatty acids have similar combustion characteristics to petroleum diesel fuel. Properties of biodiesel are variable and dependent on the source of oils or fats used to produce the fuel. Plant oils contain a mixture of saturated and unsaturated fatty acids. Animal fats contain larger amounts of saturated fatty acids compared to plant oils (Table 2-1). Saturated fatty acids have the best combustion characteristics and oxidation stability, but behave poorly in cold temperatures due to the high melting points. Unsaturated fatty acids have better low temperature properties but sacrifice oxidation and storage stability [13]. Methyl esters with high molecular weight are more likely to contain unsaturated bonds and contain less oxygen. Oxygen content in the fuel increases ignitibility and cetane while unsaturated bonds reduce cetane [14]. Blends of these fatty acids can be produced to achieve maximum performance for specific climates.

Table 2-1: Fatty Acid Composition of Plant Oils and Beef Tallow (adapted from [15]).

Material	Lauric	Myristic	Saturated				Unsaturated			
			Palmitic (% Total Fatty Acids)	Stearic	Arachidic	Palmitoleic	Oleic	Linoleic (% Total Fatty Acids)	Liolenic	Other ^a
Corn oil		1.4	10	3.2	5.8	1.5	49.6	34.3		
Canola oil			1				32	15	1	50
Soybean oil	0.2	0.1	9.8	2.4	0.9	0.4	28.9	50.7	6.5	0.1
Sunflower oil			5.6	2.2	0.9		25.1	66.2		
Beef tallow		6.3	27.4	14.1			49.6	2.5		

Source: Data from Lide, D. R., ed. 1992. *CRC Handbook of Chemistry and Physics*, 73rd ed., section 7-29. Boca Raton, FL: CRC Press.

^a Erucic (canola); C14 monoethenoic (soybean).

2.2 Biodiesel Production

Biodiesel is produced by the transesterification of triglycerides. The transesterification process shown in Figure 2-1 is a reaction between one mole of triglyceride and three moles of alcohol. The products of the reaction are one mole of glycerol and three moles of biodiesel. Using methanol as the alcohol in the reaction produces fatty acid methyl esters; whereas, ethanol produces fatty acid ethyl esters. Typically, methanol is used in the reaction because it produces the most volatile fatty acid esters [15].

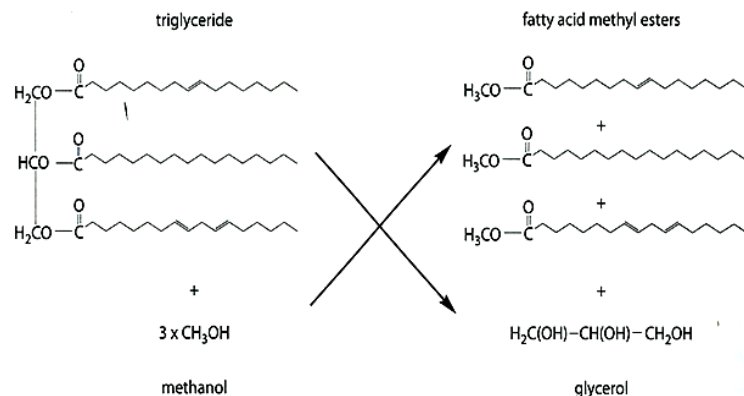


Figure 2-1: Transesterification of triglycerides to fatty acid methyl esters (adapted from [15]).

A schematic of a typical biodiesel production process is shown in Figure 2-2. From the schematic, oil and methanol are added to a reactor with a catalyst (KOH). Catalysts are commonly used to increase reaction rates for the transesterification process. Alkaline catalysts (such as sodium methoxide, potassium methoxide, sodium hydroxide, and potassium hydroxide) are typically used during transesterification by large scale biodiesel plants. The result is increased conversion rate and shorter reaction times at relatively low temperatures. Sodium and potassium hydroxide are cheaper catalysts and can cause the formation of methanolate and water. Sodium and potassium methoxide catalyst work well with high quality vegetable oils and do not produce additional water. Deacidification steps are required when using alkaline catalyst with highly acidic waste oils. Acid catalysts (such as concentrated sulphuric acid) are better suited for highly acidic oils [13]. The settling process allows the glycerol to separate from the biodiesel. After separation has occurred, washing and purification processes are performed to remove unwanted contaminants before excess alcohol is evaporated off and reused.

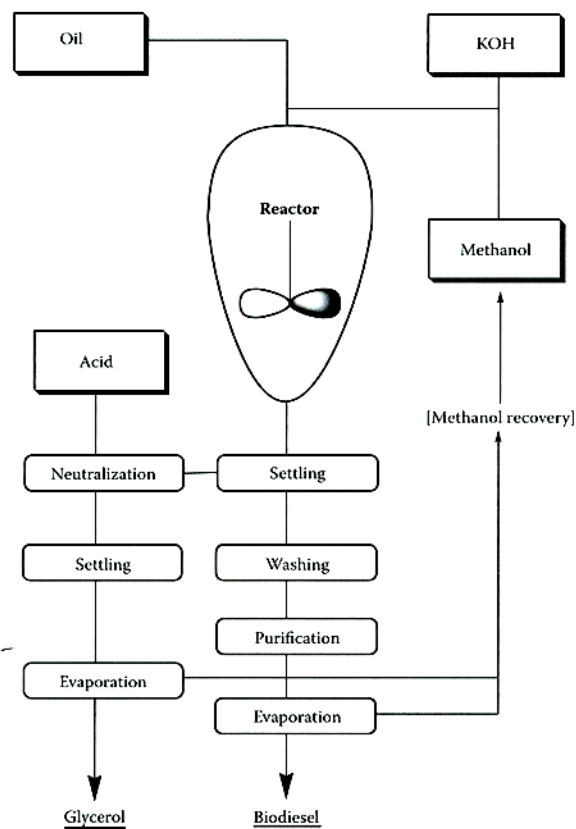


Figure 2-2: Schematic of typical biodiesel production process (adapted from [15]).

2.3 Biodiesel Sustainability

Biodiesel has a positive net energy balance making it a sustainable alternative to petroleum. The U.S. Department of Energy claims that soybean derived biodiesel contains 3.2 units of energy for each unit of energy required to produce the fuel, while conventional diesel fuel yields 0.83 units [16]. Reports of this calculation vary, but discrepancies are due to how the co-products of the process are handled. According to

the American Soybean Association, “When processed, a 60 pound bushel of soybeans yields approximately 48 pounds of protein rich soybean meal (80 percent) and 11 pounds of crude soybean oil (18 percent).” Only the oil is used for biodiesel production; so, for every 1.5 gallons of biodiesel produced, nearly 50 pounds of soybean meal is available for animal and human consumption [17].

2.4 Published Testing and Results

The U.S. Department of Energy claims that biodiesel is a clean burning and renewable substitute for petroleum diesel fuel. Significant reductions of particulate matter, carbon monoxide, and hydrocarbon emissions have been shown when burning biodiesel and blends of biodiesel with standard diesel fuel (Figure 2-3). The U.S. Department of Energy claims a small increase in NO_x emissions [16]. Many studies have been performed to investigate the effect of biodiesel on NO_x emissions with conflicting results. The discrepancies seem to stem from differences in engine characteristics, operating conditions, and testing methods.

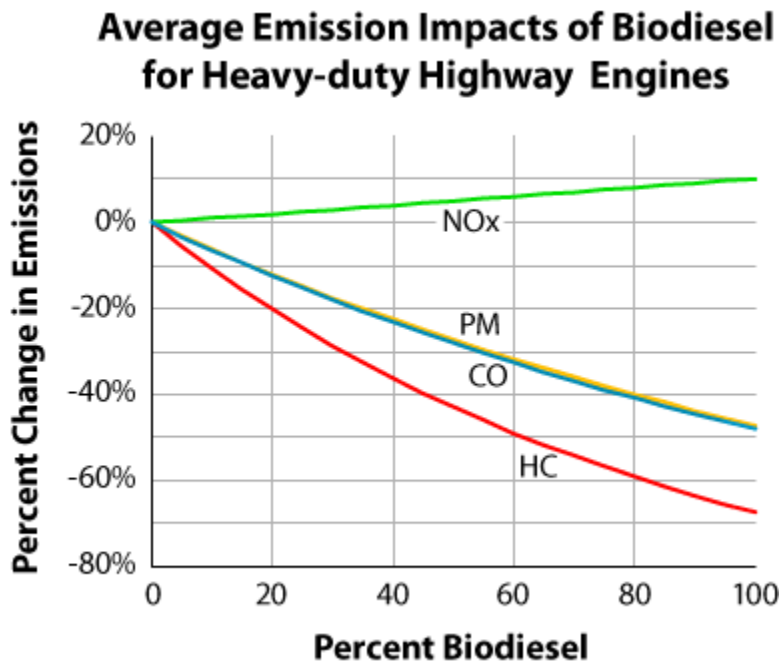


Figure 2-3: Emissions reduction from biodiesel blending (adapted from [16]).

2.5 Physical Property Effects

Compared to standard diesel fuel, biodiesel has a higher kinematic viscosity, density, and surface tension. These physical characteristics have an important effect on the injection quality and, therefore, engine performance and emissions. Deng et al. [18] reports the increased viscosity, density, and surface tension of biodiesel causes a small increase in spray penetration and a slight decrease in spray angle. Vaporization of fuel is required for combustion, and the quality of vaporization directly affects the quality of combustion. This interaction between fuel droplets and nitrogen in the combustion chamber is

promoted by lower surface tension and viscosity, making smaller droplet size and larger spray angle. The increased viscosity and surface tension of biodiesel make the droplets harder to break up, decreasing the interaction with nitrogen and increasing the droplet size. Biodiesel droplets are therefore larger and of higher density, resulting in more kinetic energy of the spray and increased spray penetration. As injection pressure is increased, kinetic energy is also increased. The droplets move faster, which increases the spray penetration and enhances the droplet and nitrogen interaction, causing reduced droplet size and increased spray angle. Spray penetration increases rapidly at the beginning of injection but, as the spray breaks up and the nitrogen interacts with the droplets, the penetration increases less. Spray pattern is also affected by ambient density. Increased ambient density results in more nitrogen interaction with the spray and increases spray angle while decreasing spray penetration. Low ambient density, as a result of low ambient pressure, causes an increased pressure difference between ambient and injection pressures. The effect is similar to increased injection pressure [18].

Ahmed et al. [19] concluded viscosity and surface tension are important factors in atomization in a study on analytical comparisons of the atomization characteristics for different biofuels. “Use of higher viscosity fuel hinders atomization by suppressing the instabilities required for the fuel jet to disintegrate. An increase in fuel surface tension resists the formation of droplets from the liquid fuel jet and can also lead to changes in the atomization characteristics.” Sauter Mean Diameter (SMD) is used to characterize

drop size based on fuel properties, and is defined as “The diameter of the drop whose ratio of volume to surface area is equal to that of the spray.” The equation for SMD with units of micrometers is:

$$SMD = 6156 v_L^{0.385} \gamma^{0.737} \rho_L^{0.737} \rho_A^{0.06} \Delta P_L^{-0.54} \quad (1)$$

where, $v_L =$ Kinematic Viscosity (m^2/sec)
 $\gamma =$ Surface Tension (N/m)
 $\rho_L =$ Liquid fuel density (kg/m^3)
 $\rho_A =$ Air Density (kg/m^3)
 $\Delta P_L =$ Pressure difference between ambient and injection bar

Atomization characteristics of different fuels are compared using the SMD. Compared to standard diesel, the results show a 9% increase of SMD for pure biodiesel derived from coconut oil and a 40% increase for pure biodiesel derived from canola and peanut oil. Similar atomization to standard diesel fuel can be achieved with biodiesel derived from coconut oil and its blends. Similar atomization of biodiesel derived from canola and peanut oil could be achieved by increasing the injection pressure.

Basavaraja et al. [20] investigated the effect of injection pressure for standard diesel and blends of biodiesel derived from pongamia oil. Pongamia Methyl Ester (PME) has similar properties to other biodiesels. Compared to standard diesel, PME has increased viscosity and density, and a decreased calorific value. The testing was performed with a

single cylinder diesel engine at full load and a speed of 1500 rpm. For each fuel the injection pressure was varied from 16-22 MPa. For biodiesel, thermal efficiency increased with injection pressure up to 20 MPa then decreased. For standard diesel, thermal efficiency increased with injection pressure up to 18 MPa and then decreased with increasing pressure. The 20% biodiesel blend had the best thermal efficiency while all blends performed better than standard diesel. The results at low injection pressures are explained by poor atomization and mixture formation. At injection pressures above 20 MPa, fuel droplet size is reduced and the spray becomes very fine, resulting in reduced penetration and momentum of fuel droplets. Brake Specific Fuel Consumption (BSFC) for biodiesel blends was similar to standard diesel at injection pressures below 20 MPa, and better at 20 MPa and above. Exhaust Gas Temperature (EGT) was highest for all fuels at low injection pressures. Low injection pressure is believed to cause coarse spray formation and increased combustion delay, effectively retarding timing and increasing EGT. NO_x, UHC, and CO emissions decrease with injection pressure up to 20 MPa, following the same trend as thermal efficiency. Due to lower compressibility of biodiesel as a result of increased density, injection pressure is thought to increase the speed of injection [21].

2.6 Chemical Property Effects

The chemical composition of biodiesel differs largely from standard diesel by the presence of oxygen atoms and the increased number of hydrogen atoms. According to Stone [22], increased number of hydrogen atoms and presence of oxygen atoms in the fuel molecule decreases energy content. The presence of oxygen represents partial oxidation of the fuel resulting in decreased energy content, but adds a significant benefit to the combustion process. Sebastian and Nagarajan [23] reported a study on the influence of fuel oxygen content on combustion and emissions characteristics of a single cylinder direct injection CI engine. Different blends of standard diesel, ethanol, and biodiesel derived from coconut oil were designed to have similar physical properties to standard diesel fuel and variable oxygen content. Coconut oil was selected for its high oxygen content compared to other available oils. When mixed together, the lower cetane of ethanol offset the increased cetane of biodiesel. The high kinematic viscosity of biodiesel is also offset by the lower viscosity of the ethanol. Viscosity was held relatively constant and oxygen content varied by changing the amount of each component in the mixture. Testing was performed at a constant speed of 1500 rpm from zero to full load and fuel oxygen content was varied from 0-13% by mass. It was determined that fuel with more than 13% oxygen content had high rates of fuel consumption due to a decreased Lower Heating Value (LHV) or energy content. Up to 60% by mass of standard diesel could be replaced by the blend without a decrease in thermal efficiency.

At full load, NO_x was reduced by 12% and HC by 20% compared to standard diesel. CO_2 was slightly increased and CO was significantly increased by 38%. At high loads, increased oxygen content increases the availability of oxygen during combustion and increases combustion efficiency.

Research by Kawano et al. [24] compares the effects of Biodiesel blending on emissions characteristics of a modern diesel engine. The engine is a four cylinder intercooled direct injection turbo diesel and utilizes exhaust gas recirculation, diesel particulate filter, and lean NO_x trap. Biodiesel derived from rapeseed, Rapeseed Methyl Ester (RME) was blended with standard diesel in proportions of 0%, 5%, 20%, and 80%. Steady state testing was performed at a constant speed of 1600 rpm and BMEP of 0.38 MPa. Because of the decreased LHV, increased biodiesel blending required a longer injection time to achieve the same amount of torque. The premixed combustion caused by increased injection duration is believed to be the reason for increased NO_x emissions. Increased oxygen content of the biodiesel blends caused a reduction in CO and hydrocarbon emissions. Hydrocarbon emissions are reduced even at low blends of RME. A 5% blend showed a 50% reduction in hydrocarbons compared to standard diesel. Although the low volatility of RME inhibits lean mixture formation, the increased oxygen content is thought to induce oxidation of hydrocarbons in the localized fuel rich regions of the combustion chamber and reduce unburned hydrocarbon emissions.

The effect of reduced fuel energy content on performance and emissions is further reinforced by Dulger and Kaplan [25] who performed a similar experiment using Sunflower Methyl Ester (SME). The experiment was performed with a four cylinder direct injection turbocharged diesel engine at full load and varying engine speed from 1000-4500 rpm in 250 rpm increments. Measurements of torque, power, specific fuel consumption, particulate matter, unburned hydrocarbons, and carbon monoxide were compared for pure SME and standard diesel. Maximum torque for each fuel is similar and occurs at the same engine speed. At the maximum engine speed of 4500 rpm the engine torque for standard diesel fuel is 10% greater compared to SME. Dulger and Kaplan [25] also report a similar drop in power for SME at speeds above 2500 rpm. They attribute the losses to lower energy content and fuel pumping problems due to increased density and viscosity of SME. The lower energy content of the fuel also causes a 2-5% increase in specific fuel consumption for the range of engine speeds. Because the test engine is turbocharged, only a small reduction in soot, carbon monoxide, and hydrocarbon emissions is observed for SME. Although small, the drop in soot, carbon monoxide, and hydrocarbon emissions is attributed to the higher oxygen content of SME.

Previous work by Suryawanshi [12] investigated the effects on performance and emissions of biodiesel derived from coconut oil burned in a single cylinder diesel engine. Comparisons of thermal efficiency, brake specific energy consumption, cylinder pressure, exhaust gas temperature, smoke, unburned hydrocarbons, and NO_x were made between

standard diesel fuel and blends of Coconut Methyl Ester (CME). Testing was performed at a constant engine speed of 1500 rpm and various loads from zero to full load. Suryawanshi [12] identifies the density, viscosity, and calorific value of biodiesel as important characteristics. These properties were measured and recorded for standard diesel and blends of CME with diesel in 20% increments up to 100% CME. As the proportion of CME increased, the density and viscosity of the fuel blend slightly increased. The calorific value of the pure CME drops 9% from the value for standard diesel. For all blends and loading points, Suryawanshi reports similar results of thermal efficiency, brake specific energy consumption, cylinder pressure, exhaust gas temperature, and NO_x . A proportional reduction in smoke is reported with increasing blends of CME. Testing of pure CME resulted in a 42% reduction in smoke compared to standard diesel. This is thought to be a result of more complete combustion due to the oxygenated nature of biodiesel. For the same reason, unburned hydrocarbons fell as the blend was increased and dropped a total of 25% for pure coconut methyl ester.

To isolate the effects of fuel properties on performance and emissions Kumar et al. [26] investigate the effect of varying cetane number, aromatic content, and distillation temperature of standard diesel fuel in compression ignition engines. Understanding the effect of these fuel properties for standard diesel fuel is helpful in understanding the performance effects of biodiesel with similar properties. Kumar et al. [26] identify cetane number and aromatic content as important chemical characteristics of diesel fuel. Steady

state emissions and performance testing of fuel properties was performed with a light duty engine modified for single cylinder operation at Cummins. The test was performed at mid load and constant speed. They tested standard diesel fuel with variations of cetane number, aromatic content, and distillation temperature. Distillation temperature is the temperature required to reach a distillate level, for example T50 represents the temperature required to reach 50% distillate level. They concluded that NO_x and smoke are impacted by mid-distillation temperature and cetane number. Lower mid-distillation temperature fuels having lower poly-aromatic content resulted in significant NO_x and smoke reduction. Increased cetane, correlating to lower mono-aromatic content resulted in a small reduction of NO_x . Higher loads are characterized by diffusion flame combustion and low loads are characterized as premixed combustion. Increased aromatic content increases NO_x emissions for diffusion combustion and decreases NO_x emissions for pre-mixed combustion.

2.7 Testing Methods

The testing mentioned in all of the above cases was performed exclusively with an actual engine on a dynamometer. A dynamometer measures engine torque by applying a resistive load to the engine. Several types of dynamometers exist, but the principle of operation is the same (Figure 2-4). In each type, the engine is connected to the dynamometer rotor which is coupled to a stator. Each type of dynamometer differs in the

way the rotor is coupled to the stator. Examples of this are electromagnetic, hydraulic, and mechanical friction. The stator is mounted in low friction bearings and engine torque is found by measuring the force at a moment arm connected to the stator, typically with a load cell [2].

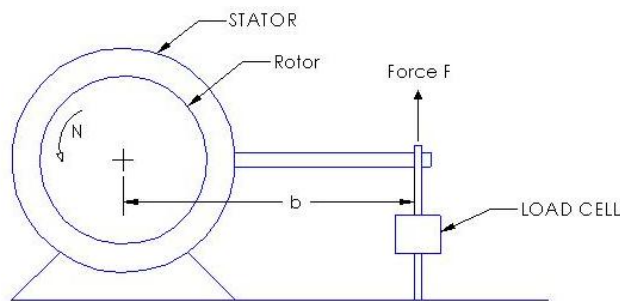


Figure 2-4: Dynamometer Schematic (reproduced from [2]).

Many results have been published showing the emissions and performance characteristics of biodiesel for steady state testing. Although, the typical operating conditions for transportation engines are transient, this type of testing is rarely investigated. This is due to the complexity of transient testing and the need for special equipment. At the University of Huddersfield, Tesfa et al. [21] investigated emissions behavior of biodiesel under transient conditions. The authors used three different acceleration sequences at four different loads to test standard diesel, 100% biodiesel derived from rapeseed, and a blend containing 25% biodiesel. The acceleration sequences were 900 rpm to 1200 rpm, 1200 rpm to 1500 rpm, and 1500 to 1800 rpm. A program was used to control the speed and

load parameters of each test. Measurements of CO, CO₂, NO_x, UHC, and O₂ were made using a Horiba EXSA-1500 gas test bench. A measurement delay of 21 seconds was determined to compensate for the analyzer response time and the transfer of sample gas through the heated sample line. For all loading conditions the authors report a higher peak cylinder pressure for biodiesel fuel as a result of more complete combustion compared to standard diesel. For 25% and 100% biodiesel the NO_x levels are reported to increase by 13% and 17%, respectively, for transient testing. The authors attribute the increase to the advanced combustion caused by the physical properties of the fuel. The lower compressibility of biodiesel causes an increased pressure and a faster injection time. The effect is increased NO_x formation because the cylinder gases are rich in fuel at the peak temperature. As the speed increased in each transient test cycle the NO_x emissions were observed to decrease. Increased gas flow rate and volumetric efficiency are claimed to promote faster mixing and minimize the ignition delay. CO was reported to decrease with biodiesel and increased engine speed. Conversion of CO to CO₂ is increased with temperature. Increased engine speeds and the better combustion of biodiesel result in decreased CO. Due to the decrease in carbon molecules of biodiesel, CO₂ emissions were shown to decrease by 52%. A 38% reduction in UHC emissions was reported for biodiesel as a result of more complete combustion from the 11% oxygen content and increased cetane. Increased cetane reduces combustion delay, allowing more time for the combustion, resulting in more complete combustion [21].

CHAPTER 3 TEST CELL DESIGN

This chapter will discuss the design of the test cell, including the selection of components and the modification of existing equipment required to perform the desired testing. After reviewing commercially available test cells and the equipment available in the Bucknell Hybrid Powertrain Lab, design criteria and constraints were established. The test cell was then designed and built around these constraints.

3.1 Design Criteria

Safe and user friendly operation is the most critical goal for the testing apparatus. A dynamometer offers safe and controlled testing of internal combustion engines, but is not fail safe. Testing an engine on a dynamometer involves many parts rotating at high speeds. In the event of a failure, rotating parts could cause injury to the test cell operator and observers. Special guards and procedures must be utilized to prevent injuries from engine or dynamometer failures. In addition to general safety criteria, the success of the project depends largely on performance criteria. To make consistent and accurate measurements worthy of comparisons between tests, the test cell must offer accurate and repeatable measurements for the entire range of speed and load for the engine being tested. These measurements include engine speed, engine torque, fuel consumption, air consumption, ambient weather conditions, various temperatures, and exhaust composition. All data needs to be recorded by a computer and saved in a file that can be

accessed for later analysis. The operator must also have precise control of engine speed and load. Meeting these criteria was accomplished with careful component selection, test cell design, calibration methods, and operation procedures.

3.2 Design Constraints

Design of the alternative fuel testing apparatus was largely constrained by budget and time. Initial funding for the project provided by the Mechanical Engineering Department was set at \$2500.00. Careful selection and procurement of quality components meeting the design criteria had to be made to meet the budget constraints. Time had to be balanced between design, procurement, fabrication, and use of the test cell. For this reason, adaptation of a dynamometer already established at Bucknell University was necessary. A transmission dynamometer designed and built by Michael DeVita in 2006 offered an excellent foundation for the test cell. The remainder of the test cell would have to be designed and built around this foundation.

3.3 Previous Work and Modifications

The dynamometer designed and built by DeVita consisted of a control box, DC absorbing motor, and resistor bank with a capacity of 20 horsepower [27]. The test bench featured precision loading control and measurement designed for ease of operation, but lacked computerized data acquisition, and required modifications to perform the engine testing needed. Modifications were made to the dynamometer while preserving the option to test

transmissions on the test bench if needed. The transmission and driving motor were removed from the test bench and replaced with a compression ignition engine with a speed reduction system. Necessary engine controls were added to a separate panel attached to the dynamometer control box (Figure 3-1) and computerized data acquisition equipment was implemented. Air intake, fuel delivery, and exhaust systems were also added to the test cell.



Figure 3-1: Dynamometer Control Box

3.4 Engine Selection

Based on research of current technology, it was determined that a diesel engine would provide the most relevant alternative fuel testing. To maximize the simplicity of the test cell, a single cylinder, high quality, air cooled compression ignition engine was desired. Development and evaluation of new ideas and components is simplified by a one cylinder test engine. This reduces development time and cost and simplifies data analysis. When

selecting an engine it was desired that the engine be a reputable engine known to industry. Parts must be readily available to rebuild the engine if needed and to make modifications to parts, such as the cylinder head and piston. For this reason a Yanmar 10 HP direct injection diesel engine was selected. The Yanmar Company is well known for high quality dependable engines, and resources are readily available.

3.5 Engine Implementation

Because diesel engines are more robust and expensive to produce, the cost for a brand new Yanmar engine is approximately \$3000.00 and did not meet the constraints of the project budget. A used version was desired but not immediately located. During the procurement process a Briggs and Stratton 10HP spark ignition engine was used to temporarily complete the set up and allow for functionality testing of the dynamometer (Figure 3-2).



Figure 3-2: Briggs and Stratton 10 HP Configured to the Test Bench

After months of searching, a used 2004 10 HP Yanmar engine was purchased locally at a flea market for \$110.00. The engine was part of a nonfunctional generator set, but the engine was functional. The engine was removed from the generator and implemented to the test cell. Specifications for the engine are listed in Table 3-1.

Table 3-1: Yanmar L100EE Specifications (reproduced from Yanmar Manual)

Specification		Unit	Detail
Engine Model			2004 Yanmar L100EE
Engine Type			Single-cylinder, vertical-4cycle diesel
Cooling System			Forced air cooling by flywheel fan
Combustion System			Direct injection system
Starting System			Starting motor with recoil starter
Number of cylinder-BoreXStroke		mm	1-86-72
Displacement		liters	0.418
Output	Continuous	kW(HP)	6.3(8.6)
	Maximum	kW(HP)	7.1(9.6)
Rated engine speed (crankshaft)		rpm	3600
Idle engine speed at no-load high/low		rpm	3780/1200
Compression Ratio			20.0
PTO shaft	PTO Position		Crankshaft
	Direction of rotation		Counterclockwise viewed from PTO
Fuel oil system	Fuel injection pump		Bosch type YANMAR PFE-M type
	Fuel injection timing (FIC: bTDC)	deg	17.0
	Fuel injection nozzle		VCO nozzle Bosch made
	Fuel injection pressure	Mpa (kgf/cm ²)	19.6 (200)
Lubricating oil system	Type of lubrication		Forced lubrication via trochoid pump: splash lubrication for valve rocker arm chamber
	Lubricating oil filter		Resin, 60 mesh
	Lubricating oil selection		SAE10W30, API grade CC or higher
	Lubricating oil capacity full/effective	liters	1.65/0.6
Governor			All speed type mechanical
Engine Dimensions (Length X Width X Height)		mm	392 X 470 X 494
Dry Mass		kg	54
Balancer shaft			Single shaft

The first step in implementing the engine to the test cell was modeling the engine and the test cell in Solidworks. Modeling of the components would allow for visualization of the test cell and aid in the design process. Dimensions were obtained by manually measuring each component. An assembly was then created by combining each component model. This allowed for easy design and fitment verification of all new components of the test cell.

3.6 Intake System

An intake system was required to channel air from the room through a measurement device and through a filter before being delivered to the engine without any leaks. A Meriam Laminar Flow Element (LFE) was used to measure the volumetric flow rate of the air. Flexible tubing connects the LFE to a custom tubular air box containing a high performance K&N air filter to minimize airflow resistance. The air needed to be filtered at the engine inlet to prevent any contaminants from entering the engine. The stock air box could not be modified to meet these constraints, so a new intake system was designed. A two piece adapter was designed to locate the K&N filter inside of the tubular air box and allow both to be mounted to the engine (Figure 3-3). The tubular air box was fabricated from a clear acrylic tube. Use of a clear air box would allow for easy inspection of the air filter and also give the user and observers a unique and interesting view of the intake system.

3.7 Exhaust System

An exhaust system was required to channel exhaust gases from the engine to the outside of the building. A muffler would also be required to reduce noise and potential disturbances to other buildings. An exhaust system routed to the outside of the building with a muffler was already in place for the Hybrid Electric Vehicle (HEV) dynamometer. To meet time and budget constraints, it was necessary to tap into this system. A special exhaust header pipe was designed and built to attach to the Yanmar engine and route the exhaust gas upward (Figure 3-3). The header pipe features flanges at each end for ease of assembly and disassembly and includes ports for temperature and emissions sampling in addition to a condensation trap. In order to preserve the tuning of the engine, the inside diameter of the header pipe was kept the same as the stock exhaust system. Flexible galvanized exhaust pipe was connected to the header flange and routed toward the pre-existing muffler of the HEV exhaust system. A cable operated exhaust switch was installed at the inlet of the muffler to enable exhaust flow to be switched between the HEV engine and the Yanmar engine. Switching of the flow prevents exhaust gas backflow into either system.

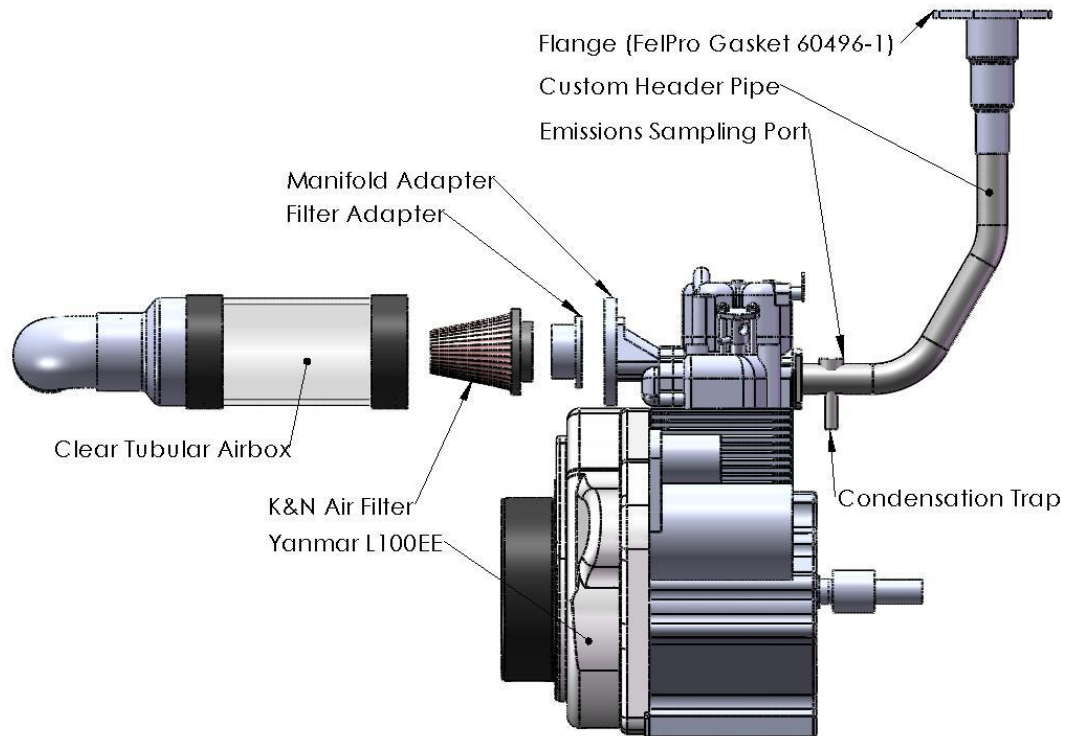


Figure 3-3: Intake and Exhaust System Design

3.8 Speed Reduction System

To maintain the speed of the dynamometer below the maximum rated speed of 1750 rpm, a speed reduction system was designed to reduce the speed of the engine by a factor of two. Reducing the speed of the DC absorbing motor also increases the torque applied by the test engine by a factor of two. Special precautions needed to be taken to ensure the dynamometer could handle the increased torque at decreased speeds. This was verified by

plotting the maximum torque output of the engine and the maximum torque absorption of the dynamometer as a function of engine speed (Figure 3-4). Data for the plot was obtained by interpreting and reproducing plots of rated power from Yanmar and maximum continuous torque versus speed for the DC absorbing motor.

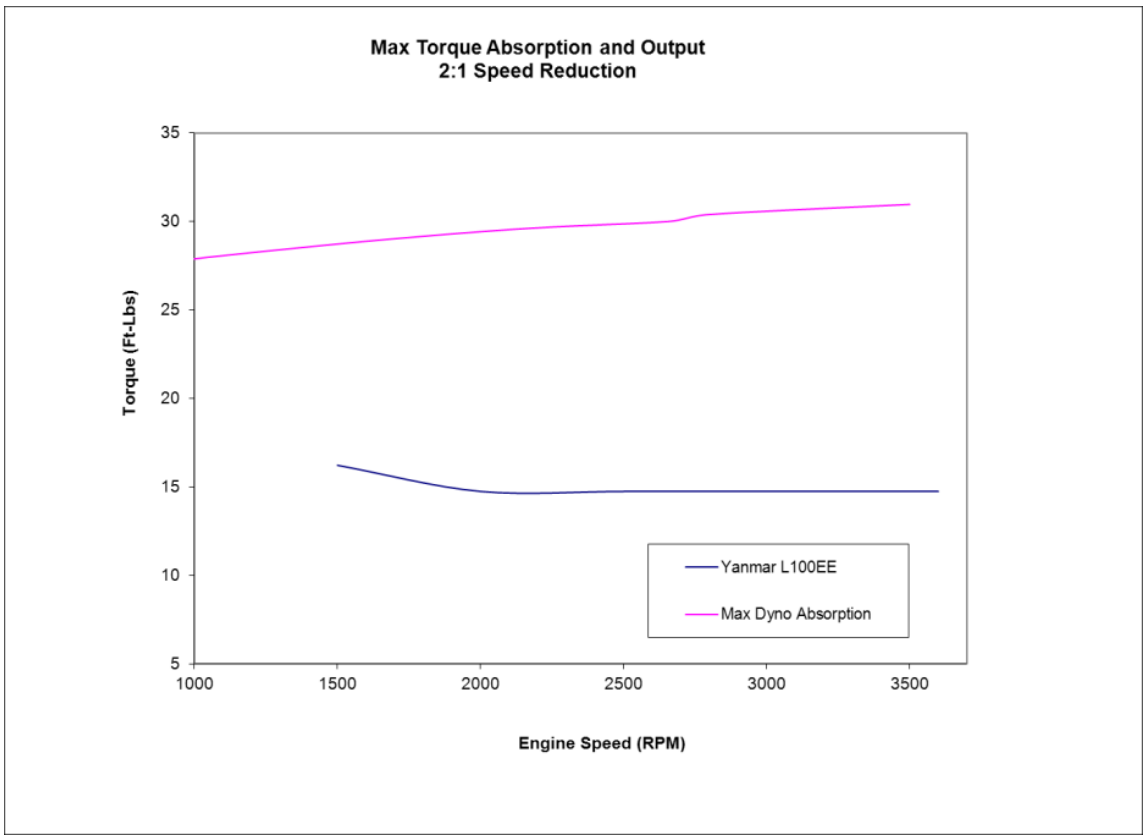


Figure 3-4: Torque Verification Plot

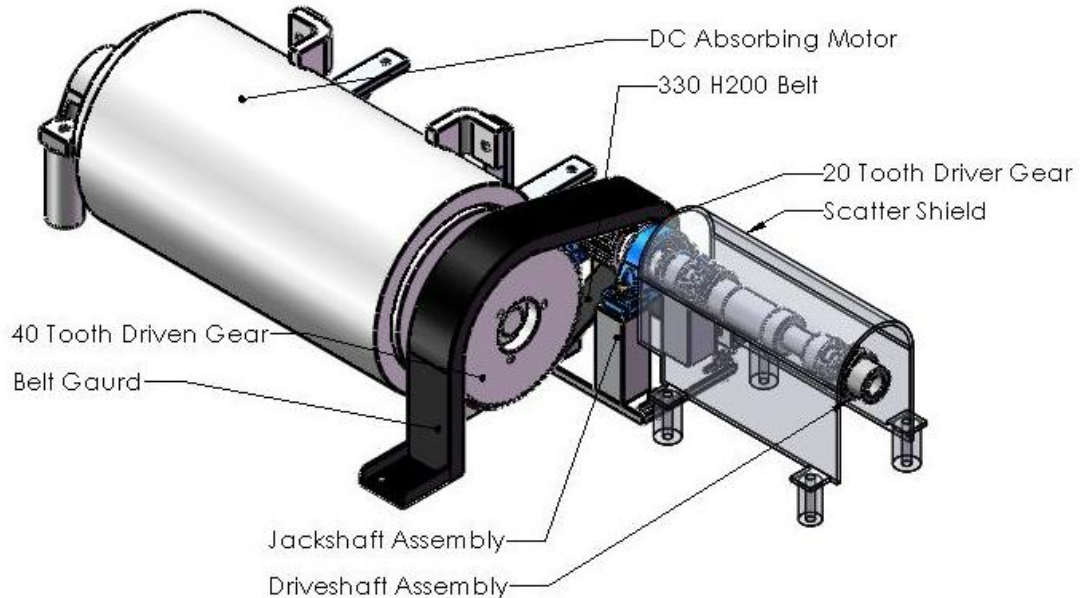


Figure 3-5: Speed Reduction System

The speed reduction system shown in Figure 3-5 was accomplished with a timing pulley system, jack shaft assembly, and driveshaft assembly. The jack shaft assembly shown in Figure 3-6 is mounted to the table and features precision adjusters to meet alignment and belt tension requirements. The jack shaft is designed to be at the same height as the crank shaft of the engine. Any misalignment is compensated by the dual universal joint driveshaft but perfect alignment is desired to minimize frictional losses. To achieve a 2:1 speed reduction, the driver pulley connected to the jackshaft is half the size of the driven pulley connected to the absorbing motor. The layout of the test bench required the

maximum center distance of the belt reduction system to be ten inches. To maintain clearance and adjustability of the system, a minimum center distance of eight inches was desired. Using Martins stock drive selection charts (Figure 3-7), pulley sizes were selected based on the maximum center distance and available belt lengths while maintaining a 2:1 speed ratio and proper power capacities. Using “H” series pulleys, a driver pulley with 20 teeth and a driven pulley with 40 teeth were selected to maintain the correct speed ratio and handle 11.77 horsepower per inch of belt width at a driver speed of 3500 rpm. The “200” series belt and pulleys selected are two inches wide and have a capacity of 23.54 horsepower at the maximum dynamometer speed. This combination was chosen so the pulley system capacity exceeded the power capacity of the dynamometer. A “330H” belt with 66 teeth provides a center distance of 8.86 inches between the pulleys, meeting the space constraints of the test bench. The jackshaft and engine are located on the front side of the test bench (away from the wall) in order to maintain proper direction of rotation for the absorbing motor and the test engine. A belt guard was designed and built to enclose the pulley system and protect the user from debris in the event of a belt failure. The guard was designed to be compatible with a driven pulley size of up to 60 teeth in case a different speed ratio was desired in the future. A similar shield was also designed and built to enclose the driveshaft connecting the engine to the speed reduction system. This shield is labeled “Scatter Shield” in Figure 3-5.

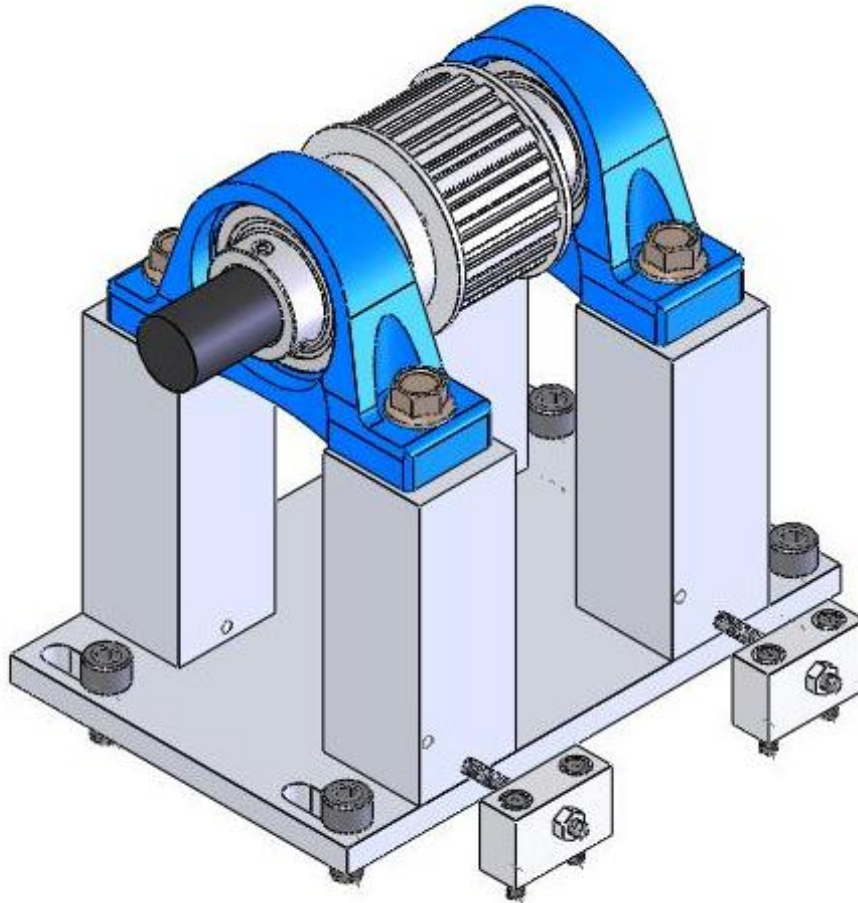


Figure 3-6: Jack Shaft Assembly

speed ratio □	pulley combination				driveN speed and hp capacity						center distance, inches†							
	driveR		driveN		3500 rpm driveR speed		1750 rpm driveR speed		1160 rpm driveR speed		according to belt pitch length (PL), inches and corresponding code number (bold type)							
	code: no. of grooves	pitch diameter in.	code: no. of grooves	pitch diameter in.	driveN speed rpm	hp for 1 inch belt	driveN speed rpm	hp for 1 inch belt	driveN speed rpm	hp for 1 inch belt	PL: 24.00 48 teeth 240 H	PL: 27.00 54 teeth 270 H	PL: 30.00 60 teeth 300 H	PL: 33.00 66 teeth 330 H	PL: 36.00 72 teeth 360 H	PL: 39.00 78 teeth 390 H	PL: 42.00 84 teeth 420 H	
1.56	18 H	2.865	28 H	4.456	2250	10.71	1125	5.52	746	3.68	6.21	7.72	9.22	10.73	12.23	13.74	15.24	
1.57	28 H	4.456	44 H	7.003	2227	15.74	1114	8.46	738	5.68	—	—	—	7.40	8.92	10.43	11.94	
1.58	19 H	3.024	30 H	4.775	2217	11.24	1108	5.81	735	3.88	5.82	7.33	8.84	10.35	11.85	13.36	14.86	
1.60	30 H	4.775	48 H	7.639	2188	16.59	1094	9.03	725	6.08	—	—	—	6.60	8.13	9.65	11.17	
	20 H	3.183	32 H	5.093	2188	11.77	1094	6.11	725	4.08	5.42	6.94	8.45	9.96	11.47	12.97	14.48	
1.63	44 H	7.003	72 H	11.459	2139	21.01	1069	12.84	709	8.80	—	—	—	—	—	—	—	
	22 H	3.501	36 H	5.730	2139	12.84	1069	6.71	709	4.48	—	6.16	7.68	9.19	10.70	12.21	13.71	
	16 H	2.546	26 H	4.138	2154	—	1077	4.91	714	3.27	6.71	8.22	9.73	11.23	12.73	14.24	15.74	
1.67	36 H	5.730	60 H	9.549	2100	18.89	1050	10.71	696	7.26	—	—	—	—	—	—	8.80	
	24 H	3.820	40 H	6.366	2100	13.82	1050	7.30	696	4.89	—	—	6.89	8.41	9.93	11.44	12.95	
	18 H	2.865	30 H	4.775	2100	10.71	1050	5.52	696	3.68	5.93	7.45	8.96	10.46	11.97	13.48	14.98	
1.68	19 H	3.024	32 H	5.093	2078	11.24	1039	5.81	689	3.88	5.54	7.06	8.57	10.08	11.59	13.09	14.60	
1.69	26 H	4.138	44 H	7.003	2068	14.80	1034	7.88	685	5.28	—	—	6.09	7.62	9.15	10.66	12.17	
1.71	28 H	4.456	48 H	7.639	2042	15.74	1021	8.46	677	5.68	—	—	—	6.82	8.35	9.88	11.40	
	21 H	3.342	36 H	5.730	2042	12.31	1021	6.41	677	4.28	4.73	6.27	7.79	9.31	10.82	12.33	13.83	
1.75	48 H	7.639	84 H	13.369	2000	21.63	1000	13.84	663	9.55	—	—	—	—	—	—	—	
	16 H	2.546	28 H	4.456	2000	—	1000	4.91	663	3.27	6.44	7.95	9.46	10.97	12.47	13.98	15.48	
1.78	18 H	2.865	32 H	5.093	1969	10.71	985	5.52	652	3.68	5.65	7.17	8.69	10.20	11.71	13.21	14.72	
1.80	40 H	6.366	72 H	11.459	1944	20.08	972	11.79	644	8.03	—	—	—	—	—	—	—	
	20 H	3.183	36 H	5.730	1944	11.77	972	6.11	644	4.08	4.84	6.38	7.90	9.42	10.93	12.44	13.95	
1.82	22 H	3.501	40 H	6.366	1925	12.84	963	6.71	638	4.48	—	5.57	7.11	8.64	10.16	11.67	13.18	
1.83	24 H	3.820	44 H	7.003	1909	13.82	955	7.30	633	4.89	—	—	6.30	7.84	9.37	10.89	12.41	
1.85	26 H	4.138	48 H	7.639	1896	14.80	948	7.88	628	5.28	—	—	—	7.04	8.58	10.11	11.63	
1.88	32 H	5.093	60 H	9.549	1867	17.40	933	9.60	619	6.48	—	—	—	—	—	7.68	9.24	
	16 H	2.546	30 H	4.775	1867	—	933	4.91	619	3.27	6.16	7.68	9.19	10.70	12.21	13.71	15.22	
1.89	19 H	3.024	36 H	5.730	1847	11.24	924	5.81	612	3.88	4.94	6.49	8.02	9.54	11.04	12.56	14.07	
1.90	21 H	3.342	40 H	6.366	1838	12.31	919	6.41	609	4.28	—	5.68	7.22	8.75	10.27	11.79	13.30	
1.91	44 H	7.003	84 H	13.369	1833	21.01	917	12.84	607	8.80	—	—	—	—	—	—	—	
2.00	48 H	7.639	96 H	15.279	1750	21.63	875	13.84	580	9.55	—	—	—	—	—	—	—	
	36 H	5.730	72 H	11.459	1750	18.89	875	10.71	580	7.26	—	—	—	—	—	—	—	
	30 H	4.775	60 H	9.549	1750	16.59	875	9.03	580	6.08	—	—	—	—	—	7.89	9.45	
	24 H	3.820	48 H	7.639	1750	13.82	875	7.30	580	4.89	—	—	—	7.25	8.80	10.33	11.85	
	22 H	3.501	44 H	7.003	1750	12.84	875	6.71	580	4.48	—	—	—	6.52	8.07	9.60	11.12	
	20 H	3.183	40 H	6.366	1750	11.77	875	6.11	580	4.08	—	5.78	7.33	8.86	10.39	11.90	13.41	
	18 H	2.865	36 H	5.730	1750	10.71	875	5.52	580	3.68	5.05	6.60	8.13	9.65	11.16	12.68	14.19	
	16 H	2.546	32 H	5.093	1750	—	875	4.91	580	3.27	5.87	7.40	8.92	10.43	11.94	13.45	14.96	
2.09	21 H	3.342	44 H	7.003	1670	12.31	835	6.41	554	4.28	—	—	—	6.63	8.18	9.71	11.23	
2.10	40 H	6.366	84 H	13.369	1667	20.08	833	11.79	552	8.03	—	—	—	—	—	—	—	
2.11	19 H	3.024	40 H	6.366	1663	11.24	831	5.81	551	3.88	—	5.89	7.44	8.98	10.50	12.02	13.53	

Figure 3-7: Belt Reduction Pulley Selection Chart (reproduced from [28]). The highlighted row of data shows the specifications and belt options for the combination selected.

3.9 Engine Mount

Vibrations are an issue for all internal combustion engines and must be dealt with to ensure the durability and longevity of the apparatus. The engine mount needed to secure the engine to the test bench, absorb engine vibrations, and offer adjustability to

compensate for alignment with the jackshaft and consequently belt tension adjustments. Four Anchor Industries #2265 engine mounts (Figure 3-8) were used in conjunction with a slotted steel plate to achieve these constraints. One side of each vibration absorbing mount is bolted to the test bench and the other side bolted through the slotted portion of the steel plate (Figure 3-9). The engine is bolted to the steel plate and the assembly is adjustable until tightened to the vibration absorbing mounts.



Figure 3-8: Anchor Industries #2265 Engine Mount

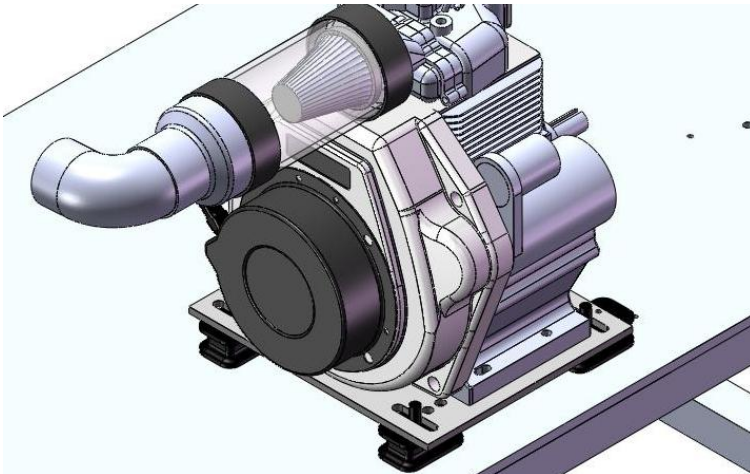


Figure 3-9: Yanmar Engine Mount

3.10 Fuel Delivery System

A fuel delivery system was necessary to deliver fuel to the Yanmar engine at a constant temperature of 40°C. The fuel flowing to the engine also needed to be measured and filtered. The system was largely constrained by delivery pressure, method of fuel measurement, temperature control, and material compatibility. Since biodiesel has corrosive properties, yellow metals such as copper and brass are not suitable for long term use. Stainless steel fittings and yellow Tygon tubing were selected because of their compatibility with gasoline, diesel, alcohol, and biodiesel. Yellow Tygon tubing also offers flexibility for easy line routing and is transparent which allows easy visualization of air in the fuel line. A 5 micron fuel filter with water separator was used to filter any contaminants from the fuel to prevent clogging of the precision injector nozzle. A water bath was used in conjunction with a stainless steel coil to condition the fuel to a constant temperature of 40°C. A low pressure diesel transfer pump was purchased and used to pump fuel to the engine from the fuel tank through the chiller coil, filter, and line. To avoid damage to the engine's fuel injection pump, the pressure of the fuel delivered to the engine must be kept to a minimum. The transfer pump selected has a maximum output pressure of 2 psi and is compatible with biodiesel. A Sartorius explosion proof paint scale was selected to measure the change in mass of the fuel tank for determining the mass flow rate of the fuel. A semi-transparent plastic one gallon fuel tank compatible

with all fuel types was selected to fit on the fuel scale and offer visibility of the fuel level.

The fuel system schematic is shown in Figure 3-10.

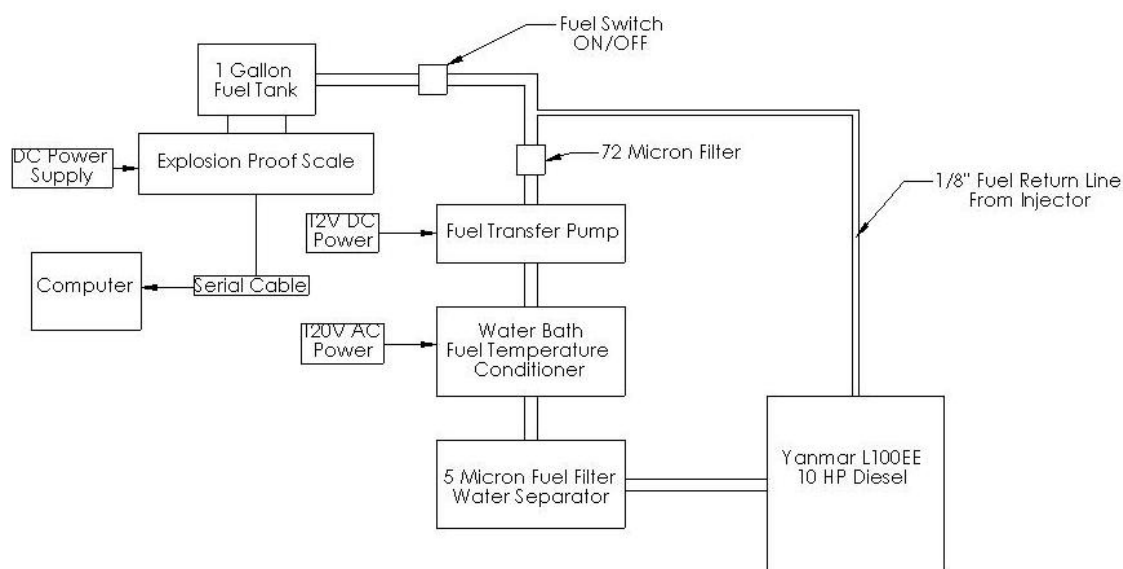


Figure 3-10: Yanmar fuel delivery system schematic

3.11 Speed Control System

For the Yanmar engine selected, engine speed is controlled by manually adjusting the position of the engine governor. The governor controls the variable displacement injection pump and therefore directly controls engine speed by varying the volume of fuel injected into the cylinder. The range of adjustment between the idle and full speed positions of the governor is about one inch. A control cable with a precision knob

adjustment was used to translate rotary motion of the control knob to precise linear motion of the governor control from the control desk. The full adjustment range of the governor is accomplished by 25 turns of the precision control knob. A quick release button on the speed control knob allows for rapid shut down of the engine. In the home position of the speed control knob (all the way clockwise) fuel flow to the engine is stopped. Since CI engines have no ignition system, the only way to turn off the engine is by stopping the fuel flow to the cylinder. Emergency shutdown of the engine is achieved by pressing the quick release button.

3.12 Engine Starting System

The L100EE Yanmar engine comes equipped with a manual recoil starter and an electric starting system. A battery is located under the test bench to power the starter and the fuel transfer pump. A charging system is located inside of the engine flywheel to charge the battery and run accessories but in order to minimize the power losses on the engine, the charging system is only used to operate a small LED on the user control panel to indicate the engine is running. The starter and fuel pump are controlled by an ignition switch located in the control panel. Power from the battery is connected to the system by a battery disconnect switch. The safety switch allows the battery to be disconnected from the system when not in use; this also prevents draining of the battery.

3.13 Emissions Analysis Equipment

To determine exhaust gas composition, it was desired to measure the concentrations of the following exhaust components: unburned hydrocarbons, oxides of nitrogen, carbon dioxide, carbon monoxide, oxygen, and sulfur dioxide. The emissions equipment used for this project was new to Bucknell University and required a significant amount of setup preparation. A heated stainless steel sample line is used to carry a sample gas to two separate analyzers. Heating of the line is required to prevent the moisture in the sample gas from condensing and damaging the equipment. A heated filter is also used to remove particulate matter that could also damage the equipment. After the filter, the sample line is split to deliver sample gas to a Total Hydrocarbon Analyzer (THC) and a Multi gas analyzer. The THC analyzer manufactured by California Analytical Instruments (CAI) uses a Heated Flame Ionization Detector (HFID) to measure the concentration of hydrocarbons or unburned fuel in the exhaust gas. The multi-gas analyzer manufactured by Horiba measures NO_x, SO₂, CO, CO₂, and O₂. NO_x is measured using a chemiluminescence method. SO₂, CO, and CO₂ are measured using a non-dispersive infrared method. O₂ is measured using a galvanic cell method. Special equipment including high purity regulators, burner fuel, zero gases, and span gases are required to operate this equipment. A schematic of the equipment and required plumbing is shown in Figure 3-11.

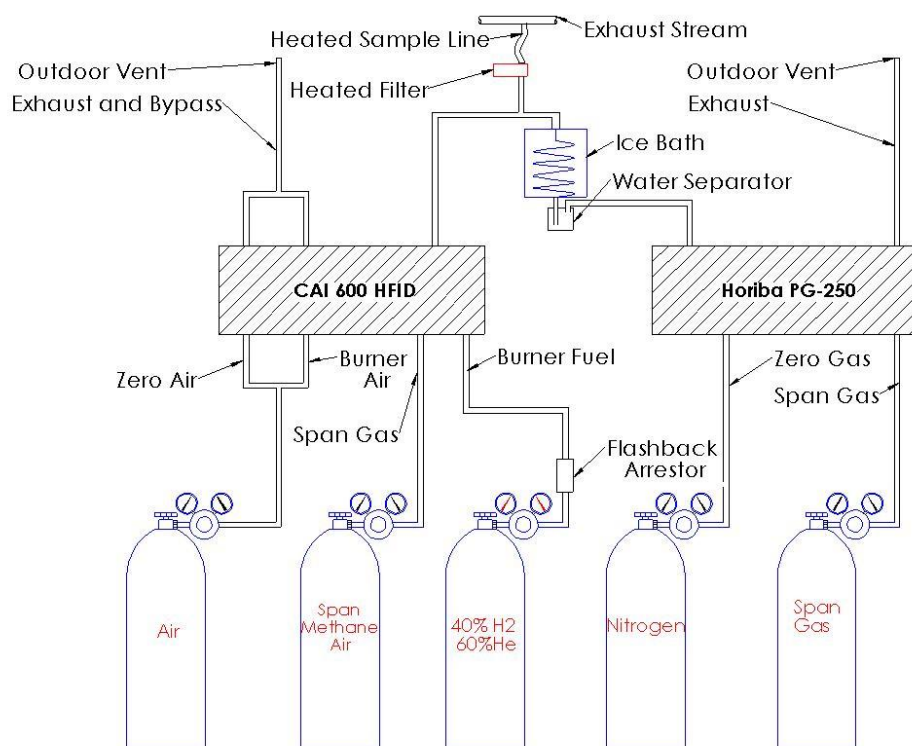


Figure 3-11: Emissions analyzer plumbing schematic

The emissions analysis equipment was intended to be shared between the Hybrid Powertrain Lab and the Combustion Research Lab. Making the equipment mobile allowed the equipment to be easily transferred between labs in a reasonable amount of time. A cart was purchased and modified to contain the analyzers, heated filter, ice bath, water separator, and temperature controllers for the heated line and filter. A heated sample line was fabricated for each lab. Five gas bottles are required for operation and

also needed to be portable. A special cart was designed and built during the summer of 2010 to contain all the gas bottles (Figure 3-12).

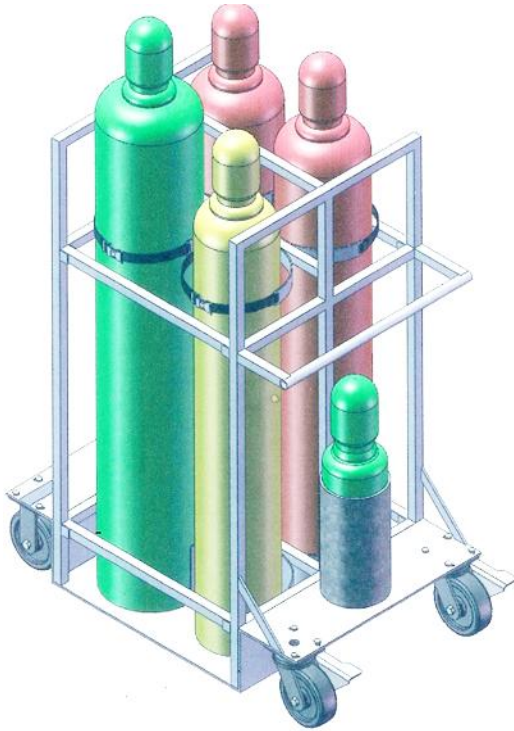


Figure 3-12: Emissions gas bottle cart

The cart features lockable, six inch diameter wheels for easy rolling and low ground clearance for easy loading and unloading of heavy gas bottles. The width of the cart was kept to a minimum for maneuverability in the elevator and through doorways. Each bottle is secured to the cart with an adjustable strap and in case of strap failure; a safety bar is located at the top and bottom of each side.

3.7 Data Acquisition

Data acquisition is performed with a custom LabVIEW® program in conjunction with an Agilent 34970A Data Acquisition Unit. The Agilent reads signals from the load cell, optical speed sensor, emissions equipment, and thermocouples. The LabVIEW® program calls and records this data in addition to air and fuel flow data every ten seconds. The data is displayed to the user and also saved to an excel spreadsheet for later analysis.

Note/Set	Elapsed Time (s)	Fuel Weight (g)	RPM	Torque (ft-lbf)	Air Flow (CFM)	EGT (C)	Air T (C)	Oil T (C)	Calculated HP	O2	NOx	CO2	HC	SO2	CO
0.000	0.000	1861.100	0.000	-0.189	-0.025	19.824	20.394	19.666	0.000	4.345	0.995	0.992	0.188	1.163	0.995
0.000	10.000	0.000	0.000	-0.190	-0.025	19.885	20.489	19.678	0.000	4.345	0.997	0.992	0.186	1.165	0.995
0.000	20.000	1861.100	0.000	14.285	-0.025	19.847	20.410	19.686	0.000	4.345	0.997	0.992	0.186	1.165	0.995
0.000	30.000	1861.100	0.000	14.266	-0.025	19.847	20.445	19.667	0.000	4.345	0.997	0.992	0.185	1.165	0.995
0.000	40.001	1861.000	0.000	14.261	-0.025	19.847	20.423	19.673	0.000	4.345	0.997	0.992	0.183	1.163	0.995
0.000	50.001	1861.100	0.000	14.258	-0.025	19.872	20.451	19.676	0.000	4.345	0.997	0.992	0.182	1.165	0.995
0.000	60.001	1861.100	0.000	14.257	-0.025	19.872	20.493	19.667	0.000	4.345	0.995	0.992	0.180	1.163	0.995
0.000	70.001	1861.100	0.000	14.255	-0.025	19.869	20.451	19.663	0.000	4.345	0.995	0.992	0.180	1.163	0.995
0.000	80.001	1861.100	0.000	14.255	-0.025	19.866	20.489	19.695	0.000	4.345	0.995	0.992	0.180	1.165	0.995
0.000	90.001	1861.100	0.000	14.254	-0.025	19.881	20.445	19.689	0.000	4.345	0.997	0.992	0.180	1.165	0.995
0.000	100.001	1861.100	0.000	14.254	-0.025	19.897	20.432	19.695	0.000	4.345	0.995	0.992	0.179	1.163	0.995
0.000	110.001	1861.100	0.000	14.254	-0.025	19.875	20.426	19.695	0.000	4.345	0.995	0.992	0.177	1.163	0.995

Figure 3-13: User interface of custom LabVIEW® program

Measurements and displays for dynamometer load and engine speed were already established in the control panel created by DeVita. In order to record the speed and load data, signals from the load cell and optical speed sensor were wired into the Agilent data acquisition unit. The custom LabVIEW® program communicates with the Agilent and uses the voltage from the load cell to calculate a force and the frequency signal from the

optical speed sensor to calculate speed. Within the calculations, the speed is doubled and the torque is decreased by a factor of two. This is necessary to represent actual engine speed and torque since the belt reduction system increases the torque and decreases the speed applied to the dynamometer. K type thermocouples are wired into the Agilent to read temperatures of exhaust gas (EGT), engine oil, and combustion air. The custom LabVIEW® program configures the Agilent to sequentially read and record the temperatures with rest of the data. Also wired into the Agilent are voltage signals from the emissions analysis equipment. Voltages from the emissions equipment are linearly proportional to the measurement being made but are dependent on the range of each measurement. For this reason, the voltages are recorded and measurement values are calculated during the data analysis. The LabVIEW® program collects data from the Agilent in ten second intervals. The data collection process could be performed in less than one second but a quality filter placed on the load cell measurement increases the time collection time to approximately six seconds. The filter configured in the LabVIEW® program samples the signal for an extended period of time to filter out interference and errors. This is important for obtaining good torque data. Vibrations from the engine and absorbing motor create a somewhat noisy signal from the load cell. Averaging the data over a longer sample time increases the quality of the measurement.

Measurements of airflow and fuel mass are made by the LabVIEW® program by directly communicating with each measurement device. A Meriam Laminar Flow Element (LFE)

is used to measure the volumetric flow rate of air consumed by the engine. A MKS Baratron pressure transducer measures the pressure drop across the LFE from the flowing air. A MKS Type 670 signal conditioner controls the pressure transducer and outputs the pressure drop to the desktop computer via serial communication. A pressure drop of eight inches of water across the LFE correlates to a volumetric flow rate of one hundred cubic feet per minute. The custom LabVIEW® program interprets the data and uses the linear relationship to calculate the volumetric flow rate of air. Mass of the fuel is measured with a Sartorius PMA 7200-X explosion proof paint scale (Figure 3-14). The serial communications output of the scale is connected to the desktop computer with a USB converter. The data is then interpreted and recorded by the custom LabVIEW® program in ten second intervals. The mass flow rate of the fuel is then calculated using the difference in mass and time between each data point during the data analysis.

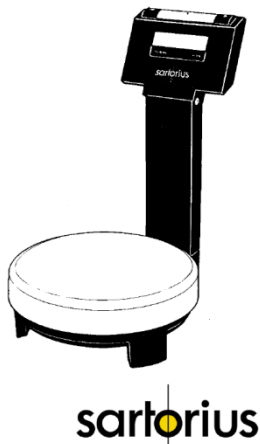


Figure 3-14: Sartorius PMA 7200-X Explosion Proof Paint Scale used to Measure Mass of Fuel (adapted from [29]).

CHAPTER 4 TESTING AND DESIGN VERIFICATION

4.1 Test Plan

The purpose of the experiment was to determine the feasibility of biodiesel as an alternative fuel. It was desired to study the effect on performance and emissions of the engine burning different blends of biodiesel and standard diesel. After some preliminary testing, it was found that the Yanmar engine was most efficient at full load and speeds from 2000-3000 rpm. Although the maximum torque for the Yanmar L100EE engine is approximately 14.5 ft-lbs, the maximum continuous output torque is 12.75 ft-lbs. Some torque is also lost in the speed reduction system and the DC absorbing motor. Therefore the maximum stable loading point for the desired speed range was found to be 12 ft-lbs.

Blends of biodiesel and diesel would be tested starting with standard diesel and adding biodiesel in 20% increments. In the state of Pennsylvania, all diesel fuel is mandated to contain 2% biodiesel. Standard diesel fuel containing 2% biodiesel is commonly known as B2. B2 was used as the standard fuel, and biodiesel derived from soybean oil was added to achieve the required blend percentage. Blends were mixed in six liter batches. Composition of each blend is shown in Table 4-1. A small sample of each fuel was kept for testing energy content and kinematic viscosity.

Table 4-1: Fuel Blending Data

Blend Name	Diesel % (Volume)	Biodiesel % (Volume)	Volume B2 (Liters)	Volume B100 (Liters)	Total Volume (Liters)
B2	98	2	6	0	6
B20	80	20	4.898	1.102	6
B40	60	40	3.673	2.327	6
B60	40	60	2.449	3.551	6
B80	20	80	1.225	4.775	6
B100	0	100	0	6	6

For each fuel blend, testing was performed at a constant torque of 12 ft-lbs starting at a speed of 2000 rpm, increasing to 3000 rpm in 100 rpm increments (Table 4-2). Special attention was given to perform the required warm up period and testing operation as consistently as possible for each fuel. Data was recorded for five minutes at each test point after reaching steady state operation of the engine for a minimum of one minute. To reduce measurement errors, the five minutes of data at each test point are averaged with exception to emissions measurements. An emissions measurement delay exists because the emissions sample line is 25 feet in length. Measurement delay is shown to be approximately 90 seconds (Table 4-3). Another 60-90 seconds is required after the measurement delay to allow the measurement to stabilize. For this reason, only the last minute of emissions data is averaged for each test point. Careful attention was also given when changing test fuels. To prevent fuel contamination, each time a new fuel was tested the entire fuel system was drained before adding the new fuel.

Table 4-2: Fuel Blend and Engine Operating Point Test Plan

Fuel Blend	Test Point	Engine Speed (RPM)	Engine Torque (ft-lbs)
B2, B20, B40, B60, B80, B100	1	2000	12
	2	2100	12
	3	2200	12
	4	2300	12
	5	2400	12
	6	2500	12
	7	2600	12
	8	2700	12
	9	2800	12
	10	2900	12
	11	3000	12

Table 4-3: Emissions Sample Measurement Delay

Note/Set	Time (Sec)		O2 (%)	NOx (ppm)	CO2(%)	
2612	3460		13.21	425.50	5.81	
2612	3470		13.21	426.00	5.82	
2612	3480		13.21	426.50	5.82	
2612	3490		13.21	426.50	5.82	
2612	3500		13.22	427.00	5.82	
2612	3510		13.22	426.50	5.82	
Speed and Load Change						
0	3520	80-90 Second Measurement Delay	13.22	426.50	5.82	
0	3530		13.22	426.00	5.81	
0	3540		13.22	425.50	5.81	
0	3550		13.22	425.50	5.81	
0	3560		13.22	425.50	5.81	
0	3570		13.21	425.50	5.81	
0	3580		13.22	426.00	5.81	
0	3590		13.21	425.50	5.82	
0	3600			13.19	424.50	5.83
0	3610			13.17	422.50	5.84
0	3620	13.14		420.50	5.86	
0	3630	13.12		418.50	5.89	

4.2 Operation Procedures

The first step of the test cell operation is to prepare the emissions analysis equipment. This equipment takes almost two hours to prepare before measurements can be made so it is necessary to do this first. Detailed instructions are available in the “Emissions Analyzer Equipment Operation Procedure” (Appendix A). After the emissions equipment preparation has been completed, the data file for the LabVIEW® program needs to be prepared. This should be performed by following the “Data File Preparation Procedure” (Appendix B). After this has been completed, preparation of the engine and the dynamometer can begin. This should be completed by following the “Dynamometer Startup and Operation Procedure” (Appendix C). This procedure also discusses how to operate the dynamometer to complete a test, and how to properly shut down the dynamometer. Instructions for shutdown of the emissions equipment are given in Appendix A. Post testing data analysis should be performed by following the “Data File Analysis Procedure” (Appendix D). Instructions for changing the test fuel are given in the “Fuel Changing Procedure” (Appendix E)

4.3 Measurement Calibrations

The most critical component of the testing apparatus is the load cell used to measure engine torque. Any error in this measurement has a direct effect on the calculations of power, specific fuel consumption, and thermal efficiency. For example, a 1% change in

torque causes a 1% change in each calculation. For this reason, a load cell calibration procedure was developed and should be performed before each test. The procedure involves placing the calibration weight onto the calibration arm of the dynamometer absorbing motor. The weight contains a pin that fits into the calibration arm ensuring consistent placement of the calibration weight and an accurate calibration. The load cell calibration procedure is included in the “Dynamometer Startup and Operation Procedure” (Appendix C).

Calibration of the engine speed measurement is not as critical as the load cell but nonetheless important for calculations. Independent measurements read from the optical sensor are made by the programmable tachometer located in the control box and by the LabVIEW® program. By visually comparing the two speed measurements, the user can determine any error between the two. A handheld tachometer should also be used periodically to confirm the accuracy of both measurements. Typical engine speed fluctuation of 10-15 rpm is normal when operating the engine. Engine speed data is averaged to compensate for the fluctuation but keeping the variation below 1% of the set speed is ideal.

The process for calibrating the Sartorius fuel scale is similar to the load cell calibration. After zeroing the scale and allowing a thirty minute warm up time, a 5000 gram (+/- 0.03 grams) calibration weight is placed in the center of the scale. The calibration is complete

if the measurement matches the known mass of the weight. Because the data of concern is the change in fuel mass, the linearity of the measurement is much more important than the actual accuracy of the measurement at full scale. For example, if the known weight of an object was 5000 grams and the scale read 4500 grams the measurement accuracy is not valid. However, if you added or removed a known mass and the scale measurement correctly represented the change, the linearity of the measurement is accurate and sufficient for taking data. The linearity can be checked by placing five 1000 gram calibration weights on the scale. Regardless of the initial measurement, removal of one weight should result in the measurement decreasing by 1000 grams. Each successive removal of weight should result a 1000 gram decrease in the measurement value. If the calibration cannot be confirmed, the scale needs to be recalibrated by the manufacturer.

Calibration of the Meriam LFE is performed by the manufacturer. Records of this calibration were not available and, because of the age of the unit, the manufacturer was not willing to perform a new calibration. However, the MKS signal conditioner used to read the pressure drop from the LFE is zeroed and calibrated before each test. Instructions for this process are included in the “Dynamometer Startup and Operation Procedure” (Appendix A.3). Consistent measurements of airflow are verified by comparing data from the same test performed on two different days. This is discussed in the next section.

Calibration of the emissions analysis equipment is performed before each test. The process, which is explained step by step in the “Emissions Analyzer Equipment Operation Procedure” (Appendix A.2), involves zero and span calibrations for each measurement. Each instrument is first zeroed with a designated zero gas. High purity air is used as the zero gas for the HFID and high purity nitrogen is used as the zero gas for the Horiba multi gas analyzer. After zeroing each unit, span calibration of each measurement can be performed. The concentration of span gas for each measurement is determined by taking 90% of the expected full scale range. Span calibration verifies the upper limit of the measurement and enables accurate measurements between the zero and span points. The span gas selected for the HFID unit consists of high purity air and 1000 parts per million (ppm) of methane. The multi component span gas used for the Horiba multi gas analyzer is shown in Table 4-4. Span calibration for oxygen is performed with the oxygen contained in room air.

Table 4-4: Horiba Span Gas Concentrations

Component	Requested Concentration	Actual Concentration	Analytical Uncertainty Concentration
Sulfur Dioxide	150 ppm	147.7 ppm	+/- 2%
Nitric Oxide	1000 ppm	1019 ppm	+/- 2%
Carbon Monoxide	4000 ppm	3930 ppm	+/- 2%
Carbon Dioxide	15%	14.98%	+/- 2%
Nitrogen	Balance		

4.4 Design Verification

Design verification was originally performed by testing the functionality of the dynamometer and data acquisition equipment with a 10 HP Briggs and Stratton Engine. After implementing the Yanmar diesel engine, the next stage of design verification was completed by confirming the engine would run and that the speed and load controls functioned properly. Successfully testing the engine from zero to full load at speeds from idle to full speed (3500 rpm) proved the apparatus to be safe and functional. The best specific fuel consumption for the engine should be 245 grams of fuel per kilowatt hour at a speed of 2500 rpm. Testing the engine with B2 resulted in a specific fuel consumption of 247 grams of fuel per kilowatt hour. A comparison of specific fuel consumption data obtained and the data provided by Yanmar showed a variation of less than 1% thus proving the validity of the apparatus and data acquisition equipment. Data obtained seemed accurate and consistent but further testing was performed to establish repeatability.

4.5 Accuracy and Repeatability

Following the test method presented in (Table 4-2) the torque and speed are set for each test point. Achieving the speed and torque values at each test point would prove the accuracy and repeatability of the dynamometer controls. Test point deviations of speed and torque from a test of B80 on May 25th, 2011 show minimal deviations between the

test point and actual values with a maximum deviation of 0.55% (Table 4-5). Comparing test point data from the same test on May 12th, 2011, the deviation of actual speed and torque values between the two tests are less than 1% (Table 4-6). Performing the same test on different days and obtaining data with less than 2% deviation would prove the accuracy and repeatability of the measurements and the test method. This test of repeatability was performed on numerous occasions with minimal deviations for most measurements (Table 4-7, Table 4-8, and Table 4-9). Deviations for CO and UHC between tests of B80 on May 12th and May 25th are much higher than acceptable (Table 4-10). The deviations are larger at low speeds and could represent unstable combustion at low speeds. Further comparison of CO and UHC measurements for tests of B2, B20, B40, and B80 performed on different days shows no clear deviation trend (Table 4-11). The large deviations are most likely due to combustion instabilities or measurement errors. Uncertainty of the measurements made by the emissions analyzers are known to be 2% of the measurement range. The CO and UHC measurement ranges are 5000 ppm and 3000 ppm, respectively. The result is a measurement uncertainty of 100 ppm for CO and 60 ppm for UHC. With exception to the first two test points, the known measurement uncertainty is greater than the measurement deviation.

Table 4-5: Test Point Deviations of Speed and Torque from B80 Test May 25, 2011

Test Point	Set Speed (rpm)	Set Torque (ft-lb)	Actual Speed (rpm)	Actual Torque (ft-lb)	Speed Deviation (%)	Torque Deviation (%)
1	2000	12	2002.25	11.93	0.11	0.55
2	2100	12	2100.09	11.97	0.00	0.22
3	2200	12	2205.33	11.97	0.24	0.23
4	2300	12	2298.07	12.01	0.08	0.10
5	2400	12	2398.47	12.00	0.06	0.02
6	2500	12	2503.69	12.00	0.15	0.04
7	2600	12	2603.24	12.02	0.12	0.16
8	2700	12	2703.82	12.02	0.14	0.13
9	2800	12	2808.08	12.06	0.29	0.49
10	2900	12	2898.90	12.03	0.04	0.25
11	3000	12	2999.69	11.99	0.01	0.04

Table 4-6: Speed and Torque Deviations of B80 Tests on 5-12 and 5-25

Test Point	B80 5-12 Actual Speed (rpm)	B80 5-12 Actual Torque (ft-lb)	B80 5-25 Actual Speed (rpm)	B80 5-25 Actual Torque (ft-lb)	Speed Deviation (%)	Torque Deviation (%)
1	2013.62	12.00	2002.25	11.93	0.56	0.58
2	2101.55	11.97	2100.09	11.97	0.07	0.06
3	2203.11	12.03	2205.33	11.97	0.10	0.49
4	2299.92	12.04	2298.07	12.01	0.08	0.27
5	2399.63	12.04	2398.47	12.00	0.05	0.35
6	2498.69	12.03	2503.69	12.00	0.20	0.24
7	2597.70	12.04	2603.24	12.02	0.21	0.17
8	2698.88	12.05	2703.82	12.02	0.18	0.31
9	2795.41	11.98	2808.08	12.06	0.45	0.64
10	2896.63	11.99	2898.90	12.03	0.08	0.35
11	3001.13	11.96	2999.69	11.99	0.05	0.28

Table 4-7: Deviation of Airflow and BSFC: B80 Testing on 5-12 and 5-25

Test Point	B80 5-12 Airflow (cfm)	B80 5-12 BSFC (g/kW-hr)	B80 5-25 Airflow (cfm)	B80 5-25 BSFC (g/kW-hr)	Airflow Deviation (%)	BSFC Deviation (%)
1	12.18	269.35	12.19	272.35	0.06	1.11
2	12.64	268.33	12.69	271.24	0.37	1.09
3	13.16	268.77	13.21	269.20	0.39	0.16
4	13.64	268.48	13.69	269.74	0.35	0.47
5	14.32	269.32	14.36	269.91	0.26	0.22
6	14.90	269.56	14.97	269.11	0.47	0.17
7	15.46	270.50	15.50	268.78	0.24	0.64
8	16.32	272.82	16.37	273.16	0.32	0.12
9	16.87	278.58	16.91	278.80	0.27	0.08
10	17.23	282.56	17.29	283.06	0.36	0.18
11	17.84	286.52	17.90	287.27	0.32	0.26

Table 4-8: Deviation of Thermal Efficiency and NO_x: B80 Testing on 5-12 and 5-25

Test Point	B80 5-12 Thermal Efficiency (%)	B80 5-12 NO _x (ppm)	B80 5-25 Thermal Efficiency (%)	B80 5-25 NO _x (ppm)	Thermal Efficiency Deviation (%)	NO _x Deviation (%)
1	34.64	508.80	34.26	528.20	1.10	3.81
2	34.77	496.20	34.40	512.10	1.08	3.20
3	34.71	489.10	34.66	495.20	0.16	1.25
4	34.75	466.10	34.59	471.40	0.47	1.14
5	34.64	451.10	34.57	446.65	0.22	0.99
6	34.61	439.30	34.67	426.65	0.17	2.88
7	34.49	426.50	34.71	413.15	0.64	3.13
8	34.20	411.20	34.15	398.75	0.12	3.03
9	33.49	394.40	33.46	386.45	0.08	2.02
10	33.02	381.45	32.96	374.45	0.18	1.84
11	32.56	365.75	32.48	355.05	0.26	2.93

Table 4-9: Deviation of Oxygen and Carbon Dioxide: B80 Testing on 5-12 and 5-25

Test Point	B80 5-12 O2 (%)	B80 5-12 CO2 (%)	B80 5-25 O2 (%)	B80 5-25 CO2 (%)	O2 Deviation (%)	CO2 Deviation (%)
1	12.82	6.08	12.88	6.09	0.44	0.13
2	12.88	6.04	12.84	6.13	0.32	1.41
3	12.87	6.06	12.95	6.05	0.65	0.17
4	12.95	5.99	13.01	6.00	0.49	0.30
5	13.07	5.91	13.08	5.95	0.11	0.71
6	13.14	5.86	13.11	5.93	0.24	1.23
7	13.21	5.82	13.21	5.87	0.01	0.86
8	13.04	5.94	13.10	5.96	0.39	0.30
9	12.93	6.02	12.98	6.04	0.38	0.27
10	13.04	5.94	13.03	6.00	0.12	1.04
11	13.08	5.91	13.09	5.96	0.05	0.74

Table 4-10: Deviation of UHC and CO: B80 Testing on 5-12 and 5-25

Test Point	B80 5-12 UHC (ppm)	B80 5-12 CO (ppm)	B80 5-25 UHC (ppm)	B80 5-25 CO (ppm)	UHC Deviation (%)	CO Deviation (%)
1	386.16	569.25	312.24	515.75	19.14	9.40
2	394.80	525.75	314.16	494.75	20.43	5.90
3	367.08	464.25	327.36	481.00	10.82	3.61
4	395.88	515.75	338.16	484.25	14.58	6.11
5	366.96	493.75	348.00	511.25	5.17	3.54
6	379.56	494.75	346.44	507.75	8.73	2.63
7	360.36	452.75	313.44	456.25	13.02	0.77
8	334.56	427.25	294.72	418.75	11.91	1.99
9	330.60	432.75	305.40	431.25	7.62	0.35
10	292.92	394.75	288.60	400.75	1.47	1.52
11	285.00	379.25	282.72	393.75	0.80	3.82

Table 4-11: Deviations of Carbon Monoxide (CO) and Unburned Hydrocarbons (UHC) Measurements Between Tests of B2, B20, B40, and B80.

CO Test Deviations (%)				
Test Point	Fuel Blend			
	B2	B20	B40	B80
1	16.55	1.96	8.34	9.40
2	1.73	3.52	5.18	5.90
3	1.66	4.41	3.17	3.61
4	3.71	2.43	4.14	6.11
5		2.89	2.12	3.54
6	2.04	5.61	2.23	2.63
7		4.44	3.01	0.77
8	6.96	0.52	3.68	1.99
9		0.88	0.57	0.35
10		0.99	3.86	1.52
11		2.74	3.50	3.82

UHC Test Deviations (%)				
Test Point	Fuel Blend			
	B2	B20	B40	B80
1	6.79	6.57	18.11	19.14
2	0.85	0.12	18.39	20.43
3	5.58	6.32	19.47	10.82
4	9.20	9.77	17.00	14.58
5		6.96	15.63	5.17
6	6.47	8.76	12.32	8.73
7		2.46	23.42	13.02
8	11.66	2.49	29.19	11.91
9		5.72	24.14	7.62
10		4.85	18.96	1.47
11		10.28	22.65	0.80

CHAPTER 5 EXPERIMENTAL RESULTS

This chapter will present the experimental results of the testing discussed in Chapter 4. Experimentally obtained fuel properties and experimental methods will be presented first followed by the experimental emissions and performance data from the dynamometer testing. Important calculations from this data are then discussed and results presented. Validity and repeatability of experimental data is discussed in Chapter 4.

5.1 Fuel Properties

The Biodiesel (NEXSOL BD-0100) obtained for testing was purchased from Peter Cremer North America, LP [30]. From the data sheet provided with the fuel (Figure 5-1), the Cetane and Kinematic Viscosity are known to be 48 and 4.0 mm²/second respectively. It should be noted that this biodiesel meets ASTM D 6751-09 and EPA 4627 specifications.

NEXSOL BD-0100 Biodiesel

ASTM D 6751-09 (EPA 4627)

Lot #: PN027410202

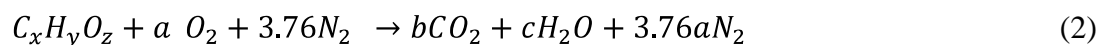
Property	ASTM Method	Limits	Results
Flash Point	D93	93° C min	173°C
Water & Sediment	D2709	0.050 % vol. max	0.000
Kinematic Viscosity, 40° C	D445	1.9-6.0 mm ² /sec.	4.0
Sulfated Ash	D874	0.020 % mass max	0.000
Sulfur	D5453	15ppm max	0
Copper Strip Corrosion	D130	No. 3 max	1a
Cetane	D613 / D6890	47 min.	48
Cloud Point	D2500	Report to customer	0°C
Carbon Residue, 100% sample	D4530	0.050 % mass max	0.000
Acid Number	D664	0.50 mg KOH/gm max	0.14
Free Glycerin	D6584	0.020 % mass max	0.016
Monoglycerides	D6584	0.8% (m/m) max	0.029
Diglycerides	D6584	0.2% (m/m) max	0.003
Triglycerides	D6584	0.2% (m/m) max	0.091
Total Glycerin	D6584	0.240 % mass max	0.213
Phosphorus Content	D4951	0.001 % mass max	0.000
Distillation temp., atmospheric equiv. temp., 90% recovered	D1160	360 °C max	354° C
Sodium & Potassium Metals	EN 14538	Sppm max combined	1.2
Calcium & Magnesium Metals	EN 14538	Sppm max combined	0.0
Oxidation Stability	EN 14112	3 hours minimum	7
Visual Inspection	D 4176 (#2)	2 maximum	1
Cold Soak Filtration	D6751 Appendix	360 seconds max ¹	97
Water Content by Karl Fisher	D6304	500ppm	372

¹ B100 (or B99.9) intended for blending into diesel fuel that is expected to give satisfactory vehicle performance at fuel temperatures at or below -12°C shall comply with a cold soak filterability limit of 200 seconds maximum.

Figure 5-1: Biodiesel property sheet (adapted from [30]).

Other characteristics of the fuel such as chemical composition and energy content were not provided and needed to be determined. Analysis of the biodiesel was performed by Huan Luong from the Environmental Engineering and Science Lab. Results from the fuel composition analysis show large percentages of Linoleic Acid (70.7%), Palmitic Acid (20.5%), and Stearic Acid (8.7%). The chemical formula for Linoleic Acid, Palmitic

Acid, and Stearic Acid are ($C_{18}H_{32}O_2$), ($C_{16}H_{32}O_2$), and ($C_{18}H_{36}O_2$), respectively [31]. Referring to Table 2-1, the Biodiesel obtained is believed to be derived from a blend of soybean oil and beef tallow. The exact source of the oil is not known and unimportant providing the chemical and physical properties of the fuel are known. Energy content for each fuel blend was determined using a Bomb Calorimeter. The process involved igniting a known mass of fuel and measuring the resulting temperature increase. The water produced from combusting the fuel is condensed during the process so the calculated energy content is known as the gross heating value. For internal combustion engines the water formed during combustion remains as a vapor. The energy associated with the phase change of vapor condensing to a liquid is lost. For this reason, the relevant energy content is known as the Lower Heating Value (LHV). LHV is calculated from the net heating value by subtracting the energy of vaporization of water. Energy of vaporization is found using the enthalpy of vaporization and the mass of water produced during combustion. The mass of water produced is directly related to the fuel chemistry and can be found by balancing the basic equation for combustion:



$$\text{Carbon Balance:} \quad x = b \quad \rightarrow \quad b = x \quad (3)$$

$$\text{Hydrogen Balance:} \quad y = 2c \quad \rightarrow \quad c = y/2 \quad (4)$$

$$\text{Oxygen Balance:} \quad z + 2a = 2b + c \quad \rightarrow \quad a = x + y/4 - z/2 \quad (5)$$

For every one mole of fuel combusted, c moles of water are produced. From a hydrogen balance, we see the molar value of water produced is equal to half the number of hydrogen atoms in the fuel. The chemical composition of standard diesel and biodiesel varies with the source of the oil used to produce the fuel. To complete the energy analysis, some fuel chemistry assumptions were made. The chemical formula for Linoleic Acid ($C_{18}H_{32}O_2$) was used to represent the fuel because it represents the major component of biodiesel and the other components have very similar chemical formulas. Using fuel properties from Heywood [3], the chemical equation for standard diesel is assumed to be $C_{12.3}H_{22.1}$. The chemical composition and molecular weight for standard diesel, biodiesel, and blends are shown in Table 5-1.

Table 5-1: Fuel Blend Chemical Composition

Fuel:	B0	B2	B20	B40	B60	B80	B100
Carbon Atoms	12.300	12.414	13.440	14.580	15.720	16.860	18.000
Hydrogen Atoms	22.100	22.298	24.080	26.060	28.040	30.020	32.000
Oxygen Atoms	0.000	0.040	0.400	0.800	1.200	1.600	2.000
Molecular Weight	170.011	172.220	192.099	214.187	236.275	258.363	280.451

With the number of hydrogen atoms known for each fuel, the amount of water produced for each mole of fuel burned can be found. For stoichiometric combustion, 1 mole of B100 produces 16 moles of water. The measured mass of each fuel used in the bomb calorimeter and the calculated molecular weight of each fuel is then used to find the number of moles of fuel combusted in each test. For B100, 0.708 grams or 0.00252 moles

of fuel were combusted during the calorimeter test. The molar value of fuel combusted is found by dividing the mass of fuel by the molecular weight of the fuel. The molar value of water produced is found by multiplying the molar value of fuel burned by the molar value of water produced per mole of fuel. For B100, 0.04039 moles of water were produced. This equates to 0.728 grams of water by multiplying the molar value by the molecular weight of water. Heat of vaporization is then found by multiplying the mass of water formed in each test by the enthalpy of vaporization for water (2442.83 joules/gram). Results for heat of vaporization of water for each test are shown in Table 5-2. The lower heating value is found by subtracting the heat of vaporization of water from the net heating values obtained from the test. Experimental heating value data is shown in Table 5-3 and compared to theoretical values obtained from the National Biodiesel Board for biodiesel meeting the same standards [32]. As seen in Table 5-3, the difference between experimental and theoretical values of lower heating value for each fuel is less than 0.75%.

Table 5-2: Mass and Molar Values of Water and Fuel from Bomb Calorimeter Testing

Fuel:	B2	B20	B40	B60	B80	B100
Mass of fuel used (grams)	0.633	0.635	0.655	0.669	0.684	0.708
Moles Fuel	0.00368	0.00331	0.00306	0.00283	0.00265	0.00252
Moles H ₂ O per mole fuel	11.149	12.040	13.030	14.020	15.010	16.000
Moles H ₂ O	0.04098	0.03980	0.03985	0.03970	0.03974	0.04039
Mass H ₂ O (grams)	0.738	0.717	0.718	0.715	0.716	0.728
H ₂ O Heat of Vaporization (J)	1803.40	1751.50	1753.59	1746.99	1748.80	1777.59
H ₂ O Heat of Vap. (J/gram fuel)	2848.97	2758.27	2677.23	2611.35	2556.73	2510.72

Table 5-3: Experimental Net and Lower Heating Values for Biodiesel Blends

Fuel:	B2	B20	B40	B60	B80	B100
Net Heating Value (kJ/g)	45.2731	44.3107	43.2730	42.3225	41.1271	40.1355
H ₂ O Heat of Vap. (J/g fuel)	2848.97	2758.27	2677.23	2611.35	2556.73	2510.72
Experimental QLHV (kJ/g)	42.4242	41.5524	40.5958	39.7112	38.5704	37.6248
Theoretical QLHV (kJ/g)	42.3423	41.4382	40.4252	39.4264	38.4411	37.4692
% Difference	0.1930	0.2749	0.4202	0.7171	0.3352	0.4136

The kinematic viscosity of each fuel blend was tested using a calibrated Ubbelohde type viscometer. Results from the testing are shown in Table 5-4. Each blend was tested three times and the results averaged to minimize error. The experimental kinematic viscosity value for B100 (3.9863 mm²/sec) is very close to the value reported by the fuel supplier (4.0 mm²/sec).

Table 5-4: Kinematic Viscosity Test Results for Biodiesel Blends

Matt Tanner		Biodiesel Blend: Kinematic Viscosity Test Results			
Viscometer type: UBBELOHDE		Test Date: June 9th 2011			
Viscometer ID: E955		Test Location: Dana 244			
Viscometer Size: 1		Water Bath Temp: 40 C			
Range: 2-10 mm ² /sec					
Viscometer Constant:		0.01039 mm ² /s ²			
Fuel Blend	Trial	Efflux Time (seconds)	Viscosity (mm ² /sec)	Average (mm ² /sec)	
B2	Trial 1	228.38	2.37287	2.38627	
	Trial 2	228.94	2.37869		
	Trial 3	231.69	2.40726		
B20	Trial 1	248.22	2.57901	2.57513	
	Trial 2	247.22	2.56862		
	Trial 3	248.1	2.57776		
B40	Trial 1	282.31	2.93320	2.89774	
	Trial 2	277.47	2.88291		
	Trial 3	276.91	2.87709		
B60	Trial 1	308.5	3.20532	3.20545	
	Trial 2	310.22	3.22319		
	Trial 3	306.82	3.18786		
B80	Trial 1	343.15	3.56533	3.58552	
	Trial 2	345.07	3.58528		
	Trial 3	347.06	3.60595		
B100	Trial 1	384.06	3.99038	3.98630	
	Trial 2	383.72	3.98685		
	Trial 3	383.22	3.98166		

5.2 Experimental Testing Data

This section presents the experimental testing measurement data for the test plan discussed in Chapter 4. Data for B2, B20, B40, B60, B80, and B100 test fuels are shown in Table 5-5, Table 5-6, Table 5-7, Table 5-8, Table 5-9, and Table 5-10, respectively. Each test was performed at a constant torque of 12 ft-lbs and engines speeds from 2000-3000 rpm in 100 rpm increments. Each table includes raw data measurements and fuelling and emissions data converted from raw data. Each test point represents data averaged over a five minute period. Calculations from this data are presented and discussed in Section 5.3.

Table 5-5: B2 Experimental Data

Test Fuel: B2 Date: 4/28/11 Weather: BP: 29.00 (inhg) DP: 59.6 F RH: 57%												
Test Point	Fueling (g/s)	Speed (RPM)	Torque (ft-lb)	Airflow (cfm)	Ex.Temp (C)	AirTemp (C)	Oil Temp (C)	O2 (vol %)	NOx (ppm)	CO2 (vol %)	UHC (ppm)	CO (ppm)
1	0.236	2002.1	12.02	12.18	351.48	23.12	70.42	12.53	525.17	6.12	650.40	757.08
2	0.245	2100.4	11.97	12.69	357.28	23.12	75.75	12.50	509.25	6.16	617.80	699.17
3	0.258	2199.5	12.07	13.21	362.69	23.37	78.28	12.46	503.83	6.19	611.70	625.83
4	0.270	2299.3	12.03	13.74	365.62	23.37	80.28	12.78	475.58	5.96	649.30	669.58
6	0.293	2507.1	11.96	14.98	376.34	23.68	80.68	12.88	441.79	5.90	691.40	638.75
8	0.324	2704.2	12.01	16.36	390.92	23.29	82.80	12.83	411.83	5.95	605.70	562.92
9	0.341	2799.9	11.97	16.88	404.66	23.55	84.16	12.66	394.58	6.08	568.10	546.67
10	0.359	2907.4	11.99	17.33	416.92	23.99	85.65	12.63	379.25	6.10	480.30	495.00
11	0.378	3004.2	12.01	17.93	430.85	24.26	87.34	12.59	356.17	6.12	441.80	502.50

Table 5-6: B20 Experimental Data

Test Fuel: B20 Date: 5/5/11 Weather: BP: 29.52 (inhg) DP: 41.4 F RH: 38.5%												
Test Point	Fueling (g/s)	Speed (RPM)	Torque (ft-lb)	Airflow (cfm)	Ex.Temp (C)	AirTemp (C)	Oil Temp (C)	O2 (vol %)	NOx (ppm)	CO2 (vol %)	UHC (ppm)	CO (ppm)
1	0.236	2005.5	11.97	12.08	337.37	19.36	57.75	12.94	558.83	5.82	509.90	580.42
2	0.246	2109.2	11.96	12.58	343.42	19.34	64.50	12.86	544.42	5.88	513.00	524.58
3	0.258	2205.6	11.97	13.00	348.42	19.57	68.38	12.91	528.67	5.84	485.20	521.25
4	0.270	2302.6	12.00	13.59	353.18	19.44	69.66	12.99	502.00	5.78	492.90	544.17
5	0.289	2422.2	12.17	14.35	362.90	19.55	71.12	13.01	477.42	5.77	519.30	547.92
6	0.291	2497.1	11.96	14.87	361.52	19.63	72.11	13.22	470.67	5.62	532.60	521.25
7	0.309	2605.5	12.03	15.47	368.79	19.85	73.40	13.21	448.92	5.63	476.70	490.00
8	0.325	2697.5	12.05	16.29	377.86	19.91	74.84	12.97	433.75	5.80	445.20	481.25
9	0.344	2798.0	11.99	16.85	392.49	20.12	77.54	12.88	414.58	5.86	433.50	487.50
10	0.362	2894.6	12.00	17.12	403.64	20.26	78.66	12.97	401.50	5.79	397.70	465.83
11	0.380	3006.5	12.04	17.83	415.00	20.61	79.11	12.93	379.00	5.82	425.20	499.58

Table 5-7: B40 Experimental Data

Test Fuel: B40 Date: 5/20/11 Weather: BP: 29.39 (inhg) DP: 57.8 F RH: 63%												
Test Point	Fueling (g/s)	Speed (RPM)	Torque (ft-lb)	Airflow (cfm)	Ex.Temp (C)	AirTemp (C)	Oil Temp (C)	O2 (vol %)	NOx (ppm)	CO2 (vol %)	UHC (ppm)	CO (ppm)
1	0.249	1997.1	11.96	12.08	341.23	20.92	61.29	12.85	526.50	6.03	404.10	580.42
2	0.259	2102.2	12.04	12.61	349.14	20.97	66.87	12.74	505.33	6.09	397.30	545.00
3	0.268	2200.2	11.99	13.07	351.51	20.93	70.46	12.83	489.42	6.04	382.70	491.67
4	0.281	2304.7	12.04	13.60	357.08	20.95	71.71	12.93	466.13	5.95	376.40	528.75
5	0.292	2408.1	11.99	14.28	362.13	21.01	72.84	13.02	441.08	5.89	397.20	526.67
6	0.303	2502.9	12.02	14.87	368.24	21.08	73.19	13.04	427.50	5.89	391.30	508.33
7	0.317	2596.7	12.01	15.39	372.76	20.97	73.82	13.20	410.58	5.78	503.10	478.75
8	0.332	2701.7	12.00	16.26	379.19	21.05	74.55	13.11	398.67	5.86	482.90	455.42
9	0.348	2790.5	11.94	16.78	390.04	20.96	77.28	12.98	384.58	5.95	455.40	441.25
10	0.371	2909.1	12.00	17.16	403.10	21.13	78.70	13.01	365.33	5.93	408.70	405.00
11	0.386	2990.3	12.03	17.71	413.36	21.31	79.92	13.04	349.33	5.91	405.20	404.58

Table 5-8: B60 Experimental Data

Test Fuel: B60 Date: 5/6/11 Weather: BP: 29.37 (inhg) DP: 39.6 F RH: 33.6%												
Test Point	Fueling (g/s)	Speed (RPM)	Torque (ft-lb)	Airflow (cfm)	Ex.Temp (C)	AirTemp (C)	Oil Temp (C)	O2 (vol %)	NOx (ppm)	CO2 (vol %)	UHC (ppm)	CO (ppm)
1	0.255	2003.4	11.99	12.10	341.66	20.66	60.59	12.91	535.75	5.93	414.12	624.75
2	0.265	2099.5	11.99	12.59	347.63	20.69	65.88	12.88	516.35	5.96	441.48	605.25
3	0.276	2205.2	11.99	13.08	351.16	20.63	69.11	12.98	504.10	5.89	408.36	532.25
4	0.287	2296.7	12.00	13.60	355.33	20.72	71.19	13.06	481.50	5.83	411.36	535.25
5	0.302	2402.5	12.06	14.29	363.21	20.73	72.38	13.13	462.20	5.78	441.72	532.75
6	0.312	2493.7	12.04	14.89	367.93	20.90	73.22	13.17	452.00	5.75	426.48	521.25
7	0.326	2601.8	11.97	15.46	371.46	20.98	75.17	13.29	440.10	5.67	383.16	462.25
8	0.343	2695.2	12.04	16.31	379.15	21.00	76.49	13.08	428.00	5.82	348.00	426.25
9	0.363	2801.9	12.03	16.83	392.87	21.35	78.95	13.06	414.40	5.85	343.56	426.25
10	0.378	2903.1	11.95	17.14	401.43	21.45	79.62	13.18	402.30	5.75	300.84	386.25
11	0.395	2999.8	11.98	17.82	410.57	21.53	80.40	13.12	382.40	5.80	308.64	396.25

Table 5-9: B80 Experimental Data

Test Fuel: B80 Date: 5/12/11 Weather: BP: 29.43 (inhg) DP: 53.2 F RH: 46.9%												
Test Point	Fueling (g/s)	Speed (RPM)	Torque (ft-lb)	Airflow (cfm)	Ex.Temp (C)	AirTemp (C)	Oil Temp (C)	O2 (vol %)	NOx (ppm)	CO2 (vol %)	UHC (ppm)	CO (ppm)
1	0.257	2013.6	12.00	12.18	341.63	21.80	63.18	12.82	508.80	6.08	386.16	569.25
2	0.266	2101.5	11.97	12.64	346.95	21.92	68.17	12.88	496.20	6.04	394.80	525.75
3	0.281	2203.1	12.03	13.16	352.43	21.92	71.37	12.87	489.10	6.06	367.08	464.25
4	0.293	2299.9	12.04	13.64	357.66	21.95	73.08	12.95	466.10	5.99	395.88	515.75
5	0.307	2399.6	12.04	14.32	363.88	22.19	73.67	13.07	451.10	5.91	366.96	493.75
6	0.320	2498.7	12.03	14.90	368.45	22.29	74.37	13.14	439.30	5.86	379.56	494.75
7	0.334	2597.7	12.04	15.46	373.98	22.64	75.99	13.21	426.50	5.82	360.36	452.75
8	0.350	2698.9	12.05	16.32	381.81	22.98	78.04	13.04	411.20	5.94	334.56	427.25
9	0.368	2795.4	11.98	16.87	394.33	23.11	80.07	12.93	394.40	6.02	330.60	432.75
10	0.387	2896.6	11.99	17.23	405.49	23.23	81.16	13.04	381.45	5.94	292.92	394.75
11	0.406	3001.1	11.96	17.84	413.83	23.34	82.41	13.08	365.75	5.91	285.00	379.25

Table 5-10: B100 Experimental Data

Test Fuel: B100 Date: 5/13/11 Weather: BP: 29.34 (inhg) DP: 51.7 F RH: 49.6%												
Test Point	Fueling (g/s)	Speed (RPM)	Torque (ft-lb)	Airflow (cfm)	Ex.Temp (C)	AirTemp (C)	Oil Temp (C)	O2 (vol %)	NOx (ppm)	CO2 (vol %)	UHC (ppm)	CO (ppm)
1	0.265	2002.2	11.96	12.14	341.02	21.22	61.20	12.92	533.50	6.04	389.10	586.25
2	0.277	2105.1	11.99	12.61	349.27	20.98	68.06	12.95	512.67	6.02	392.00	592.08
3	0.287	2197.5	12.02	13.06	353.79	21.16	71.76	12.94	494.42	6.03	373.50	530.00
4	0.302	2303.2	12.01	13.64	357.52	20.94	73.11	13.08	472.00	5.95	372.50	526.04
5	0.317	2398.4	12.01	14.25	363.79	20.94	73.79	13.10	448.17	5.93	379.60	538.75
6	0.332	2501.0	12.06	14.87	369.74	21.03	74.48	13.16	438.25	5.89	364.90	513.75
7	0.343	2599.7	12.03	15.41	373.43	21.14	76.12	13.29	425.42	5.79	335.40	469.58
8	0.359	2705.4	12.00	16.27	379.67	21.22	77.06	13.15	411.50	5.89	314.30	432.50
9	0.385	2804.0	12.05	16.79	393.44	21.00	79.18	13.04	396.25	5.96	291.50	408.75
10	0.401	2897.7	12.03	17.07	402.11	21.03	80.65	13.10	385.00	5.90	268.00	371.25
11	0.416	2995.0	11.93	17.69	409.31	21.19	81.08	13.18	364.96	5.84	273.10	373.75

5.3 Calculated Data

The experimental measurements presented in Section 5.2 were used to calculate the following engine performance parameters: power, Brake Mean Effective Pressure (BMEP), Brake Specific Fuel Consumption (BSFC), thermal efficiency, air mass flow rate, air fuel ratio, corrected NO_x, energy lost to exhaust, and heat rejection. The importance of each calculation is discussed and justified, and results for each are presented.

5.3.1 Power

Power produced by the engine is a function of torque and speed. The desired speed and torque at each test point remain constant so comparisons of power between tests are pointless. However, power is used in the calculations of BMEP, specific fuel

consumption and thermal efficiency, so it does need to be calculated. Because torque measurements are made in units of foot pounds, power is first calculated in units of horsepower and then converted to kilowatts. Calculated power results are shown in Table 5-11 and Table 5-12.

$$\text{Power HP} = \frac{\text{Engine Speed rpm} * \text{Torque (ft}\cdot\text{lb)}}{5252} \quad (6)$$

$$\text{Power kilowatts} = \text{Power(HP)} \times 0.7457 \quad (7)$$

Table 5-11: Calculated Power Values (Horsepower)

Test Point	Calculated Power (HP)					
	B2	B20	B40	B60	B80	B100
1	4.58	4.57	4.55	4.58	4.60	4.56
2	4.79	4.80	4.82	4.79	4.79	4.81
3	5.05	5.03	5.02	5.04	5.05	5.03
4	5.27	5.26	5.28	5.25	5.27	5.27
5		5.61	5.50	5.52	5.50	5.49
6	5.71	5.69	5.73	5.72	5.73	5.74
7		5.97	5.94	5.93	5.95	5.95
8	6.18	6.19	6.17	6.18	6.19	6.18
9	6.38	6.39	6.35	6.42	6.38	6.43
10	6.64	6.61	6.65	6.60	6.61	6.64
11	6.87	6.89	6.85	6.84	6.84	6.80

Table 5-12: Calculated Power Values (kilowatts)

Test Point	Calculated Power (kW)					
	B2	B20	B40	B60	B80	B100
1	3.42	3.41	3.39	3.41	3.43	3.40
2	3.57	3.58	3.59	3.57	3.57	3.58
3	3.77	3.75	3.75	3.76	3.76	3.75
4	3.93	3.92	3.94	3.91	3.93	3.93
5		4.19	4.10	4.11	4.10	4.09
6	4.26	4.24	4.27	4.26	4.27	4.28
7		4.45	4.43	4.42	4.44	4.44
8	4.61	4.62	4.60	4.61	4.62	4.61
9	4.76	4.76	4.73	4.79	4.76	4.80
10	4.95	4.93	4.96	4.92	4.93	4.95
11	5.12	5.14	5.11	5.10	5.10	5.07

5.3.2 Brake Mean Effective Pressure (BMEP)

BMEP is used to make relative performance comparisons between engines of different sizes and is a function of torque and engine displacement. According to Heywood, maximum BMEP values are constant for most engine sizes and BMEP can be used to evaluate the effectiveness of the displaced volume of an engine. For naturally aspirated diesel engines, meeting maximum BMEP values of 700-900 kPa confirms a good engine design [2]. Calculated BMEP data for each test is shown in Table 5-13. BMEP results are discussed in Section 6.2.1.

$$BMEP \text{ kPa} = \frac{\text{Power kW} * n_R * 1000}{\text{Volume dm}^3 * \text{Engine Speed (rev/sec)}} \quad (8)$$

where, $n_R = \text{Revolutions per power stroke} \quad n_R = 2$
 $\text{Yanmar Displacement Volume} = 0.418 \text{ dm}^3$

Table 5-13: Calculated BMEP Values (kPa)

Test Point	Calculated BMEP (kPa)					
	B2	B20	B40	B60	B80	B100
1	490.11	488.10	487.51	488.89	489.28	487.60
2	488.00	487.39	490.84	488.54	487.75	488.80
3	491.79	487.80	488.89	488.85	490.40	490.14
4	490.32	488.94	490.77	489.18	490.95	489.38
5		496.14	488.55	491.48	490.94	489.61
6	487.40	487.50	490.13	490.82	490.52	491.71
7		490.41	489.40	487.74	490.75	490.24
8	489.55	491.31	489.13	490.64	491.26	489.13
9	487.88	488.83	486.83	490.56	488.37	491.25
10	488.68	489.08	489.24	486.92	488.67	490.44
11	489.59	490.61	490.40	488.30	487.57	486.39

5.3.3 Brake Specific Fuel Consumption

BSFC is a measure of how efficiently an engine uses the mass of fuel supplied to produce work [2]. This calculation is similar to the commonly used “miles per gallon” rating of automobiles. Because the test engine is stationary, power output is used instead of mileage. BSFC is a function of fuel mass flow and power output. According to Heywood, the best BSFC value for diesel engines is around 200 grams per kilowatt hour [2]. Calculated BSFC data for each test is shown in Table 5-14.

$$BSFC \frac{g}{kW \cdot hr} = \frac{\text{fuel mass flow rate}(g/hr)}{\text{Power}(kW)} \quad (9)$$

Table 5-14: Calculated BSFC Values (g/kW-hr)

Test Point	Calculated BSFC (g/kW-hr)					
	B2	B20	B40	B60	B80	B100
1	248.70	249.30	264.32	269.25	269.35	280.54
2	247.52	247.32	259.41	266.84	268.33	277.89
3	246.88	247.83	257.81	264.92	268.77	275.70
4	247.21	248.16	257.06	264.10	268.48	277.22
5		248.20	256.22	264.63	269.32	278.70
6	247.81	247.06	255.27	263.45	269.56	279.29
7		249.66	257.53	265.38	270.50	278.41
8	252.94	253.18	259.91	267.81	272.82	280.40
9	257.72	259.93	265.00	272.87	278.58	288.61
10	260.90	264.51	269.65	276.36	282.56	291.39
11	265.61	266.02	272.27	278.46	286.52	295.13

5.3.4 Thermal Efficiency

Thermal efficiency or fuel conversion efficiency is the measure of how well an engine converts energy contained in fuel to work. It is a unit less ratio of energy produced by the engine to the energy contained in the fuel supplied to the engine. The rate of energy supplied to the engine is found by multiplying the mass flow rate of fuel by the energy content or LHV of the fuel. The equation used for thermal efficiency (Heywood 2.24c) uses values of BSFC (Table 5-14) and the experimental lower heating value (Q_{LHV}) (Table 5-3). Calculated thermal efficiency values for each test are shown in Table 5-15.

$$\text{Thermal Efficiency (\%)} : \eta_f = \frac{3600}{BSFC \frac{g}{kW \cdot h} * Q_{LHV} \frac{MJ}{kg}} * 100\% \quad (10)$$

Table 5-15: Calculated Thermal Efficiency Values (%)

Test Point	Calculated Thermal Efficiency (%)					
	B2	B20	B40	B60	B80	B100
1	34.12	34.75	33.55	33.67	34.65	34.11
2	34.28	35.03	34.18	33.97	34.78	34.43
3	34.37	34.96	34.40	34.22	34.73	34.70
4	34.33	34.91	34.50	34.33	34.76	34.51
5		34.91	34.61	34.26	34.66	34.33
6	34.24	35.07	34.74	34.41	34.63	34.26
7		34.70	34.43	34.16	34.50	34.37
8	33.55	34.22	34.12	33.85	34.21	34.12
9	32.93	33.33	33.46	33.22	33.50	33.15
10	32.53	32.75	32.89	32.80	33.03	32.84
11	31.95	32.57	32.57	32.56	32.58	32.42

5.3.5 Air Mass Flow Rate

To determine the Air/Fuel ratio discussed in the next section, the mass flow rate of combustion air is needed. The Laminar Flow Element (LFE) is used to measure volumetric flow rate of combustion air. The mass flow rate of air is found by using the volumetric flow rate and the density of the air. Air density is a function of pressure and temperature, and is directly affected by ambient weather conditions. Because air is a mixture of dry air and water vapor, the density of dry air and the density of water vapor are added together to find the density of humid air [33]. Partial pressures of dry air and water vapor are calculated from the barometric pressure and the dew point temperature. Equations and examples for calculating partial pressures are included in Appendix F.

$$\text{Air Density } \frac{kg}{m^3} = \frac{P_d}{R_d * T} + \frac{P_v}{R_v * T} \quad (11)$$

where,

P_d = Partial pressure of dry air (Pa)

P_v = Partial pressure of water vapor (Pa)

R_d = Specific gas constant for dry air = 287.05 (J/(kg-K))

R_v = Specific gas constant for water vapor = 461.495 (J/(kg-K))

T = Temperature (K)

The desired unit for mass flow is grams per second. Because the volumetric flow of air has units of cubic feet per minute, converting air density to grams per cubic foot is necessary. Air density is calculated using the air temperature at each test point, values with units of grams per cubic foot are shown in Table 5-16.

$$\text{Air Density } \frac{kg}{m^3} * \frac{1000 \text{ grams}}{1 \text{ kg}} * \frac{1 \text{ meter}}{3.2808399 \text{ feet}}^3 = \text{Air Density } \frac{g}{ft^3} \quad (12)$$

Air mass flow rate is then calculated by multiplying air density and volumetric flow rate after converting the volumetric flow rate from cubic feet per minute to cubic feet per second. Calculated values of air mass flow rate are shown in Table 5-17.

$$\text{Air mass flow rate } \frac{g}{sec} = \text{Density } \frac{g}{ft^3} * \text{Vol. flow } \frac{ft^3}{minute} * \frac{1 \text{ minute}}{60 \text{ sec}} \quad (13)$$

Table 5-16: Calculated Air Density Values (g/ft³)

Test Point	Calculated Air Density (g/ft ³)					
	B2	B20	B40	B60	B80	B100
1	32.479	33.600	33.180	33.289	33.158	33.131
2	32.480	33.603	33.174	33.286	33.144	33.157
3	32.452	33.577	33.178	33.292	33.144	33.137
4	32.452	33.591	33.176	33.282	33.140	33.162
5		33.579	33.169	33.281	33.114	33.162
6	32.419	33.570	33.162	33.261	33.103	33.152
7		33.544	33.174	33.252	33.064	33.140
8	32.461	33.538	33.165	33.250	33.026	33.130
9	32.432	33.513	33.175	33.211	33.011	33.155
10	32.384	33.498	33.156	33.199	32.998	33.152
11	32.356	33.458	33.135	33.190	32.985	33.133

Table 5-17: Calculated Values of Air Mass Flow Rate (g/s)

Test Point	Calculated Air Mass Flow Rate (g/s)					
	B2	B20	B40	B60	B80	B100
1	6.595	6.765	6.680	6.714	6.732	6.705
2	6.872	7.047	6.970	6.983	6.984	6.969
3	7.147	7.275	7.225	7.256	7.272	7.210
4	7.432	7.610	7.517	7.546	7.533	7.538
5		8.033	7.892	7.928	7.903	7.878
6	8.093	8.319	8.219	8.253	8.221	8.214
7		8.650	8.507	8.569	8.520	8.510
8	8.849	9.107	8.986	9.036	8.981	8.985
9	9.126	9.413	9.276	9.318	9.281	9.279
10	9.352	9.556	9.481	9.482	9.475	9.431
11	9.669	9.942	9.778	9.855	9.809	9.771

5.3.6 Air/Fuel Ratio

Air/fuel ratio is defined as the air mass flow rate divided by the fuel mass flow rate. The ratio of mass flow rates is useful in analyzing combustion characteristics and defining operating conditions. Dividing each mass flow rate (units of g/s) results in a unit less

value of air fuel ratio. Heywood defines the range of air/fuel ratio for normal operating conditions of diesel engines from 18-70 [2]. Calculated values of air/fuel ratio are shown in Table 5-18.

Table 5-18: Calculated Values of Air/Fuel Ratio

Test Point	Calculated Air/Fuel Ratio					
	B2	B20	B40	B60	B80	B100
1	27.93	28.65	26.83	26.31	26.22	25.30
2	27.99	28.65	26.91	26.37	26.24	25.19
3	27.66	28.20	26.93	26.26	25.88	25.09
4	27.56	28.15	26.72	26.28	25.68	24.93
5		27.83	27.06	26.22	25.74	24.88
6	27.62	28.59	27.13	26.45	25.72	24.72
7		28.02	26.86	26.30	25.53	24.79
8	27.31	28.05	27.04	26.37	25.66	25.03
9	26.79	27.36	26.63	25.68	25.22	24.12
10	26.07	26.37	25.53	25.09	24.48	23.54
11	25.58	26.19	25.31	24.97	24.18	23.49

5.3.7 Corrected NO_x

NO_x is formed when atmospheric nitrogen and oxygen are exposed to the extremely high temperatures. The formation of NO_x is driven directly by the adiabatic flame temperature of combustion. Ambient air conditions affect the specific heat of combustion air and therefore the adiabatic flame temperature and the formation of NO_x. For this reason, NO_x emissions are impacted greatly by ambient air temperature, pressure, and humidity. Comparisons of NO_x emissions between tests performed in different ambient conditions are not valid unless corrected to standard conditions. The derivation for the NO_x

correction procedure for diesel engines was obtained from the Environmental Protection Agency's website [34]. The calculation of the NO_x correction factor with example calculations is given in Appendix G. The ambient weather conditions (Barometric pressure and dew point temperature) used to calculate the NO_x correction factor and the resulting calculated values are given in Table 5-19. Calculated values of corrected NO_x emissions are shown in Table 5-20.

Table 5-19: NO_x Correction Factors and Ambient Weather Conditions

	B2	B20	B40	B60	B80	B100
Barometric Pressure (inHg)	29.00	29.52	29.39	29.37	29.43	29.34
Dew Point (°F)	59.60	41.40	57.80	39.60	53.20	51.70
Calculated NO _x Corr. Factor	1.0099	0.9144	0.9943	0.9091	0.9657	0.9581

Table 5-20: Corrected NO_x Emissions (ppm)

Test Point	Corrected NO _x Emissions (ppm)					
	B2	B20	B40	B60	B80	B100
1	530.37	511.01	523.49	487.05	491.35	511.15
2	514.29	497.83	502.44	469.41	479.18	491.19
3	508.82	483.43	486.62	458.27	472.33	473.70
4	480.29	459.04	463.46	437.73	450.11	452.22
5		436.56	438.56	420.18	435.63	429.39
6	446.17	430.39	425.06	410.91	424.23	419.89
7		410.50	408.24	400.09	411.87	407.59
8	415.91	396.63	396.39	389.09	397.10	394.26
9	398.49	379.11	382.38	376.73	380.87	379.65
10	383.00	367.14	363.24	365.73	368.37	368.87
11	359.69	346.57	347.34	347.64	353.21	349.67

5.3.8 Exhaust Energy

Calculation of energy lost in the exhaust gas is necessary for determining the amount of heat transfer to the cylinder (heat rejection) and characteristics of combustion. To simplify the calculation, the exhaust gas products were assumed to be air at standard pressure. Specific heat values were interpolated from Turns [35] for air at the average temperature of the intake air and the exhaust gas. The energy lost to exhaust is then found by multiplying the mass flow rate of intake air by the specific heat and change in temperature between the intake and exhaust for each test point. The value was then divided by the energy supplied by the fuel to obtain the energy lost to exhaust as a percentage of the total energy supplied by the fuel (Table 5-21).

$$\text{Energy Lost to Exhaust } \% = 100 * \frac{\text{Mass Air Flow } \frac{\text{kg}}{\text{s}} * C_p \frac{\text{kJ}}{\text{kg}\cdot\text{K}} * \Delta T(\text{K})}{\text{Fuel Flow Rate } \frac{\text{kg}}{\text{s}} * \text{Fuel LHV } \left(\frac{\text{kJ}}{\text{g}}\right)} \quad (14)$$

Table 5-21: Calculated Values of Energy Lost to Exhaust Gas (% of total energy)

Test Point	Energy Lost to Exhaust (% of total)					
	B2	B20	B40	B60	B80	B100
1	22.05	22.35	21.57	21.68	22.16	21.92
2	22.50	22.78	22.19	22.14	22.55	22.42
3	22.58	22.76	22.37	22.29	22.62	22.63
4	22.70	23.07	22.58	22.60	22.81	22.76
5		23.49	23.21	23.09	23.29	23.15
6	23.46	24.02	23.70	23.61	23.57	23.40
7		24.04	23.79	23.71	23.77	23.71
8	24.21	24.70	24.39	24.31	24.41	24.37
9	24.65	25.10	24.77	24.58	24.84	24.44
10	24.76	24.93	24.61	24.58	24.85	24.42
11	25.16	25.48	25.06	25.07	25.09	24.83

5.3.9 Heat Rejection

Heat rejection refers to the combustion energy lost by heat transfer to the surfaces of the combustion chamber. An estimated value heat rejection can be found by subtracting the energy lost to exhaust and the usable energy produced by the engine from the total energy supplied by the fuel. The energy lost to heat transfer is only an estimated value because it includes frictional energy losses from the engine, driveshaft, speed reduction system, and the DC absorbing motor. For comparisons of the same test point, the frictional losses are constant and a change in heat transfer loss accurately represents a change in heat transfer loss. For different test points, especially as speed increases, the frictional losses are increased. As frictional losses are increased, the calculated value of heat transfer losses also increases. Although heat transfer rate does change with engine speed, comparisons at different set points should not be made. Calculated values of heat rejection are shown in Table 5-22.

Energy Lost to Heat Transfer % =

$$100 - \text{Exhaust Energy \%} - \text{Work}(\%) \quad (15)$$

Table 5-22: Energy Lost to Heat Rejection (% of total)

Test Point	Energy Lost to Heat Rejection (% of total)					
	B2	B20	B40	B60	B80	B100
1	43.83	42.90	44.87	44.65	43.19	43.97
2	43.22	42.19	43.62	43.89	42.67	43.15
3	43.04	42.28	43.23	43.49	42.65	42.66
4	42.97	42.02	42.92	43.07	42.43	42.72
5		41.61	42.18	42.65	42.06	42.52
6	42.29	40.91	41.56	41.98	41.80	42.34
7		41.26	41.78	42.13	41.73	41.92
8	42.24	41.08	41.49	41.84	41.38	41.50
9	42.43	41.57	41.76	42.19	41.65	42.41
10	42.72	42.32	42.51	42.62	42.11	42.75
11	42.89	41.95	42.37	42.37	42.34	42.75

CHAPTER 6 DISCUSSION AND CONCLUSION

This chapter will discuss the testing results, conclusions, and recommendations for future work. Testing results include fuel properties, engine performance parameters, and exhaust emissions from different blends of biodiesel. Data was plotted against the concentration of biodiesel with constant lines of speed for each test. Comparing the data against the concentration of biodiesel is helpful in separating the effects of biodiesel blending and engine speed. Trends in results are justified and the viability of biodiesel as an alternative to standard diesel fuel is assessed.

6.1 Discussion of Fuel Properties

Although similar chemically, standard diesel and biodiesel have some differences in chemical and physical properties. Chemically, biodiesel contains oxygen atoms, has lower energy content, and has a greater cetane number than standard diesel fuel. Oxygen atoms in the fuel promote better combustion by supplying oxygen to the localized fuel rich regions of the combustion chamber. The expected effect is more complete combustion and, as a result, less Carbon Monoxide (CO) and Unburned Hydrocarbon (UHC) emissions. The energy content of biodiesel is lower primarily because the fuel is already partially oxidized by the contained oxygen atoms. The expected effect of decreased energy content is increased fuel consumption on a mass and volume basis. Biodiesel has a greater cetane number than standard diesel, which means it will ignite

sooner, decreasing the ignition delay period between the start of injection and start of combustion, effectively advancing timing. Advanced timing means the combustion starts earlier and has more time to complete. The expected effect is increased efficiency, increased combustion temperatures, increased NO_x emissions, and decreased CO and UHC emissions. Physically, the biodiesel used in this study has a 67% greater kinematic viscosity than standard diesel. The increased kinematic viscosity is expected to negatively affect the spray pattern of the fuel when injected into the cylinder. The diameter of the fuel droplets is expected to increase and the spray is expected to have an increased penetration at a decreased angle.

6.2 Discussion of Engine Performance Parameters

This section will present plots and a discussion for the following engine performance parameters: Brake Mean Effective Pressure (BMEP), Brake Specific Fuel Consumption (BSFC), Thermal Efficiency, Air/Fuel ratio, and Heat losses. The calculations and calculated data are presented in Chapter 5.

6.2.1 Discussion of Brake Mean Effective Pressure Results

Comparing BMEP values presented in Table 6-1, the values are 30% lower than the range of values suggested by Heywood [2] to confirm a good engine design (700-900 kPa). The values necessary for good engine design correspond to maximum values of engine torque. The testing performed for this thesis represents the maximum continuous

torque at a range of speeds, which is 15% lower than the maximum rated torque. Justification of BMEP values is not critical for the testing performed but is necessary to validate the precision of the testing apparatus. More to the point, the BMEP values can be used to validate the repeatability of test points and thus the testing apparatus. The equation for BMEP can be reduced to a function of engine torque and engine displacement. Since the designed torque at each test point is set to 12 ft-lbs, the desired BMEP at each test point is 489.13 kPa for a 0.418 Liter engine. The average test point deviation of BMEP as a percentage of the desired value is 0.26% (Table 6-1). A BMEP deviation of 0.26% verifies the consistency and repeatability of the test method and apparatus, ensuring any variation in results is not due to variations in how the testing was performed.

Table 6-1: Deviation of Calculated BMEP Values

Test Point	Calculated BMEP (kPa)						Avg. Dev. (%)
	B2	B20	B40	B60	B80	B100	
1	490.11	488.10	487.51	488.89	489.28	487.60	0.19
2	488.00	487.39	490.84	488.54	487.75	488.80	0.24
3	491.79	487.80	488.89	488.85	490.40	490.14	0.23
4	490.32	488.94	490.77	489.18	490.95	489.38	0.17
5		496.14	488.55	491.48	490.94	489.61	0.50
6	487.40	487.50	490.13	490.82	490.52	491.71	0.34
7		490.41	489.40	487.74	490.75	490.24	0.23
8	489.55	491.31	489.13	490.64	491.26	489.13	0.21
9	487.88	488.83	486.83	490.56	488.37	491.25	0.28
10	488.68	489.08	489.24	486.92	488.67	490.44	0.16
11	489.59	490.61	490.40	488.30	487.57	486.39	0.28
						Average	0.26

6.2.2 Discussion of Brake Specific Fuel Consumption

Values of BSFC are plotted in Figure 6-1 and show a clear increase in BSFC for increased speeds and increased concentrations of biodiesel. As engine speed increases, frictional losses and pumping losses also increase. Consider the piston in the engine traveling up and down the cylinder, the piston rings are physically touching the cylinder wall and creating friction. Because of the friction between the two surfaces, each stroke of the piston requires some force to overcome the frictional forces. The piston is used as an example, but frictional losses occur at each moving part of the engine. As speed increases, the frictional losses over a period of time also increase. The same is true for pumping combustion air into the combustion chamber. Some energy is required to pump air into the engine. This is known as pumping loss and increases proportionally with the

volume of air being pumped. The volume of air pumped into the engine is directly controlled by the speed of the engine so increased speed results in increased pumping losses. To overcome increased frictional forces and pumping losses, more energy is required to achieve the desired speed and torque. Energy is added by increasing the amount of fuel injected. As speed increases more fuel is consumed to overcome frictional losses and brake specific fuel consumption is increased.

Also from the plot of BSFC (Figure 6-1), BSFC increases with increased biodiesel concentration. This trend is expected due to the lower energy content of biodiesel. BSFC relates the mass of fuel consumed to the power produced by the engine. Since biodiesel contains less energy on a volume and mass basis, more fuel must be injected to achieve the same power output. Comparing pure biodiesel (B100) to the standard fuel (B2), BSFC is increased by 12%. The increase is justified by the 11.3% decrease in energy content. How well the energy contained in the fuel is converted to work by the engine is discussed in the next section on thermal efficiency.

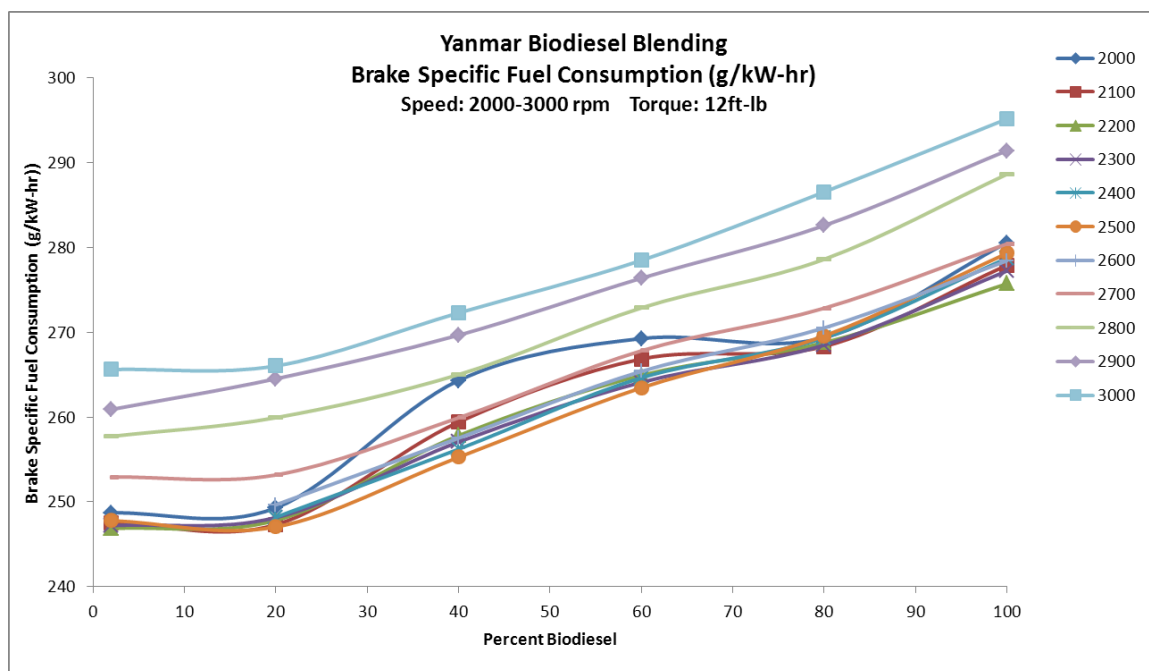


Figure 6-1: Yanmar Biodiesel Blending: Brake Specific Fuel Consumption Results

6.2.3 Discussion of Thermal Efficiency

Values of Thermal Efficiency are plotted in Figure 6-2 to show trends due to engine speed and biodiesel blending. Much like BSFC, thermal efficiency is greatly affected by engine speed. For each fuel, thermal efficiency results are similar at low speeds (up to 2500 rpm), and decrease significantly at high speeds (above 2500 rpm). The increased friction at greater speeds is likely responsible for decreased thermal efficiency. In general, the thermal efficiency at all speeds is increased for each biodiesel blend compared to the standard fuel.

Results at low speeds are unstable but the overall trend is increased efficiency from B2 to B20 and then gradually decreased thermal efficiency from B20 to B100. The cause of the instability is likely a result of poor atomization and mixing from low speed operation and increased biodiesel concentration. Biodiesel has greater kinematic viscosity (which hinders atomization) and increased cetane number (which effectively advances timing). As biodiesel concentration is increased, unstable combustion occurs at low speeds as a result of poor mixing or an effective timing that is too far advanced. The exact cause is difficult to isolate but both problems are resolved with increased engine speed, which effectively retards combustion timing and promotes better mixing.

At high speeds, where mixing issues are resolved, thermal efficiency gradually increases with the concentration of biodiesel up to B80 where it is increased by 1.8% compared to B2. From B80 to B100, thermal efficiency decreases slightly but remains 1.2% better than B2. The increased efficiency is likely a result of fuel properties such as oxygen content and increased cetane number which in theory effectively advances timing and allows more time for combustion to complete. A heat loss analysis presented in Section 6.2.5 provides supplemental information on the thermal efficiency effects of biodiesel. The small drop in efficiency from B80 to B100 could be from poor atomization caused by increased kinematic viscosity.

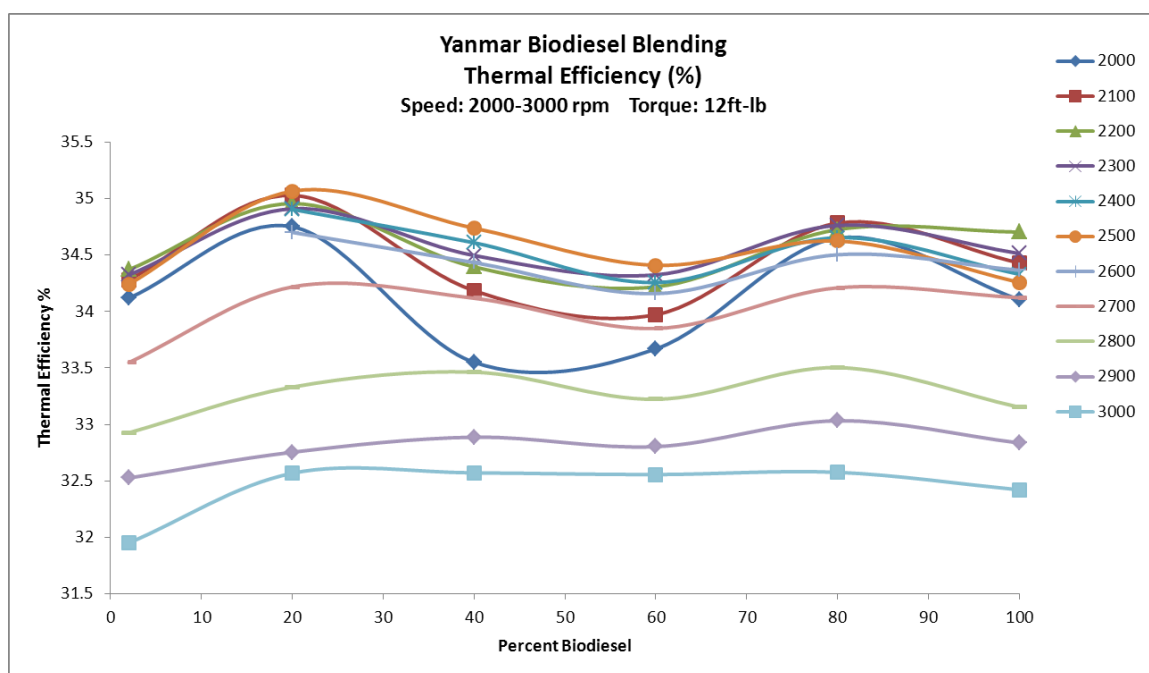


Figure 6-2: Yanmar Biodiesel Blending: Thermal Efficiency Results Plot

6.2.4 Discussion of Air/Fuel Ratio

Air/Fuel ratio is calculated from the mass flow rates of air and fuel, and plotted against speed in Figure 6-3. Because volumetric airflow is directly controlled by engine speed, the mass flow rate of air at a specific engine speed is constant with exception to small variations in air density due to ambient weather conditions. As speed is increased, the Air/Fuel ratio decreases because more fuel is required to overcome frictional losses as discussed in the previous section. Also, increased pumping losses at increased speeds decrease volumetric efficiency which is a parameter used to measure the effectiveness of

the induction process [2]. Volumetric efficiency compares the actual flow rate of air to the maximum possible flow rate of air (without losses) determined by the displacement volume and speed of the engine. Volumetric efficiency decreases with speed, contributing to decreased Air/Fuel ratio with increased speed.

Air/Fuel ratio also decreases with increasing biodiesel concentration because a greater mass of biodiesel is injected to achieve the same energy input. The increase in Air/Fuel ratio from standard fuel to B20 is explained by increased thermal efficiency with B20 and increased mass airflow rates due to ambient weather conditions (i.e. colder and thus more dense air) on the particular test date.

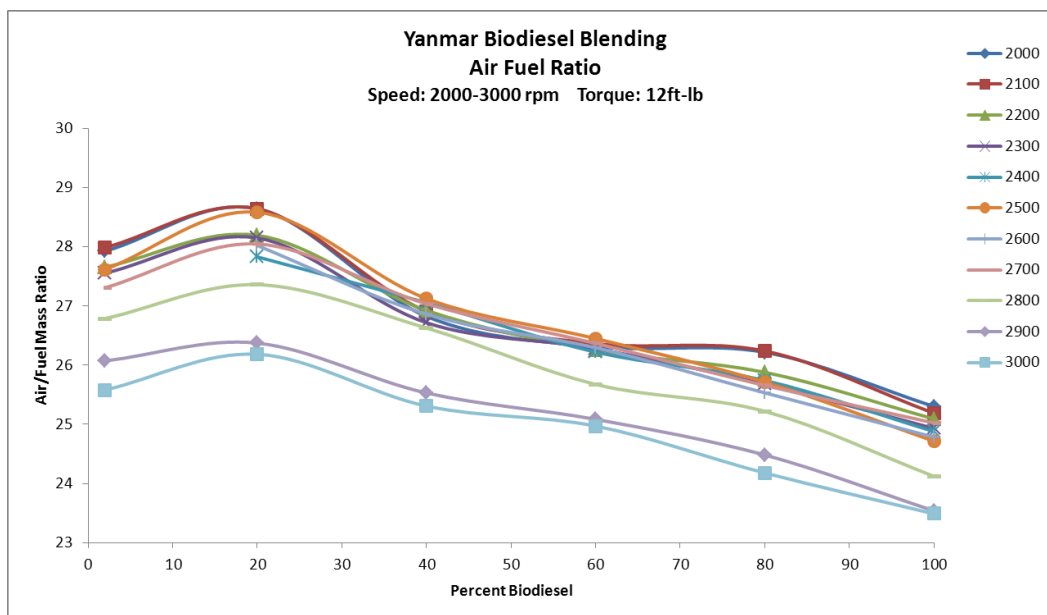


Figure 6-3: Yanmar Biodiesel Blending: Air/Fuel Ratio Results Plot

6.2.5 Discussion of Heat Losses

Heat losses include energy lost to exhaust gas and heat transfer to the combustion chamber (heat rejection). These heat losses are useful in characterizing the heat release for each fuel. From the plot of energy lost to exhaust (Figure 6-4) and the plot of heat rejection (Figure 6-5), increased engine speed correlates to increased energy lost to exhaust gas and decreased heat rejection. Increased speed effectively retards timing, decreasing peak cylinder temperatures and reducing the amount of time for heat to transfer to the engine. A later start of combustion, lower peak flame temperature, and less time for heat transfer all result in less heat rejection and increased exhaust energy.

Comparing B2 to B20, for each engine speed, the energy lost to exhaust increases and the heat rejection decreases, but the trend for increasing concentrations of biodiesel is not as clear. After discussing the heat loss data with Professor Indranil Brahma, it was determined that the variance in exhaust energy is much lower than the variance in heat rejection for each fuel blend compared to standard diesel [36]. The result is a decrease in heat rejection that is greater than the increase in exhaust energy meaning less total heat loss and increased efficiency. The decreased heat rejection is believed to be a result of a slower heat release rate and lower flame temperatures due to lower energy content with increasing biodiesel concentration [36]. Although flame temperature cannot be measured,

this claim is consistent with NO_x emissions results. As discussed in Section 6.3.4, NO_x emissions are a direct indicator of flame temperature.

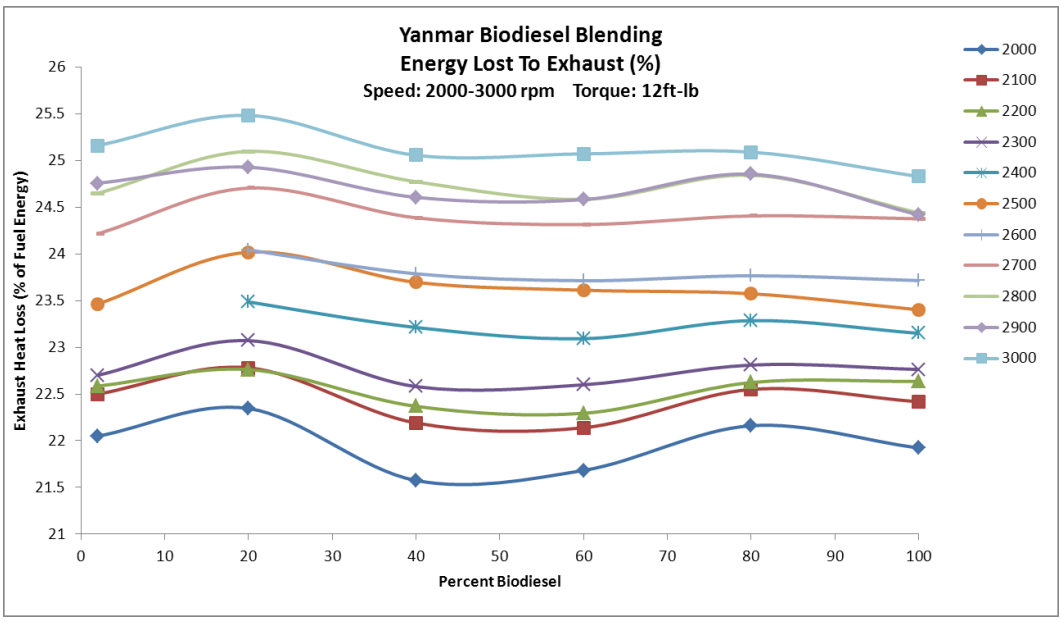


Figure 6-4: Yanmar Biodiesel Blending: Energy Lost to Exhaust

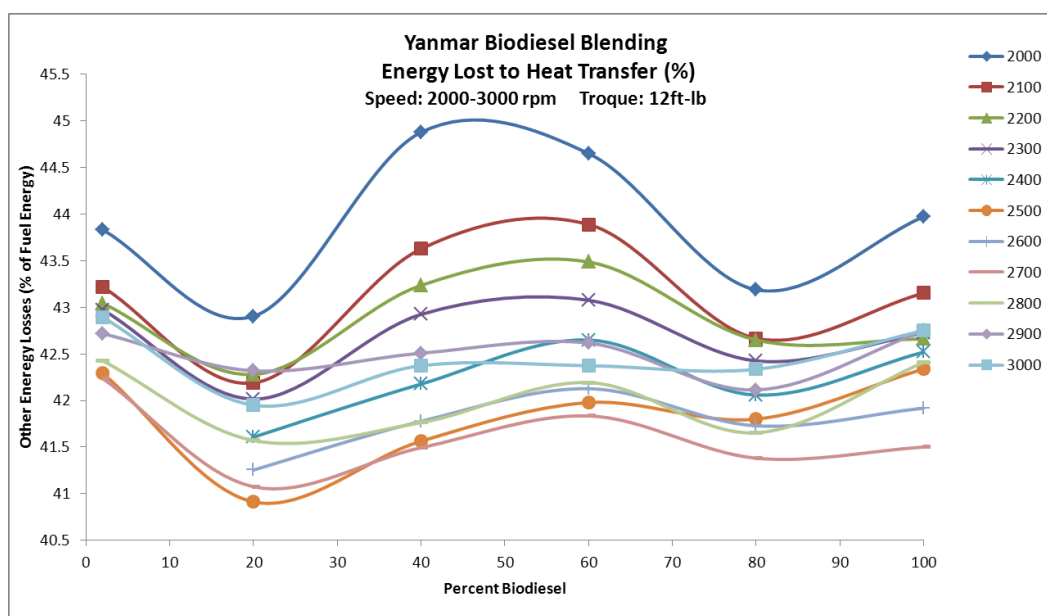


Figure 6-5: Yanmar Biodiesel Blending: Heat Rejection

6.3 Discussion of Emissions Results

The general trend in published testing results of emissions for biodiesel compared to standard diesel is a decrease in hydrocarbons, carbon monoxide, and carbon dioxide with a slight increase in NO_x. This section will present, discuss, and compare experimental results obtained with the published trends.

6.3.1 Discussion of Unburned Hydrocarbon Emissions

Comparing the UHC emissions data in Figure 6-6, a decrease is evident with increased concentrations of biodiesel and engine speed. Heywood [5] claims increased engine

speed promotes better mixing of air and fuel and reduces UHC emissions caused by under mixing of fuel. For each fuel, UHC emissions are decreased by approximately 30% from 2000 rpm to 3000 rpm. The large decrease of UHC from biodiesel is linked to fuel properties. Compared to standard diesel, biodiesel contains oxygen atoms and has an increased kinematic viscosity and cetane number. While the increased kinematic viscosity would have a negative effect on spray pattern and mixing, the effect is overcome by the positive effects of oxygen content and cetane number. Oxygen atoms contained in biodiesel suppress the effect of localized fuel rich zones in the combustion chamber. Increased cetane number means the fuel has a decreased ignition delay period. The effect is combustion starts earlier in the cycle and has more time to burn before being exhausted. The result of increased engine speed and increased concentration of biodiesel is a significant reduction in unburned hydrocarbon emissions. Comparing the measurements between B2 and B100, the average decrease of hydrocarbon emissions over the entire speed range is 43%.

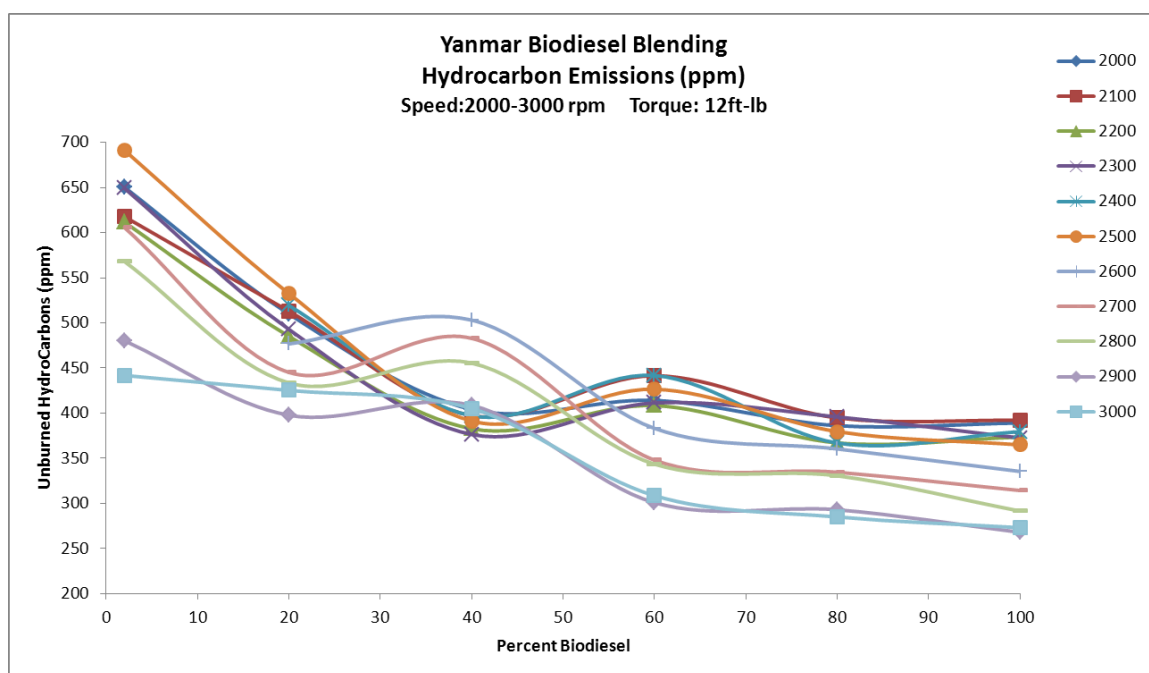


Figure 6-6: Yanmar Biodiesel Blending: Hydrocarbon Emissions Plot

6.3.2 Discussion of Carbon Monoxide Emissions

Incomplete combustion or partial oxidation of fuel is the main cause of CO formation from internal combustion engines. When a lack of oxygen exists, carbon in the fuel cannot completely oxidize to CO₂. CO emissions typically go hand in hand with hydrocarbon emissions as unburned hydrocarbons directly represent incomplete combustion of fuel. CO emissions are expected to decrease for the same reasons increased speed and concentrations of biodiesel decrease hydrocarbon emissions. For all blends, CO emissions are reduced with biodiesel (Figure 6-7). Comparing results from

B2 to B100, the average reduction in CO across the speed range is 21.4%. A clear reduction of CO is noticed at the higher speeds with biodiesel blending but the trend at lower speeds is not as clear. The instabilities at low speeds are likely caused by poor mixing or insufficient exhaust gas temperatures needed to convert CO to CO₂. The variance in CO measurements is decreased at increased speeds due to better mixing and higher temperatures later in the cycle as evidenced by increased exhaust gas temperatures (Figure 6-8).

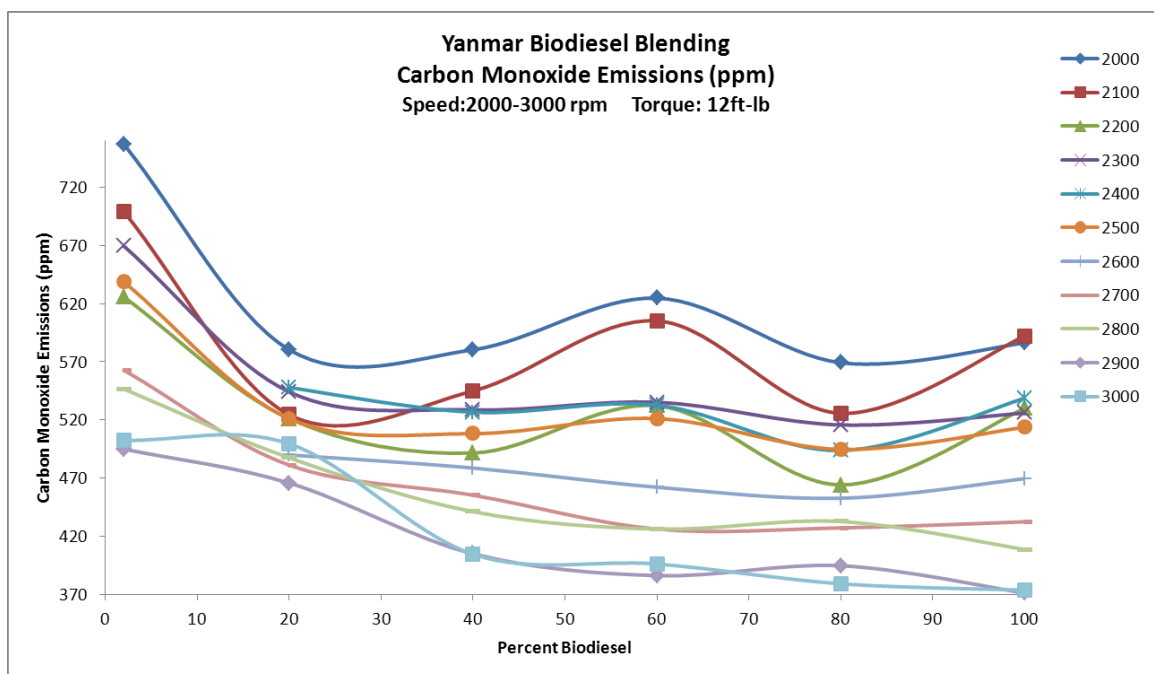


Figure 6-7: Yanmar Biodiesel Blending: Carbon Monoxide Emissions Plot

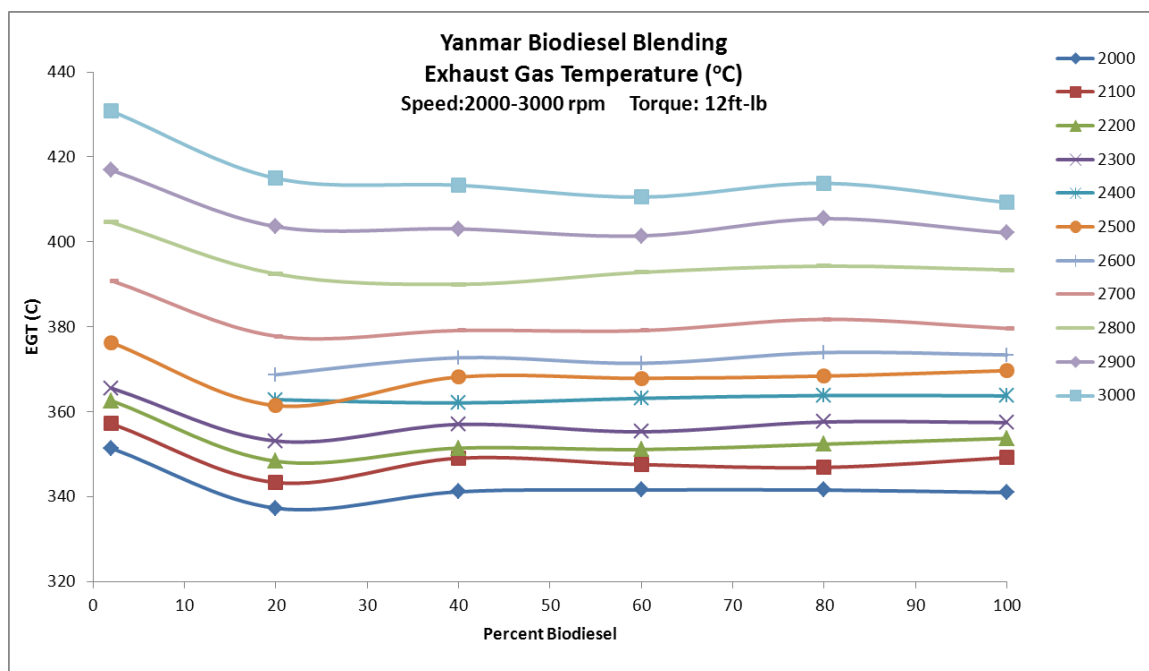


Figure 6-8: Yanmar Biodiesel Blending: Exhaust Gas Temperatures Plot

6.3.3 Discussion of Carbon Dioxide Emissions

From a balance of the stoichiometric combustion reaction, it is known that Carbon Dioxide emissions are directly related to the amount of carbon atoms in the fuel and therefore the amount of fuel consumed. Comparing fuel composition from Table 5-1, the average B2 fuel molecule contains 12.414 carbon atoms and each B100 fuel molecule contains 18 carbon atoms. On a mass basis, the carbon composition for B2 and B100 is 86.6% and 77.1%, respectively. Each gram of B2 contains 42.424 kJ of energy and 0.866 grams of carbon and each gram of B100 contains 37.625 kJ of energy and 0.771 grams of

carbon. 1.128 grams of B100 (containing 0.869 grams of carbon) is needed to achieve the same energy content as one gram of B2 resulting in the same carbon input per unit of energy for each fuel. Incomplete combustion can cause carbon monoxide formation and prevent the carbon contained in the fuel from fully converting to CO₂ but the effect is small for diesel engines. CO₂ emissions are generally an indicator of engine efficiency. Since CO₂ emissions are directly controlled by fuel consumption, a lower amount of CO₂ at a set point would indicate less fuel burned to achieve the same power output, meaning greater efficiency. CO₂ emissions for each test are plotted in Figure 6-9. The overall trend from the plot is a decrease in CO₂ with increased biodiesel concentration and the average decrease in CO₂ emissions from B2 to B100 is 2%. Because each fuel contains the same amount of carbon per unit of energy, the decrease in CO₂ represents an increase in thermal efficiency. While not generally considered a pollutant, CO₂ emissions are responsible for global warming and reduction is desired. Because biodiesel is produced from plant oil, and plants naturally absorb CO₂ the life cycle reduction of CO₂ from biodiesel can be as high as 78% [16].

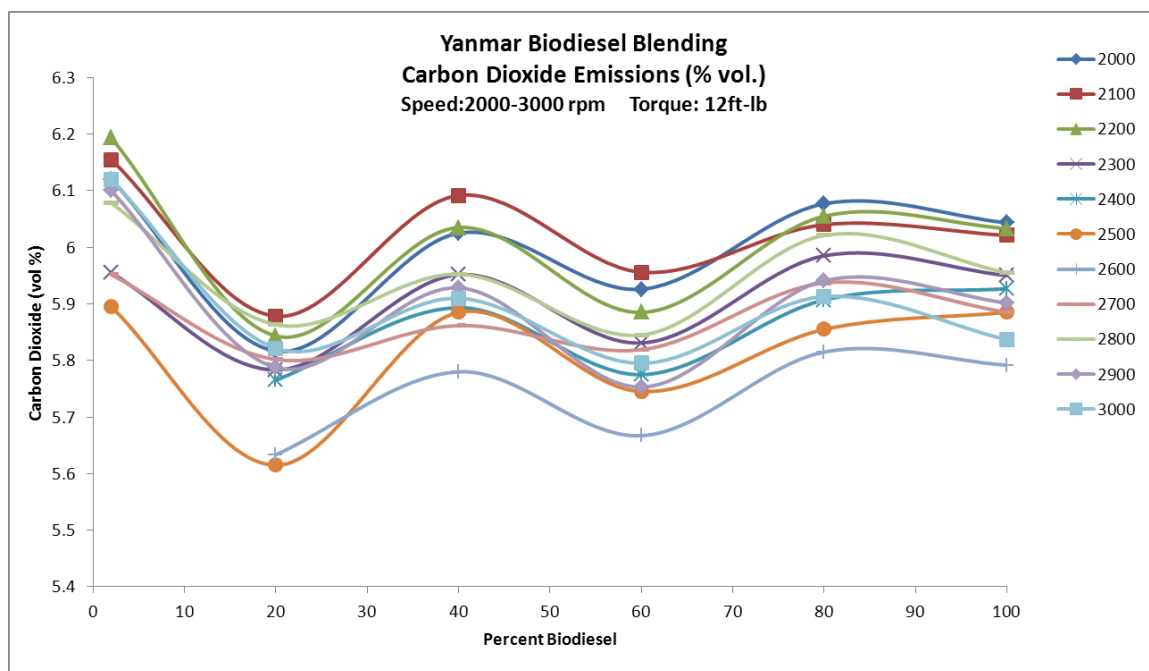


Figure 6-9: Yanmar Biodiesel Blending: Carbon Dioxide Emissions Plot

6.3.4 Discussion of NO_x Emissions

NO_x formation is driven primarily by adiabatic flame temperature with higher temperatures creating more NO_x [37]. Adiabatic flame temperature should not be confused with exhaust gas temperature which increases with engine speed because less time is available for heat to transfer to the engine and remains in the exhaust gas. To understand the effect of timing on adiabatic flame temperature, consider a case where timing is advanced. When timing is advanced, combustion starts earlier in the cycle and more fuel is burned before the piston reaches top dead center, resulting in increased peak

pressure and temperature. The diffusion flame is exposed to the increased pressure and temperature, resulting in unburned fuel inside the diffusion flame being heated. The increased fuel temperature also increases the adiabatic flame temperature and therefore increases NO_x emissions. From the plot of corrected NO_x emissions shown in Figure 6-10, the obvious trend for all fuel blends is a decrease of NO_x with increased engine speed. Increasing engine speed promotes better mixing and effectively retards timing, causing combustion to start later or closer to top dead center. Combustion occurring later in the cycle reduces the peak pressure and temperature which reduces NO_x . NO_x is further reduced by better mixing of fuel and air. Better mixing causes a more uniform distribution of fuel and air, reducing hot spots and distributing energy to the inert excess air in the cylinder. The result is a lower combustion temperature and decreased NO_x .

Biodiesel has an increased cetane number compared to standard diesel which effectively advances combustion timing. Theoretically, advancing the timing would cause more NO_x because the combustion starts earlier resulting in increased peak pressure and adiabatic flame temperature. Despite this property of biodiesel that should cause an increase in NO_x emissions and the published data that matches the theory, the experimental results show the opposite. For speeds above 2600 rpm, we see approximately a 4% reduction in NO_x for all fuel blends compared to the standard fuel. For speeds of 2500 rpm and less, we see an average NO_x decrease of 5.5% and an overall trend of decreased NO_x with increasing concentrations of biodiesel.

The only fuel properties of biodiesel that could explain the NO_x reduction phenomenon are energy content and kinematic viscosity. Biodiesel has lower energy content because it is already partially oxidized by the oxygen atoms contained in the fuel. The decreased energy content of biodiesel also causes increased injection duration. Because the fuel has less energy per volume, more volume is injected to achieve the same amount of energy injected compared to standard diesel. The physical start of fuel injection is constant regardless of the fuel, but as more fuel is injected the duration of the injection event is increased. Compared to standard fuel, the same amount of energy is extracted over a longer period of time. The believed effect is a slower heat release rate and less intense burning of fuel during combustion resulting in lower adiabatic flame temperatures which decreases NO_x emissions. The increased kinematic viscosity of biodiesel inhibits atomization because the stabilities needed for fuel disintegration are suppressed [19]. Hindered atomization reduces the mixing rate of fuel and air. According to Heywood, reducing the mixing rate of fuel and air reduces the rate of heat release during diffusion combustion [37]. The increased kinematic viscosity of biodiesel further reduces the rate of heat release resulting in decreased flame temperature and lower NO_x emissions.

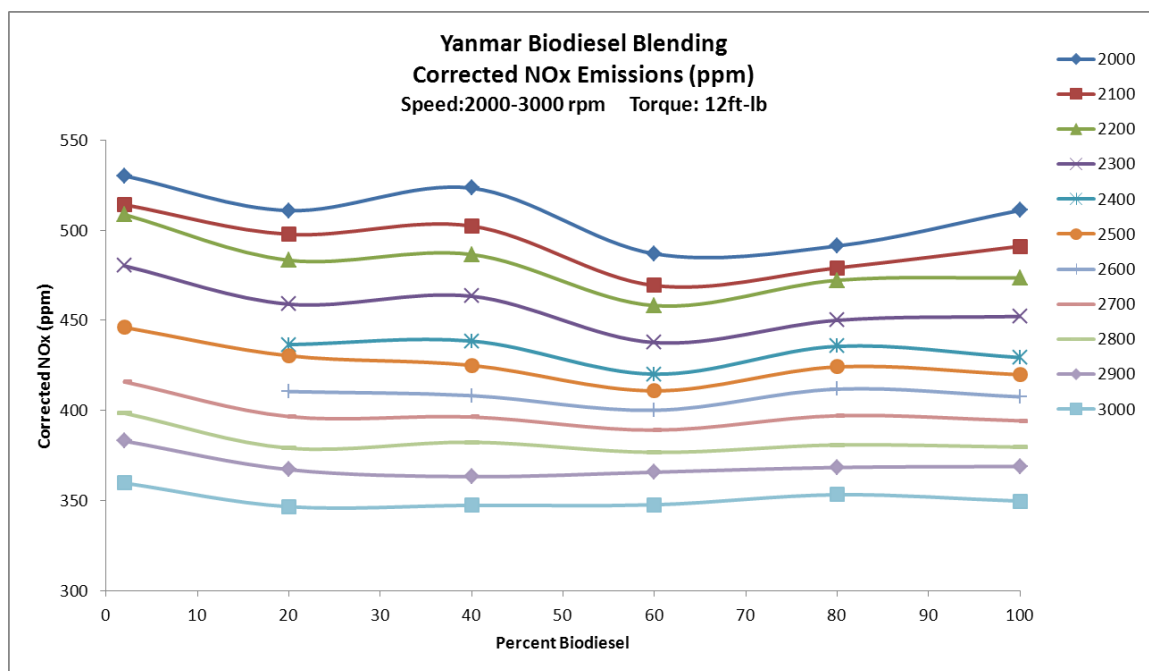


Figure 6-10: Yanmar Biodiesel Blending: Corrected NO_x Emissions Plot

6.4 Conclusions

Using biodiesel as an alternative to standard diesel fuel in a single cylinder 10 HP Yanmar diesel engine is feasible without modification or a sacrifice in performance. Test results show an increase in thermal efficiency, brake specific fuel consumption, and a decrease in harmful exhaust emissions. Small reductions of NO_x emissions and significant reductions of UHC and CO emissions are made with increasing concentrations of biodiesel. Thermal efficiency is increased for each fuel blend compared to standard diesel. Maximum thermal efficiency is obtained with B20 and decreases slightly with

increasing concentration of biodiesel. The chemical properties including reduced energy content and added oxygen content increase the mass based fuel consumption but provide increased thermal efficiency and reduced exhaust emissions. The renewable and non-toxic nature of biodiesel makes it a sustainable and safe alternative to standard diesel fuel. Another important benefit is the net reduction of carbon dioxide emissions from the plants used to produce the fuel.

The results indicate that the goals and objectives of this thesis project were met, and the project is therefore a success. A test bed for determining and comparing performance and emissions characteristics of standard and alternative fuels burned in CI engines was designed and built. The functionality of the apparatus was tested and confirmed and the accuracy and consistency of the test measurements were validated. Performance and emissions testing was performed for standard diesel fuel, pure bio-diesel derived from soybean oil, and blends of the two. Testing results were analyzed and the feasibility of biodiesel as an alternative fuel was assessed.

6.5 Recommendations for Future Work

The testing apparatus and test methods developed and used in this thesis provide a solid foundation for testing and future experiments. That being said, improvements could be made to the apparatus to make additional measurements, and increase the quality of current data measurements. Some desirable testing options not currently available are

measurements of exhaust smoke and cylinder pressure. Smoke measurements are important characteristics of exhaust analysis, especially for CI engines. An encoder could be used in conjunction with a pressure transducer to measure the crank angle and corresponding combustion pressure. Knowing the cylinder pressure for each particular crank angle would provide a clear picture of the combustion and allow for more exact heat release analysis. Due to cost constraints the equipment necessary to collect this data was not available but the addition of this equipment would be an excellent improvement to the apparatus.

To increase the quality of data measurements from the apparatus, improvements could be made to the current equipment used to measure air flow, fuel mass, and exhaust gas. The LFE used to measure airflow is very old and should be either replaced or re-calibrated. The manufacturer is not willing to calibrate the device, so a method to calibrate at Bucknell University would be useful if replacement is not an option. Fuel mass measurements made with the Sartorius paint scale are currently accurate but measurements are communicated through a serial port. Serial communications are slow and occasionally cause problems with the data acquisition program. A new version of the scale with a USB output would provide much faster and reliable data acquisition. The last recommendation for improvement is the installation of a switch between the exhaust pipe and the beginning of the emissions sample line. Controlling the emissions equipment to only make measurements at the desired testing points opposed to all the time would

reduce residual effects on measurements. The solution is not simple though. The switch needs to handle the high temperatures of exhaust gas and be remotely operated from the control desk. The switch should not restrict the flow of sample exhaust gas or allow the gas to leak into the room. When the switch is used to stop the flow of exhaust sample, it must also allow the flow of room air to the analyzers to prevent damage to the sample pumps contained in the analyzers.

REFERENCES

- [1] "Annual Energy Outlook 2011," U.S Energy Information Administration, **2011**(06/14) http://www.eia.gov/forecasts/aeo/MT_liquidfuels.cfm.
- [2] Heywood, J.B., 1988, "Internal Combustion Engine Fundamentals," McGraw-Hill, New York, pp. 45-53.
- [3] Heywood, J.B., 1988, "Internal Combustion Engine Fundamentals," McGraw-Hill, New York, pp. 1-40.
- [4] Schifsky, C., 2002, "Tech: Gas Vs. Diesel," Truck Trend, (October) .
- [5] Heywood, J.B., 1988, "Internal Combustion Engine Fundamentals," McGraw-Hill, New York, pp. 567-647.
- [6] Eastwood, P., 2000, "Critical Topics in Exhaust Gas Aftertreatment," Research Studies Press, pp. 7-20.
- [7] "Particulate Matter," U.S. Environmental Protection Agency, **2011**(6/14) <http://www.epa.gov/oar/particlepollution/>.
- [8] "Reduce Climate Change," U.S. Department of Energy, **2010**(1/10) <http://fueleconomy.gov/feg/climate.shtml>.

- [9] "Electric Vehicles (EVs)," U.S. Department of Energy, **2010**(1/10)
<http://fueleconomy.gov/feg/evtech.shtml>.
- [10] "Fuel Cell Vehicles," U.S. Department of Energy, **2010**(1/10)
<http://fueleconomy.gov/feg/fuelcell.shtml>.
- [11] "Hybrid Electric Vehicle Basics," U.S. Department of Energy, **2011**(6/14)
http://www.afdc.energy.gov/afdc/vehicles/electric_basics_hev.html.
- [12] Suryawanshi, J. G., 2006, "Performance and Emission Characteristics of CI Engine Fueled by Coconut Oil Methyl Ester," SAE Paper 2006-32-0077.
- [13] Soetaert, W., and Vandamme, E.J., 2009, "Biofuels," Wiley, Hoboken, N.J., pp. 77-90.
- [14] Bunting, B. G., Eaton, S. J., Crawford, R., 2009, "Performance of Biodiesel Blends of Different FAME Distributions in HCCI Combustion," SAE Paper 2009-01-1342.
- [15] Mousdale, D.M., 2010, "Introduction to Biofuels," CRC Press, Boca Raton, FL, pp. 301-314.
- [16] "Biodiesel Benefits," U.S. Department of Energy, **2011**(3/11)
http://www.afdc.energy.gov/afdc/fuels/biodiesel_benefits.htm.

- [17] "Myths and Realities Behind Rising Food Prices," American Soybean Association, 2008, **2011**(6/28)
<http://www.soygrowers.com/publications/MythsRealhtml/MythsRealities.htm>.
- [18] Deng, J., Li, C., Hu, Z., 2010, "Spray Characteristics of Biodiesel and Diesel Fuels Under High Injection Pressure with a Common Rail System," SAE Paper 2010-01-2268.
- [19] Ahmed, M. A., Ejim, C. E., Fleck, B. A., 2006, "Effect of Biodiesel Fuel Properties and its Blends on Atomization," SAE Paper 2006-01-0893.
- [20] Basavaraja, T., Reddy, R., and Swamy, V., 2005, "Effect of Injection Pressure on Emission Performance of Bio-Diesel and its Blends," SAE Paper 2005-26-030.
- [21] Tesfa, B., Mishra, R., Gu, F., 2010, "Emission Behavior of a CI Engine Running by Biodiesel Under Transient Conditions," SAE Paper 2010-01-1280.
- [22] Stone, R., 1999, "Introduction to Internal Combustion Engines." Society of Automotive Engineers, Warrendale, PA, pp. 52-59.
- [23] Sebastian, J., and Nagarajan, G., 2010, "Experimental Study on Influence of Fuel Oxygen Content on Combustion and Emission Characteristics of a Direct Injection C.I. Engine," SAE Paper 2010-01-1969.

- [24] Kawano, D., Ishi, H., and Goto, Y., 2008, "Effect of Biodiesel Blending on Emission Characteristics of Modern Diesel Engine," SAE Paper 2008-01-2384.
- [25] Dulger, Z., and Kaplan, C., 2001, "Utilization of Sunflower Methyl Ester as a Diesel Engine Fuel," SAE Paper 2001-01-3633.
- [26] Kumar, S., Stanton, D. W., Fang, H., 2009, " The Effect of Diesel Fuel Properties on Engine-Out Emissions and Fuel Efficiency at Mid-Load Conditions," SAE Paper 2009-01-2697.
- [27] DeVita, M., 2006, "The Design and Construction of an Infinitely Variable Transmission with Dynamometer Testing Apparatus."
- [28] "Martin Stock Timing Pulley Selection," **2011**pp. 48.
<http://www.martinsprocket.com/2001/SecKa.pdf#K13>.
- [29] "Sartorius PMA 7200-X Electronic Paint Mixing Scale for use in Hazardous Locations/Area Installation and Operating Instructions," **2011**pp. 52.
<http://www.sartorius.com>.
- [30] Peter Cremer North America, LP, 2011, **2011**(3/10) <http://www.petercremerna.com/>.
- [31] "Lipomics Fatty Acid Library," Tethys Bioscience, I., 2011, **2011**(3/10)
http://www.lipomics.com/fatty_acids.

- [32] "Energy Content," National Biodiesel Board, 2005, **2011**(3/10) pp. 1.
http://www.biodiesel.org/pdf_files/fuelsheets/BTU_Content_Final_Oct2005.pdf.
- [33] Shelquist, R., 2011, "An Introduction to Air Density and Density Altitude Calculations," **2011**(5/30) pp. 1. http://wahiduddin.net/calc/density_altitude.htm.
- [34] Courtois, W., 1997, "Derivation of Humidity and NO_x Humidity Correction Factors," **2011**(5/30) pp. 10. <http://www.epa.gov/nvfe/methods/noxcorr.pdf>.
- [35] Turns, S.R., 2000, McGraw-Hill New York, pp. 653.
- [36] Brahma, I., Personal conversation and email correspondence. Bucknell University. 2011.
- [37] Heywood, J.B., 1988, "Internal Combustion Engine Fundamentals," McGraw-Hill, New York, pp. 558-625.

APPENDIX A: EMISSIONS EQUIPMENT OPERATION PROCEDURE

Use of this equipment requires approximately two hours of setup time before any data can be taken. Plan your testing schedule accordingly.

Equipment Schematic:

**Heated Filter
Temp Controller**

**Heated Line
Temp Controller**

Heated Line

Heated Filter

Horiba PG-250

Chiller Bucket

CAI 600 HFID



Figure A-1: Equipment Schematic Overview

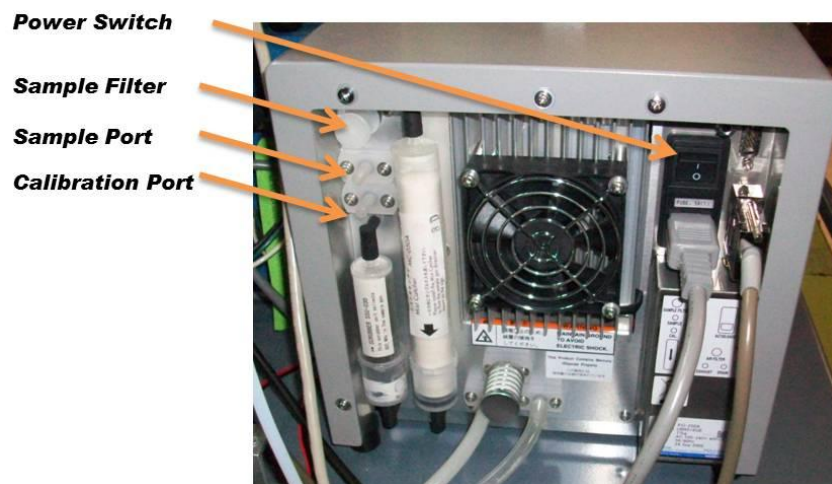


Figure A-2: Horiba PG-250 Rear Panel Schematic

Preparation and warm up:

1. Turn on Horiba PG-250, CAI HFID, Heated Filter, and Heated line.
 - a. The heated filter temperature control should be set to 170C
 - b. Heated line temperature control should be set to 300F.

2. Fill the Chiller with ice and water.
 - a. Fill a five gallon bucket with ice from the utility room located on the second floor of Breakiron and next to the men's bathroom.
 - b. Add the ice to the empty chiller. Make sure the drain valve is closed.
 - c. Add six inches of water to the ice bucket and add to the chiller. The liquid level should be just below the inlet line of the coil at the top of the chiller.

** It is important to add the ice and then the water to prevent a large mess during the transfer process.

3. Check the heated filter element (Figure A-3)
 - a. It may be necessary to replace the filter element or wipe off excess particulate matter with a paper towel.



Figure A-3: Heated Filter Element

4. Replace the sample line filter (Figure A-4) on the Horiba unit. The arrow should face towards the inside of the machine.



Figure A-4: Horiba Sample Filter

5. HFID Warm up period
 - a. The HFID unit will need to warm up until the “Oven Temperature” reaches 180°C. This will take approximately twenty minutes. Check the oven temperature by pressing “Main” then enter the Diagnostics screen by pressing “F3.”
6. HFID Burner Ignition

**Do not ignite burner until the oven temperature has reached 180°C

 - a. Verify the burner fuel and combustion air lines are connected to the HFID.
 - b. Turn on gas cylinders and verify the regulator pressures are set to 20 psi.
 - c. Verify the valves after the regulators are open.
 - d. Check for leaks by applying “Snoop” to all connections.
 - e. Bleed the fuel line by loosening the fitting at the inlet port of the HFID with a 9/16 inch wrench. After a few seconds retighten the fitting and check for leaks.
 - f. To start ignition enter the main menu by pressing “Main” and then start Ignition by pressing “F8.”

- g. After ignition has been started a warm up of one hour is required before proceeding to calibration.
7. Horiba warm up period.
- a. A one hour timer will appear on the display of the unit when the power is turned on. Calibration cannot be performed until the warm up period is complete.

Calibration Procedure

1. Zero HFID
 - a. Zero gas for the HFID is also the combustion air. No additional connections need to be made or checked providing you have correctly followed the steps up to this point.
 - b. Enter the main menu by pressing “Main”
 - c. Enter the Calibrations menu by pressing “F4.”
 - d. Enter Manual Calibrations menu by pressing “F2.”
 - e. Flow Zero gas by pressing “F1.”
 - f. Allow the measurement to stabilize (about 5 minutes)
 - g. After the zero measurement has stabilized press “F1” to save the value.
 - h. Return to the Manual Calibrations Menu by pressing “F2.”
 - i. Proceed to Step 2 of the calibration procedure to Span the HFID.
2. Span HFID
 - a. Turn on the Span gas cylinder and verify the regulator pressure is set to 25 psi.
 - b. Use “Snoop” to check for leaks at all connections.
 - c. Verify the valve after the regulator is open.
 - d. Bleed the line by loosening the connection at the HFID with a 9/16 wrench. After a few seconds retighten the connection.
 - e. Verify the span gas concentration saved in the HFID matches the concentration on the Printed analysis sheet attached to the span gas bottle.
 - f. Enter the main menu by pressing “Main”
 - g. Enter the Calibrations menu by pressing “F4.”
 - h. Enter Manual Calibrations menu by pressing “F2.”
 - i. From the manual calibrations menu press “F2” to flow the span gas.
 - j. Allow 5-10 minutes for the measurement to stabilize then press “F1” to save.
 - k. Turn off the span gas cylinder valve

- l. Bleed the line and regulator by loosening the connection at the HFID with a 9/16 wrench.
 - m. Go back to the main menu by pressing “Main.”
 - n. View the measurement screen by pressing “F1.”
3. Zero Horiba
 - a. After the one hour warm up period has expired turn on the Nitrogen tank and verify the regulator pressure is set to 50 kPa with the valve after the regulator closed.
 - b. Open the valve and connect the Nitrogen line to the sample port.
 - c. From the measurement screen press “Menu/Set”
 - d. Press “Menu/Set” again to enter the Calibration menu.
 - e. Verify span gas concentrations match the printed analysis sheet attached to the span gas bottle.
 - f. Use “R” and “F” cursor buttons to toggle between values. Use the Select arrows to change values.
 - g. Set Line to “MEAS”
 - h. Set all CAL SEL values to “ZERO”
 - i. Wait to stabilize (Approx. 5-10 minutes)
 - j. Press “Menu/Set” to save zero calibration
 - k. Turn off the Nitrogen tank and disconnect the line from the unit
4. Span Horiba
 - a. Turn on the Span gas and verify the regulator pressure is set to 50 kPa with the valve after the regulator closed.
 - b. Open the valve after the regulator and connect the line to the Cal port.
 - c. From the Calibration menu set LINE to CAL-1
 - d. Set the CAL SEL to SPAN for NO, CO, and CO₂. Set all others to “None”
 - e. Wait to stabilize (Approx. 5-10 minutes) Do not flow span gas more than 15 minutes.
 - f. Press “Menu/Set” to save span calibration
 - g. From the Calibration menu set LINE to CAL-2
 - h. Set the CAL SEL to SPAN for SO₂. Set all others to “None”
 - i. Wait to stabilize (Approx. 5-10 minutes) Do not flow span gas more than 15 minutes.
 - j. Press “Menu/Set” to save span calibration
 - k. Turn off the span gas tank and disconnect the line
 - l. From the Calibration menu set LINE to MEAS

- m. Set the CAL SEL to SPAN for O₂. Set all others to “None”
- n. For this calibration the unit will draw in room air and use the oxygen concentration as the span value. This value is set at 21.00%
- o. Wait to stabilize (Approx. 5-10 minutes)
- p. Press “Menu/Set” to save span calibration
- q. Press “Exit” two times to return to the measurement screen
- r. Change “NO_x and “SO₂” measurements to “Corr.NO_x” and “Corr.SO₂”

Shutdown Procedure

1. General Shutdown

- a. Disconnect the sample line at the engine with a 5/8 wrench
- b. Remove the sample line from the back of the Horiba unit and cap the line
- c. Run the chiller drain tube to a suitable floor drain and open the valve to drain water and melting ice
- d. Allow the analyzers to draw room air for 20-30 minutes before proceeding to the next step
- e. Turn off the heated sample line
- f. Disconnect the sample line at the heated filter with an 11/16 wrench
- g. Back flush the heated sample line with nitrogen

2. Horiba Shutdown

- a. Press the purge button
- b. Wait for the “Purge Completed” to be displayed.
- c. Turn off power switch at the back of the unit
- d. Replace the sample filter element before storage

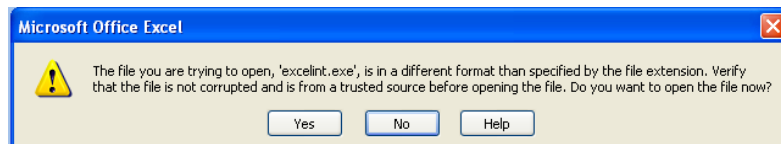
3. HFID Shutdown

- a. Enter the main menu by pressing “Main” and then purge the analyzer by pressing “F4.”
- b. Wait for the purge to complete
- c. Turn off the air and burner fuel cylinders allowing the burner to go out. The air will run out first so bleed excess fuel from the line by loosening the connection at the back of the unit
- d. Allow the unit to draw in room air for 5-10 minutes before turning off the power

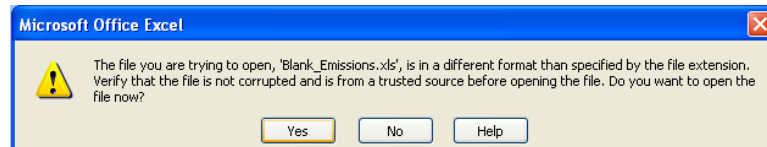
4. Turn off heated filter

APPENDIX B: DATA FILE PREPARATION PROCEDURE

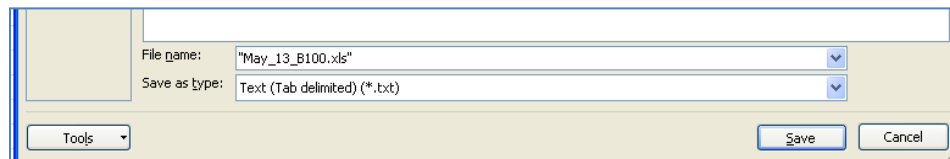
1. Log on to the computer
2. Prepare and save the data file
 - a. Locate and open the excel file named “Blank Data File” on the desktop
 - b. A dialog box will appear asking you to verify the file is not corrupted. Click Yes.



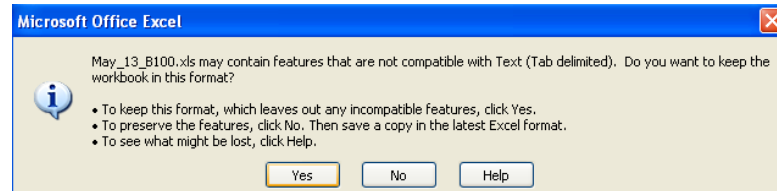
- c. Another dialog box will appear stating the file is in a different format than specified by the extension. Click yes.



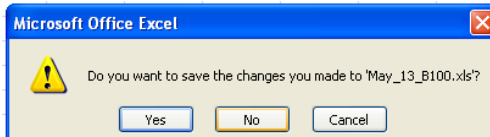
- d. With the file open, click “save as” and save the file as the Month, day, and a detail of what you will be testing. For example, testing 100% biodiesel on May 13th, the file name would be “May_13_B100.xls” Make sure the file type is “Text (Tab delimited)”



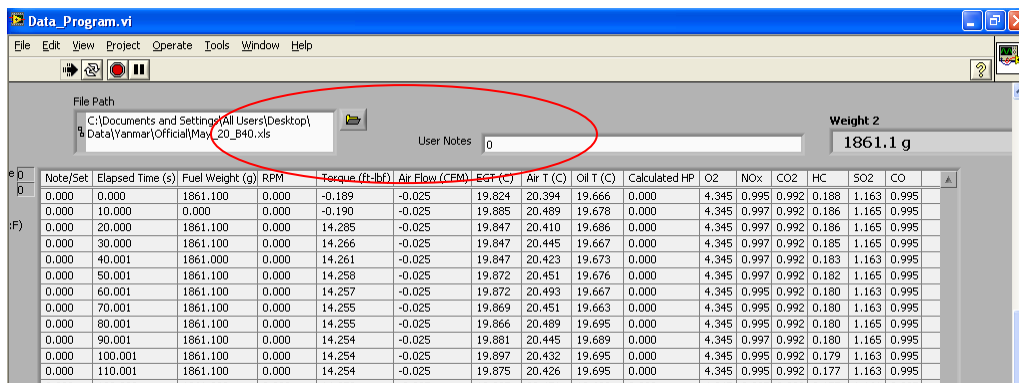
- e. A dialog box will appear stating features may not be compatible with this file type. Click yes to keep the file in this format.



- f. Exit the excel program. Another dialog will appear asking if you want to save changes to the file. Click No.



- g. From the desktop open the LabVIEW® program titled “Data_Program” Click the folder icon to set the file path for the data to be saved. Choose the file you created in the previous step.



- h. From the file menu, save the LabVIEW® program.
i. Begin collecting data by clicking the arrow in the toolbar located in the top left of the screen.

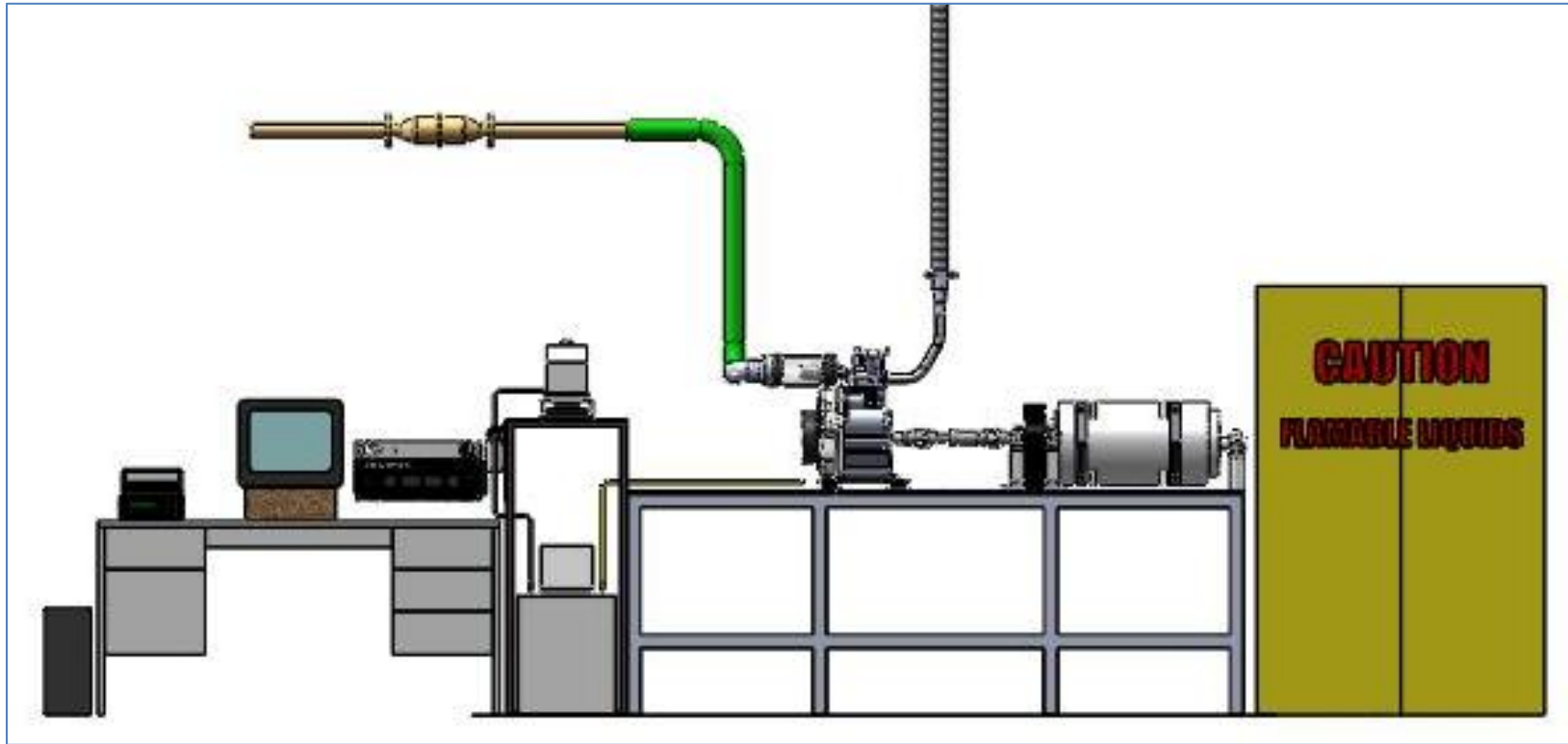
APPENDIX C: DYNAMOMETER STARTUP AND OPERATION PROCEDURE**Figure C-1: Test Cell Schematic**



Figure C-2: Dynamometer Control Box

1. Obtain proper safety equipment including safety glasses and hearing protection.
2. Locate a fire extinguisher and verify it is up to date.
3. Turn on the following equipment:
 1. Computer
 2. Agilent 34970A Data acquisition unit
 3. MKS 670 Signal Conditioner (Always on)
 4. Dynamometer control box
 5. Fuel Water Bath
 6. Handheld weather station
 7. Fuel scale (Always on)
4. Ensure the exhaust valve is correctly switched by noting the position of the cable that controls the valve (Figure C-3).

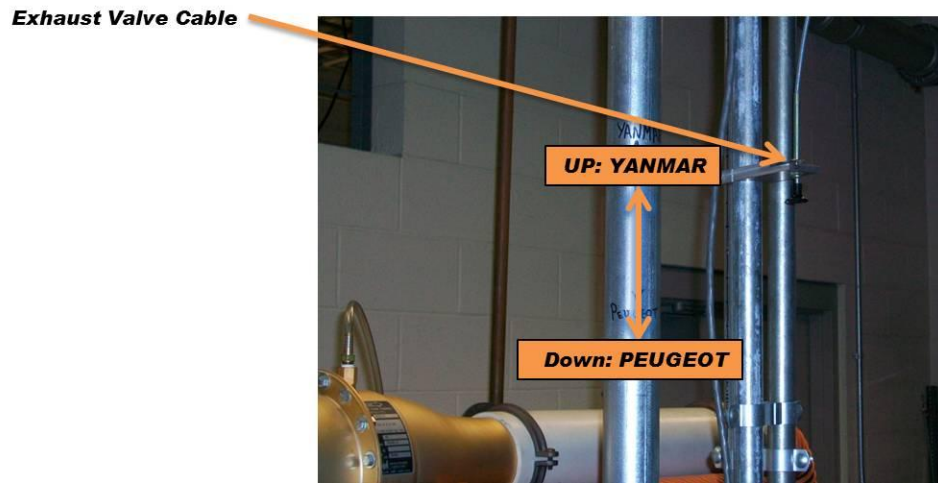


Figure C-3: Exhaust System Switch

5. Turn on and prepare the emissions equipment using the “Emissions Analyzer Equipment Operation Procedure.”
6. Prepare the data file using the “Data File Preparation Procedure.”
7. Open the garage door in room 22 approximately 18 inches.
8. Prop open the side entrance door located by the fuel cabinet.
9. Open the water valve to allow cooling water to enter the resistor bank.
10. Connect battery charger. Use the maintenance free setting.
11. Check fuel and oil levels. To change fuels use the “Fuel changing procedure.”
12. Check the overall condition of engine, driveshaft, belt, exhaust system, fuel system, etc.
13. Ensure the engine is at the compression stroke. Pulling the engine over by hand, the point at which the engine becomes hard to turn over is the beginning of the compression stroke. At this point, a mark on the large pulley of the dynamometer absorbing motor should be pointed straight down.
14. Add the calibration weight to the calibration arm of the absorbing motor. This weight is marked “14.36 lbs.” The actual weight is 28.72 pounds but half the value is used to compensate for the 2:1 speed reduction and torque increase.
15. Run the LabVIEW® program with the calibration weight for approximately 20 minutes. Then remove the weight with the program still running. Allow the program to run without the weight for approximately 5 minutes and then replace the calibration weight. Cycle this a few times. The reading should be 14.36 with the calibration weight and zero without the weight.

16. Zero the MKS signal conditioner:
 - a. Press the "Zero" button
 - i. The display should read "Press ENTER to zero" if not press the menu up arrow until it does.
 - b. Press "Enter" to zero
 - i. The display will flash "CALIBRATING" until the zero is complete
 - c. Press the "Zero" button to return to the measurement screen
17. Start data acquisition if not already running.
18. Turn battery disconnect to "ON."
19. Remove duct tape from fuel tank cap and open the fuel shut off valve to ON (Figure C-4)

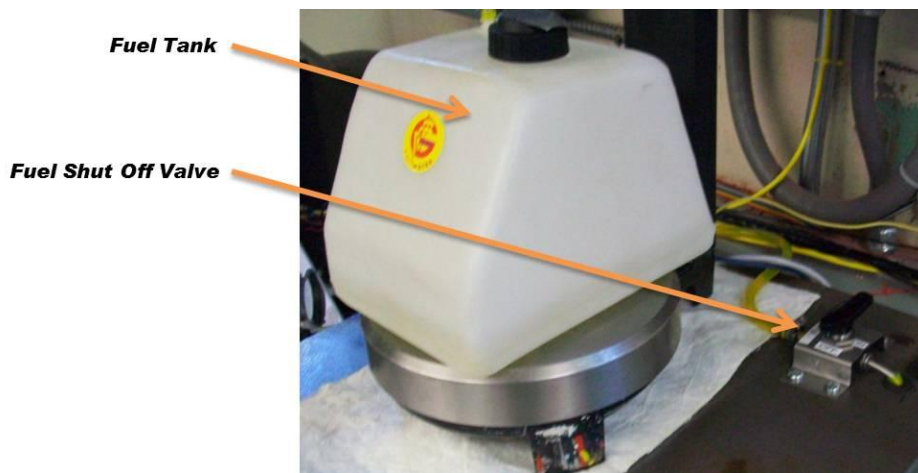


Figure C-4: Fuel Tank and Shutoff Valve

20. Turn on the room exhaust fan. Typically the low setting is adequate.
21. Open the fuel throttle by turning the "Engine Speed Control" knob counter clockwise 15-20 turns. The maximum turns out is 25.
22. Turn the ignition key to "ON" this will turn on the fuel pump and the low oil pressure warning light. The red oil pressure warning light should only be on when the engine is not running. Shut the engine down immediately if this light is illuminated during operation.

23. Ensure the "Applied Load Control" knob is turned all the way down (CCW). Only adjust this knob while the engine is running.
24. Turn the ignition key to the start position.
25. As soon as the engine starts, turn the speed control clockwise to reduce the speed of the engine to 2500 rpm as displayed on the control box.
26. If taking emissions data; remove the emissions sample port cap (Figure C-5) and install the emissions sample line to the exhaust system (Figure C-6). The line fitting should be threaded on using only fingers. Tighten with a 5/8 wrench.

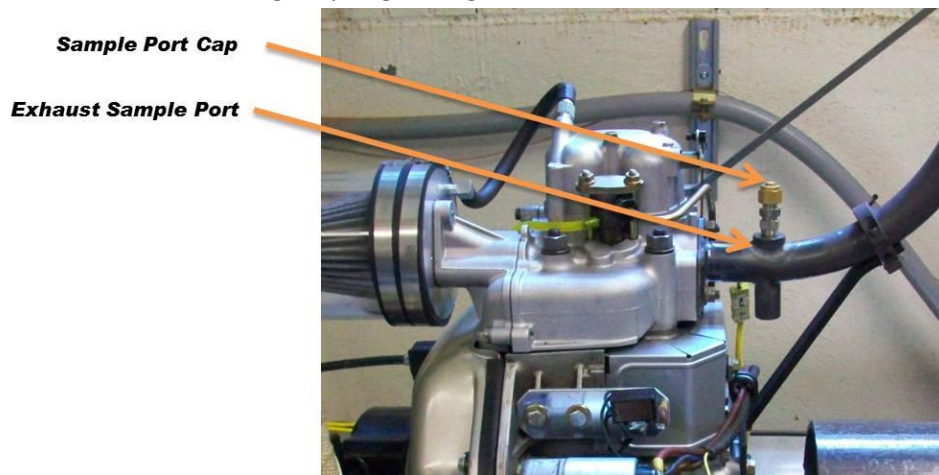


Figure C-5: Emissions Sample Port Cap

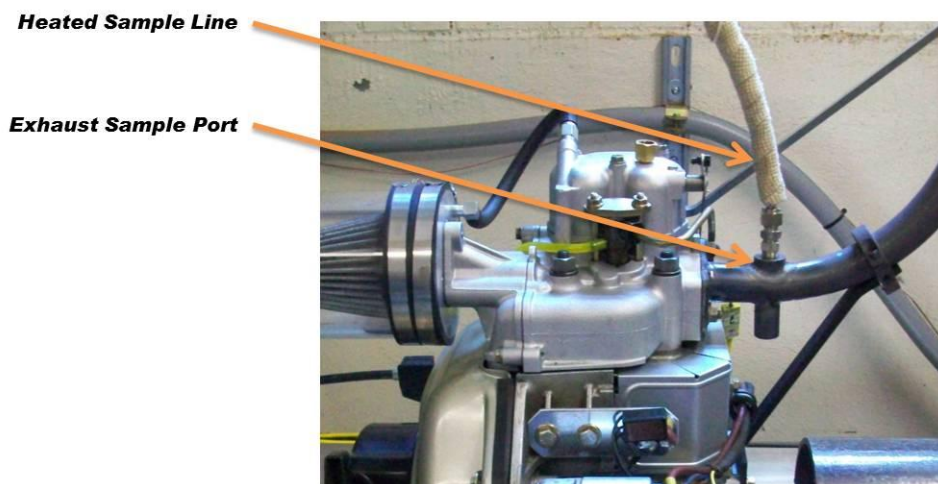


Figure C-6: Emissions Heated Sample Line

27. In case of emergency shutdown of the engine you must turn the speed control all the way inward (clockwise) to shut the engine off. This can be done by pressing the Emergency release button on the speed control knob (Figure C-2).
28. While operating the engine avoid rapid changes in speed and applied load. Rapid changes have a residual effect on the emissions data.
29. Allow the engine to warm up at zero load and 2500 rpm for five minutes. Then gradually increase the load until the torque reaches 10 ft-lbs. Allow the engine to run at this load and 2500 rpm for an additional five minutes.
30. After completing the mandatory warm up period, adjust the speed and applied load to the desired values. It is necessary to allow the engine to run at the set point for 1-2 minutes without adjusting the speed or load to reach steady state. Watch the oil temperature closely. When the engine appears to reach steady state, ensure the speed and torque remain at the desired values. After verifying, locate the "User Note" input box in the LabVIEW® program (Figure C-7). This is a numeric input only. The value should be zero for data taken during the warm-up and transients periods. After reaching steady state for the desired speed and torque enter the first two digits of the speed and torque in this box and click outside of the box to start recording the note with the data. For example, testing at 2500 rpm and 12 ft-lbs the user note would be "2512."

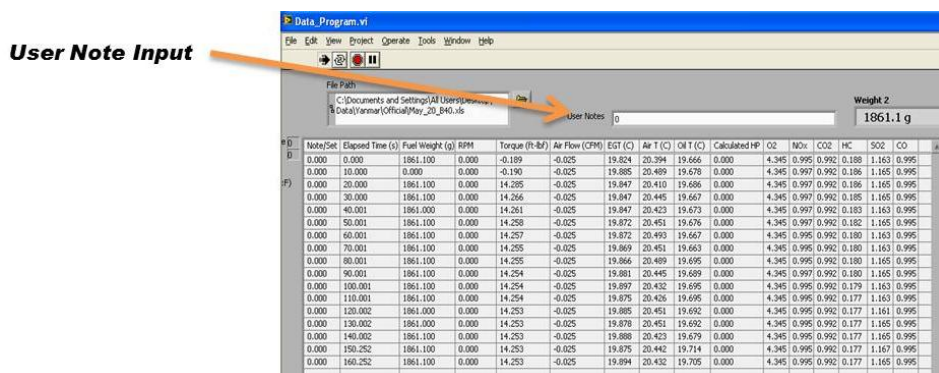


Figure C-7: LabVIEW® User Note Input

Shutdown Procedure

1. Slowly decrease the load in 1-2 ft-lb increments every 30-60 seconds until zero load is reached (keeping the speed below 3000 rpm).
2. Decrease the speed in 100 rpm increments every 30-60 seconds until 2000 rpm is reached.
3. At 2000 rpm and zero load, turn off the fuel pump by switching the ignition key to the "Off" position.
4. Allow the engine to run at 2000 rpm and zero load until the exhaust gas temperature drops to 120°C then run for an additional 2-3 minutes.
5. Turn the engine off by pressing the speed control quick release, fully disengaging the speed control knob.
6. Stop the data acquisition program.
7. Turn the engine over by hand to the beginning of the compression stroke.
8. Turn the fuel valve to "Off."
9. Place a piece of duct tape over the vent hole in the fuel tank cap.
10. Unplug the battery charger and disconnect from the battery.

11. Turn the battery disconnect to "Off"
12. Turn off the following items:
 1. Room exhaust fan
 2. Water valve
 3. Agilent 34970A Data acquisition unit
 4. Dynamometer control box
 5. Fuel water bath
 6. Handheld weather station
13. Close room and garage doors.
14. Follow the "Shutdown Procedure" located in the "Emissions Analyzer Equipment Operation Procedure."
15. To analyze results, follow the "Data File Analysis Procedure."

APPENDIX D: DATA FILE ANALYSIS PROCEDURE

1. Copy data to new Excel workbook
 - a. Open the excel file that data was written to from the LabVIEW® program
 - b. Select and copy the data columns
 - c. Paste the data columns to a new blank excel workbook
 - d. Save the new workbook in a new location
 - e. Close the original workbook

2. Rename workbook sheets
 - a. Rename Sheet 1 to "RAW"
 - b. Create a copy of "RAW" and rename it "Clean"
 - c. Rename Sheet3 to "Summary"

3. Remove unwanted data and format sheet
 - a. Select the "Clean" sheet
 - b. Delete all rows of data with "0" in the Note/Set Column
 - c. Leave ten blank rows between data sets, it may be necessary to insert additional rows

4. Format and inspect fuel weight data
 - a. Select the fuel weight data column in the "Clean" sheet
 - b. Right click the column and select "Format Cells"
 - c. Change the category to "Number" and decimal places to "2"
 - d. Inspect fuel weight data for errors

5. Calculate Fuel Consumption
 - a. Insert a new column between the Fuel (g) and RPM columns
 - b. Name the new column "Fueling (g/s)"
 - c. Fueling is the change in weight divided by the change in time (10 secs)
 - d. Subtract the fuel weight and divide the value by 10 seconds (Figure D-1)
 - e. Perform this operation for all fuel data

May_25_B80 - Microsoft Excel non-commercial use (Trial)

Formula Bar: $= (C3-C4)/10$

	A	B	C	D	E	F	G	H	I	J	K	L	M	N	O	P	Q	R
1	Note / SetTime (s)	Fuel (g)	g/s	RPM	Torque	Airflow	EGT	Air T	Oil T	HP	O2	Nox	CO2	HC	SO2	CO		
2																		
3	2012	90.033	3945.6		2019.761	12.021	12.225	342.487	22.758	61.265	4.623	3.062	3.044	2.217	0.519	1.073	1.405	
4	2012	100.033	3943.5	0.21	1992.296	12.01	12.225	342.676	22.968	61.452	4.556	3.06	3.05	2.219	0.517	1.073	1.405	
5	2012	110.033	3940.5	0.3	1992.227	12.005	12.2	343.016	22.795	61.302	4.554	3.058	3.054	2.221	0.517	1.073	1.405	
6	2012	120.034	3938.1	0.24	2011.995	11.999	12.225	342.992	22.689	61.651	4.597	3.058	3.058	2.221	0.521	1.071	1.405	

Figure D-1: Fueling Calculation

6. Average data

- a. Create a row one space below each data set for average data values
- b. The first cell of the row should contain the same value as the Note/Set value for the data set
- c. Start with the “Fueling” data and use the “average” function to average the column of data (Figure D-2)
- d. Average each column of the data set up to the emissions data
- e. The emissions data will only average the last 60 seconds of the data set
- f. Complete average calculations for each data set

D35		=AVERAGE(D3:D33)																	
	A	B	C	D	E	F	G	H	I	J	K	L	M	N	O	P	Q		
1	Note / Set	Time (s)	Fuel (g)	g/s	RPM	Torque	Airflow	EGT	Air T	Oil T	HP	O2	Nox	CO2	HC	SO2	CO		
2																			
3	2012	90.033	3945.6		2019.761	12.021	12.225	342.487	22.758	61.265	4.623	3.062	3.044	2.217	0.519	1.073	1.405		
4	2012	100.033	3943.5	0.21	1992.296	12.01	12.225	342.676	22.968	61.452	4.556	3.06	3.05	2.219	0.517	1.073	1.405		
5	2012	110.033	3940.5	0.3	1992.227	12.005	12.2	343.016	22.795	61.302	4.554	3.058	3.054	2.221	0.517	1.073	1.405		
6	2012	120.034	3938.1	0.24	2011.995	11.999	12.225	342.992	22.689	61.651	4.597	3.058	3.058	2.221	0.521	1.071	1.405		
7	2012	130.034	3935.5	0.26	2019.245	11.981	12.175	343.037	23.009	61.96	4.606	3.056	3.062	2.221	0.524	1.071	1.405		
8	2012	140.034	3932.8	0.27	1978.145	11.968	12.187	343.138	23.157	62.435	4.508	3.056	3.066	2.221	0.521	1.071	1.405		
9	2012	150.034	3930.3	0.25	1978.765	11.976	12.175	343.271	22.799	62.563	4.512	3.056	3.072	2.221	0.527	1.071	1.403		
10	2012	160.05	3927.6	0.27	2006.996	11.97	12.175	343.271	22.761	62.432	4.574	3.054	3.076	2.223	0.523	1.071	1.403		
11	2012	170.05	3925.1	0.25	1997.513	11.976	12.162	343.369	22.613	62.545	4.555	3.054	3.08	2.223	0.527	1.071	1.405		
12	2012	180.05	3922.9	0.22	2017.805	11.967	12.187	343.791	22.748	62.814	4.598	3.054	3.082	2.225	0.527	1.071	1.405		
13	2012	190.051	3920.1	0.28	2001.48	11.954	12.162	343.742	22.824	63.081	4.556	3.056	3.086	2.223	0.53	1.071	1.405		
14	2012	200.051	3917.2	0.29	1996.945	11.916	12.112	344.007	22.695	63.035	4.531	3.056	3.088	2.223	0.53	1.073	1.405		
15	2012	210.051	3914.6	0.26	1993.137	11.924	12.225	343.676	22.723	63.598	4.525	3.056	3.092	2.221	0.53	1.073	1.407		
16	2012	220.051	3912.3	0.23	2013.346	11.931	12.2	343.587	22.566	63.2	4.574	3.056	3.094	2.223	0.539	1.071	1.407		
17	2012	230.051	3909.6	0.27	2017.603	11.928	12.137	343.323	22.698	63.782	4.582	3.056	3.098	2.221	0.532	1.071	1.409		
18	2012	240.051	3907.2	0.24	1997.306	11.928	12.125	343.277	22.722	64.028	4.536	3.058	3.1	2.221	0.53	1.071	1.411		
19	2012	250.052	3904.2	0.3	2012.68	11.922	12.225	343.323	22.603	63.909	4.569	3.058	3.102	2.221	0.536	1.071	1.413		
20	2012	260.052	3901.8	0.24	1982.976	11.912	12.2	343.5	23.015	64.025	4.498	3.058	3.102	2.221	0.535	1.071	1.413		
21	2012	270.083	3899.5	0.23	2024.581	11.904	12.175	343.463	23.2	64.556	4.589	3.06	3.104	2.219	0.538	1.071	1.415		
22	2012	280.084	3896.6	0.29	2001.194	11.903	12.187	343.439	23.297	64.788	4.535	3.06	3.104	2.219	0.53	1.071	1.415		
23	2012	290.084	3894.2	0.24	2021.816	11.92	12.2	343.633	23.529	64.236	4.589	3.06	3.104	2.219	0.538	1.071	1.415		
24	2012	300.084	3891.4	0.28	2001.611	11.912	12.175	343.667	23.476	64.399	4.54	3.06	3.106	2.219	0.53	1.071	1.413		
25	2012	310.084	3888.8	0.26	2018.177	11.908	12.237	343.134	23.152	65.075	4.576	3.06	3.106	2.219	0.53	1.071	1.415		
26	2012	320.084	3886.5	0.23	1983.884	11.903	12.213	343.399	23.048	64.873	4.496	3.06	3.106	2.217	0.529	1.071	1.417		
27	2012	330.084	3884	0.25	2009.336	11.904	12.175	343.295	22.969	65.378	4.554	3.06	3.108	2.219	0.52	1.071	1.417		
28	2012	340.085	3881.4	0.26	1980.587	11.897	12.213	343.386	22.956	65.335	4.486	3.06	3.108	2.219	0.523	1.071	1.417		
29	2012	350.085	3878.5	0.29	2010.932	11.908	12.225	343.48	22.834	65.136	4.559	3.06	3.108	2.219	0.521	1.073	1.415		
30	2012	360.085	3876.2	0.23	1985.246	11.871	12.187	343.417	22.756	65.672	4.487	3.06	3.11	2.217	0.521	1.071	1.415		
31	2012	370.148	3873.8	0.24	1981.728	11.896	12.175	343.629	22.764	65.589	4.489	3.06	3.112	2.217	0.518	1.071	1.413		
32	2012	380.148	3871.1	0.27	2018.533	11.88	12.2	343.763	23.079	65.406	4.566	3.062	3.116	2.215	0.521	1.069	1.411		
33	2012	390.148	3868.6	0.25	2001.871	11.863	12.187	343.566	22.941	66.025	4.522	3.062	3.118	2.217	0.521	1.069	1.409		
34																			
35	2012			0.256667	2002.249	11.9341	12.18939	343.3792	22.90787	63.72726	4.549742	3.0608	3.1128	2.217	0.5204	1.0706	1.4126		

Figure D-2: Average Fueling Calculation

7. Format "Summary" sheet

- Copy Row 1 (data labels) and the average row of each data set to the "Summary" sheet (Figure D-3)
- Delete "Time" and "Fuel (g)" columns
- Insert 12 Columns between "HP" and "O2" (Figure D-4)
- Name the blank columns: kW, BMEP (kPa), BSFC (g/kW-h), T_eff (%), O2 (%), NOx (ppm), CO2 (%), HC (ppm), SO2 (ppm), CO (ppm), and Corr_NoX (ppm) respectively (Figure D-5)

	A	B	C	D	E	F	G	H	I	J	K	L	M	N	O	P	Q	R
1	Note / SetTime (s)	Fuel (g)	g/s	RPM	Torque	Airflow	EGT	Air T	Oil T	HP	O2	Nox	CO2	HC	SO2	CO		
2	2012		0.256667	2002.249	11.9341	12.18939	343.3792	22.90787	63.72726	4.549742	3.0608	3.1128	2.217	0.5204	1.0706	1.4126		
3	2112		0.269	2100.086	11.97355	12.68881	350.616	22.92735	68.75597	4.787774	3.0544	3.0484	2.225	0.5236	1.0706	1.3958		
4	2212		0.280333	2205.332	11.97268	13.21468	354.3361	23.02871	71.98374	5.02729	3.0724	2.9808	2.209	0.5456	1.0698	1.3848		
5	2312		0.293667	2298.066	12.01177	13.68535	359.3066	23.08813	72.385	5.255903	3.082	2.8856	2.206	0.5636	1.0718	1.3874		
6	2412		0.306452	2398.467	12.00216	14.35781	365.853	23.38155	74.31403	5.481194	3.0932	2.7866	2.1898	0.58	1.073	1.409		
7	2512		0.319	2503.69	12.00477	14.97071	372.9438	23.47068	75.43174	5.722742	3.0968	2.7066	2.1854	0.5774	1.0734	1.4062		
8	2612		0.331667	2603.239	12.01868	15.49739	378.4919	23.62016	76.30048	5.957258	3.1136	2.6526	2.173	0.5224	1.073	1.365		
9	2712		0.35	2703.821	12.01535	16.36855	385.8009	23.78245	77.40365	6.185677	3.0952	2.595	2.191	0.4912	1.0676	1.335		
10	2812		0.372333	2808.082	12.05845	16.91494	401.2705	24.14087	81.21394	6.44729	3.076	2.5458	2.2074	0.509	1.0662	1.345		
11	2912		0.389333	2898.898	12.03045	17.29029	409.4123	24.44858	82.95545	6.640258	3.084	2.4978	2.2006	0.481	1.0666	1.3206		
12	3012		0.407667	2999.693	11.99471	17.89919	419.3523	24.76797	83.92987	6.850935	3.094	2.4202	2.1914	0.4712	1.065	1.315		
13	2512		0.319032	2500.871	11.96016	14.99206	376.3798	24.58065	78.90923	5.695097	3.0992	2.7094	2.183	0.6898	1.0778	1.4386		

Figure D-3: Summary Data Sheet

	C	D	E	F	G	H	I	J	K	L	M	N	O	P	Q	R	S	T
1	RPM	Torque	Airflow	EGT	Air T	Oil T	HP											
2	2002.249	11.9341	12.18939	343.3792	22.90787	63.72726	4.549742											
3	2100.086	11.97355	12.68881	350.616	22.92735	68.75597	4.787774											
4	2205.332	11.97268	13.21468	354.3361	23.02871	71.98374	5.02729											
5	2298.066	12.01177	13.68535	359.3066	23.08813	72.385	5.255903											
6	2398.467	12.00216	14.35781	365.853	23.38155	74.31403	5.481194											
7	2503.69	12.00477	14.97071	372.9438	23.47068	75.43174	5.722742											
8	2603.239	12.01868	15.49739	378.4919	23.62016	76.30048	5.957258											
9	2703.821	12.01535	16.36855	385.8009	23.78245	77.40365	6.185677											
10	2808.082	12.05845	16.91494	401.2705	24.14087	81.21394	6.44729											
11	2898.898	12.03045	17.29029	409.4123	24.44858	82.95545	6.640258											
12	2999.693	11.99471	17.89919	419.3523	24.76797	83.92987	6.850935											
13	2500.871	11.96016	14.99206	376.3798	24.58065	78.90923	5.695097											

Figure D-4: Summary Formatting: Insert 12 Columns

	C	D	E	F	G	H	I	J	K	L	M	N	O	P	Q	R	S	T
1	RPM	Torque	Airflow	EGT	Air T	Oil T	HP	Kw	BMEP (kPa)	BSFC(g/kw-h)	T_eff (%)	O2 %	Nox ppm	CO2 %	HC ppm	SO2 ppm	CO ppm	Corr_NoX ppm
2	2002.249	11.9341	12.18939	343.3792	22.90787	63.72726	4.549742											
3	2100.086	11.97355	12.68881	350.616	22.92735	68.75597	4.787774											
4	2205.332	11.97268	13.21468	354.3361	23.02871	71.98374	5.02729											
5	2298.066	12.01177	13.68535	359.3066	23.08813	72.385	5.255903											
6	2398.467	12.00216	14.35781	365.853	23.38155	74.31403	5.481194											
7	2503.69	12.00477	14.97071	372.9438	23.47068	75.43174	5.722742											
8	2603.239	12.01868	15.49739	378.4919	23.62016	76.30048	5.957258											
9	2703.821	12.01535	16.36855	385.8009	23.78245	77.40365	6.185677											
10	2808.082	12.05845	16.91494	401.2705	24.14087	81.21394	6.44729											
11	2898.898	12.03045	17.29029	409.4123	24.44858	82.95545	6.640258											
12	2999.693	11.99471	17.89919	419.3523	24.76797	83.92987	6.850935											
13	2500.871	11.96016	14.99206	376.3798	24.58065	78.90923	5.695097											

Figure D-5: Summary Formatting: Column Titles

8. Summary Calculations

a. Power (kilowatts)

$$Power_{kW} = Power_{HP} \times 0.7457$$

$$\text{Ex: } Power_{kW} = 4.549742_{HP} \times 0.7457 = 3.39274 \text{ (kW)}$$

b. Brake Mean Effective Pressure (kilopascals)

$$BMEP_{kPa} = \frac{Power(kW) * 2000}{V_d(dm^3) * RPM / 60(\frac{sec}{min})}$$

$$\text{Ex: } BMEP(kPa) = \frac{3.392743(kW) * 2000}{0.418(liters) * 2002.249(rpm) / 60} = 486.45 \text{ (kPa)}$$

c. Brake Specific Fuel Consumption (grams fuel per kilowatt hour)

$$BSFC(\frac{g}{kW*hour}) = \frac{Fuelling \frac{g}{s} * 3600 \frac{sec}{hr}}{Power(kW)}$$

$$\text{Ex: } BSFC \frac{g}{kW*hour} = \frac{0.25667 \frac{g}{s} * 3600 \frac{sec}{hr}}{3.39274 \text{ kW}} = 272.35 \frac{g}{kW*hour}$$

d. Oxygen Content (percentage)

$$O_2 (\%) = (O_2 \text{ volts} - 1) \times \frac{Range}{4 \text{ volts}}$$

$$\text{Ex: } O_2 (\%) = (3.0608 \text{ volts} - 1) \times \frac{25\%}{4 \text{ volts}} = 12.88 (\%)$$

e. Nitrides of Oxygen Content (parts per million)

$$NO_x \text{ ppm} = (NO_x \text{ volts} - 1) \times \frac{\text{Range}}{4 \text{ volts}}$$

$$\text{Ex: } NO_x \text{ ppm} = (3.1128 \text{ volts} - 1) \times \frac{1000 \text{ ppm}}{4 \text{ volts}} = 528.2 \text{ (ppm)}$$

f. Carbon Dioxide Content (percent)

$$CO_2 \% = (CO_2 \text{ volts} - 1) \times \frac{\text{Range}}{4 \text{ volts}}$$

$$\text{Ex: } CO_2 \% = (2.217 \text{ volts} - 1) \times \frac{20 \%}{4 \text{ volts}} = 6.085 \text{ (\%)}$$

g. Unburned Hydrocarbon Content (parts per million)

$$HC \text{ ppm} = HC \text{ volts} \times \frac{\text{Range}}{5 \text{ volts}}$$

$$\text{Ex: } HC \text{ ppm} = 0.5204 \text{ volts} \times \frac{3000 \text{ ppm}}{5 \text{ volts}} = 312.24 \text{ (ppm)}$$

h. Oxides of Sulphur Content (parts per million)

$$SO_2 \text{ ppm} = (SO_2 \text{ volts} - 1) \times \frac{\text{Range}}{4 \text{ volts}}$$

$$\text{Ex: } SO_2 \text{ ppm} = (1.0706 \text{ volts} - 1) \times \frac{200 \text{ ppm}}{4 \text{ volts}} = 3.53 \text{ ppm}$$

i. Carbon Monoxide Content (parts per million)

$$CO \text{ ppm} = (CO \text{ volts} - 1) \times \frac{Range}{4 \text{ volts}}$$

$$\text{Ex: } CO \text{ ppm} = (1.4126 \text{ volts} - 1) \times \frac{5000 \text{ ppm}}{4 \text{ volts}} = 515.75 \text{ (ppm)}$$

j. Thermal Conversion Efficiency (percent)

$$\eta_f = \frac{3600}{bsfc \frac{g}{kW \cdot h} * Q_{HV} \frac{MJ}{kg}} * 100\%$$

$$\text{Ex: } \eta_f = \frac{3600}{272.346 \frac{g}{kW \cdot h} * 38.4411 \frac{MJ}{kg}} * 100\% = 34.3863\%$$

9. Weather Corrections

a. Dew Point (degrees celsius)

$$DP_{Celsius} = (DP_{Fahrenheit} - 32) \frac{5}{9}$$

$$\text{Ex: } DP_{Celsius} = (60.1_{Fahrenheit} - 32) \frac{5}{9} = 15.611_{Celsius}$$

b. Saturation Vapor Pressure (millibars)

$$e = \min(e_{water}, e_{ice})$$

$$e_{water, ice} =$$

$$a_0 + DP_c \quad a_1 + DP_c \quad a_2 + DP_c \quad a_3 + DP_c \quad a_4 + DP_c \quad a_5 + DP_c * a_6$$

where:

Water			ICE		
a0	6.1077999610		a0	6.1091779560	
a1	4.4365185210	E-01	a1	5.0346989700	E-01
a2	1.4289458050	E-02	a2	1.8860134080	E-02
a3	2.6506484710	E-04	a3	4.1762237160	E-04
a4	3.0312403960	E-06	a4	5.8247202800	E-06
a5	2.0340809480	E-08	a5	4.8388031740	E-08
a6	6.1368209290	E-11	a6	1.8388269040	E-10

$$\begin{aligned} \text{Ex: } e_{\text{water}} &= 17.7244_{\text{mb}} \\ e_{\text{ice}} &= 20.5476_{\text{mb}} \\ e &= \min 17.7244, 20.5476 = 17.7244_{\text{mb}} \end{aligned}$$

c. Barometric Pressure (millibars)

$$P_{mb} = P_{\text{inHg}} * 33.86389$$

$$\text{Ex: } P_{mb} = 29.37_{\text{inHg}} * 33.86389 = 994.5824_{\text{mb}}$$

d. Vapor Pressure Enhancement Factor

$$\text{EnhanceDew} = \min(f_{\text{water}}, f_{\text{ice}})$$

$$f_{\text{water}} = \frac{1 + 0.00041 + P_{mb} (3.48 * 10^{-6} + 7.4 * 10^{-10} DP_c + 30.6 - 0.038 * P_{mb}^2)}{1}$$

$$f_{\text{ice}} = \frac{1 + 0.00048 + P_{mb} (3.47 * 10^{-6} + 5.9 * 10^{-10} DP_c + 23.8 - 0.031 * P_{mb}^2)}{1}$$

$$\begin{aligned} \text{Ex: } f_{\text{water}} &= 1.00392 \\ f_{\text{ice}} &= 1.00397 \\ \text{EnhanceDew} &= \min 1.00392, 1.00397 = 1.00392 \end{aligned}$$

- e. Enhanced Partial Saturation Vapor Pressure (inches mercury)

$$PsatDewCorr_{inhg} = \frac{e_{mb} * EnhanceDew}{33.86389}$$

$$\text{Ex: } PsatDewCorr_{inhg} = \frac{17.7244_{mb} * 1.00392}{33.86389} = 0.525453_{inHg}$$

- f. Specific Humidity (grams per pound)

$$SpecificHumidity_{grperlb} = \frac{4347.8 * PsatDewCorr_{inHg}}{Baro_{inHg} - PsatDewCorr_{inHg}}$$

$$\text{Ex: } SpecificHumidity_{grperlb} = \frac{4347.8 * 0.525453_{inHg}}{29.37_{inHg} - 0.525453_{inHg}} = 79.203_{grperlb}$$

- g. Nox Correction Factor

$$Nox_{CF} = \frac{1}{1 - .0026 \text{ SpecificHumidity}_{grperlb} - 75}$$

$$\text{Ex: } Nox_{CF} = \frac{1}{1 - .0026 \text{ } 79.203_{grperlb} - 75} = 1.011$$

- h. Corrected Nox (parts per million)

$$Nox_{Corr} = Nox \text{ ppm} \times Nox_{CF}$$

$$\text{Ex: } Nox_{Corr} = 528.2 \text{ ppm} \times 1.011 = 534.01 \text{ (ppm)}$$

APPENDIX E: FUEL CHANGING PROCEDURE

Draining the System

1. From the toolbox, obtain the following:
 - a. One pair of rubber gloves
 - b. ¼" nut driver (red handle)
 - c. 7/16" wrench
2. Obtain a funnel and the proper fuel can to empty the unused fuel back into.
3. Open the fuel shut off valve on the fuel stand.
4. Make sure the battery disconnect is in the "off" position.
5. Turn the ignition key to the "On" position.
6. With the ¼" nut driver, loosen the fuel line hose clamp at fuel pump located on the backside of the Yanmar engine.
7. Place the fuel can in a position where you will be able to insert the fuel line into the can.
8. Squeeze the fuel line shut as close to the end as possible to prevent leakage. While squeezing the line, slide the line off the fuel pump, then place directly into the fuel can.
9. While holding the fuel line in the fuel can, reach down and turn the battery disconnect to the "on" position. With the ignition key also "on" from the previous step, this will engage the electronic fuel pump and transfer fuel from the system to the tank you are holding.
10. When the system starts to pump air, turn the battery disconnect back to the "off" position and remove the safety key.
11. Leave the fuel line disconnected but make sure it is facing in the upward position.
12. The next step is to drain the fuel filter and line coil.
13. Slide the fuel temperature conditioner to the back of the fuel stand and away from the fuel filter so the filter can be drained without fuel getting on the conditioner.

14. Remove the coil from the conditioner and let it rest above the fuel filter.
15. Position the fuel tank and funnel to catch fuel draining from the bottom of the filter.
16. Remove the drain plug with the 7/16" wrench and allow the fuel to drain for 2-3 minutes. While doing this shift the position of the coil to ensure all fuel is removed.
17. Replace the filter drain plug and the fuel coil back into the conditioner.

Filling and Purging

The following steps involve filling the fuel system with new fuel and purging air from the lines.

1. Fill the system fuel tank on the fuel stand.
2. Ensure the fuel valve is still "open" and the ignition key is in the "on" position with the battery disconnect in the "off" position
3. At the engine side of the fuel line, hold the disconnected line in the fuel can and turn the battery disconnect to the "on" position. This will engage the electronic fuel pump and start to refill the system.
4. After about one minute the fuel will start to drain into the fuel can. Wait until all the air is bled from the line before turning the battery disconnect to the "off" position.
5. While turning the battery disconnect to the "off" position, pinch the fuel line with your fingers to prevent air from re-entering the line, and slide the line back onto the fuel pump. Some air is inevitable.
6. Replace the hose clamp and tighten.
7. With a 17mm wrench loosen the fuel line at the fuel injector $\frac{3}{4}$ of a turn.
8. Place a towel in the area under and around the loosened end of the fuel line.

9. Engage the compression brake by pressing the lever down.
10. Turn the speed control knob to the “starting” position.
11. Turn the battery disconnect to the “on” position and turn the ignition key to engage the starter motor.
12. Continue to let the motor turn over for 30-45 seconds. This will allow any air in the fuel line to be bled out before entering the fuel injector.
13. Retighten the fuel injector line nut and dispose of the towel used to catch excess fuel.

APPENDIX F: PARTIAL PRESSURE CALCULATION

Convert Dew point temperature from Fahrenheit to Celsius (DP_C)

$$DP_{Celsius} = (DP_{Fahrenheit} - 32) \frac{5}{9}$$

$$\text{Ex: } DP_{Celsius} = (60.1_{Fahrenheit} - 32) \frac{5}{9} = 15.611_{Celsius}$$

Convert Barometric Pressure from inches mercury to milibars (P_{mb})

$$P_{mb} = P_{inHg} * 33.86389$$

$$\text{Ex: } P_{mb} = 29.37_{inHg} * 33.86389 = 994.5824_{mb}$$

Find the minimum vapor pressure (e) over water and ice:

$$e = \min(e_{water}, e_{ice})$$

$$e_{water, ice} = a_0 + DP_C \ a_1 + DP_C \ a_2 + DP_C \ a_3 + DP_C \ a_4 + DP_C \ a_5 + DP_C * a_6$$

Where:

Water		ICE	
a0	6.107799961	a0	6.109178
a1	0.443651852	a1	0.50347
a2	0.014289458	a2	0.01886
a3	0.000265065	a3	0.000418
a4	3.03124E-06	a4	5.82E-06
a5	2.03408E-08	a5	4.84E-08
a6	6.13682E-11	a6	1.84E-10

Ex: $e_{water} = 17.7244_{mb}$
 $e_{ice} = 20.5476_{mb}$
 $e = \min 17.7244, 20.5476 = 17.7244_{mb}$

Find the minimum vapor pressure enhancement factor (EnhanceDew) over water and ice.

$$EnhanceDew = \min(f_{water}, f_{ice})$$

$$f_{water} = 1 + 0.00041 + P_{mb} (3.48 * 10^{-6} + 7.4 * 10^{-10} DP_c + 30.6 - 0.038 * P_{mb}^2)$$

$$f_{ice} = 1 + 0.00048 + P_{mb} (3.47 * 10^{-6} + 5.9 * 10^{-10} DP_c + 23.8 - 0.031 * P_{mb}^2)$$

Ex: $f_{water} = 1.00392$
 $f_{ice} = 1.00397$
 $EnhanceDew = \min 1.00392, 1.00397 = 1.00392$

Find the Corrected Partial Pressure of Water Vapor (P_v)

$$P_v = e_{mb} * EnhanceDew * \frac{100_{Pa}}{1_{mb}}$$

$$\text{Ex: } P_v = 17.7244_{mb} * 1.00392 * \frac{100_{Pa}}{1_{mb}} = 1779.39_{Pa}$$

Find the Partial pressure of dry air in (Pa)

$$P_d = P_{mb} * \frac{100_{Pa}}{1_{mb}} - P_v$$

$$\text{Ex: } 994.5824_{mb} * \frac{100_{Pa}}{1_{mb}} - 1779.39_{Pa} = 97678.9_{Pa}$$

APPENDIX G: NOX CORRECTION FACTOR CALCULATION

Use Appendix F to find Saturation Vapor Pressure in milibars (e_{mb}) and the Vapor Pressure Enhancement Factor (EnhanceDew).

Find Enhanced Partial Saturation Vapor Pressure ($PsatDewCorr_{inhg}$)

$$PsatDewCorr_{inhg} = \frac{e_{mb} * EnhanceDew}{33.86389}$$

$$\text{Ex: } PsatDewCorr_{inhg} = \frac{17.7244_{mb} * 1.00392}{33.86389} = 0.525453_{inHg}$$

Find Specific Humidity in grams per pound

$$SpecificHumidity_{grperlb} = \frac{4347.8 * PsatDewCorr_{inHg}}{Baro_{inHg} - PsatDewCorr_{inHg}}$$

$$\text{Ex: } SpecificHumidity_{grperlb} = \frac{4347.8 * 0.525453_{inHg}}{29.37_{inHg} - 0.525453_{inHg}} = 79.203_{grperlb}$$

Find NO_x Correction Factor (NO_{xCF})

$$Nox_{CF} = \frac{1}{1 - .0026 \text{ SpecificHumidity}_{grperlb-75}}$$

$$\text{Ex: } Nox_{CF} = \frac{1}{1 - .0026 \cdot 79.203_{grperlb-75}} = 1.011$$

Find Corrected NO_x value (NO_{xCorr})

$$Nox_{Corr} = Nox \text{ ppm} \times Nox_{CF}$$

$$\text{Ex: } Nox_{Corr} = 528.2 \text{ ppm} \times 1.011 = 534.01 \text{ (ppm)}$$

APPENDIX H: ENGINEERING DRAWINGS

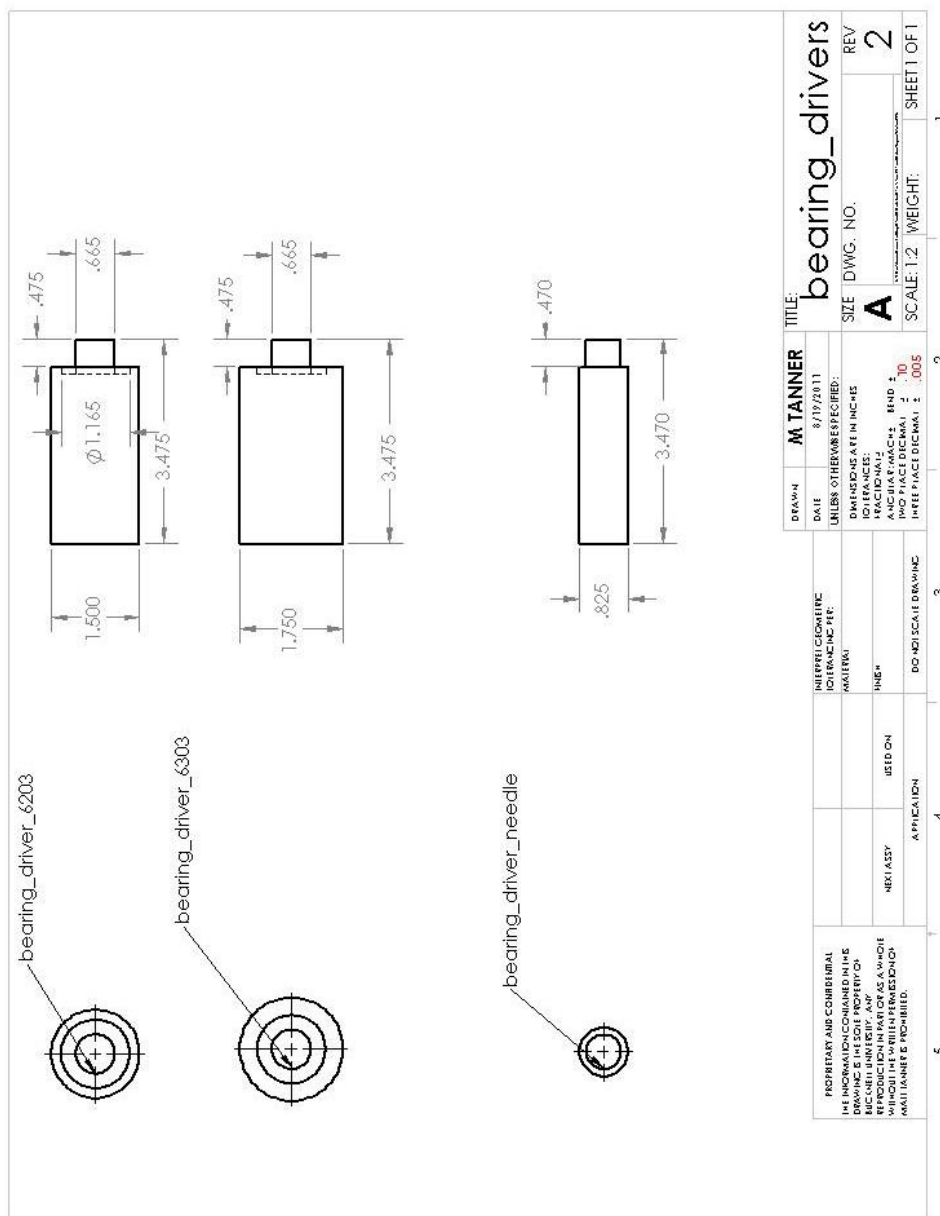


Figure H-1: Bearing Installation Drivers

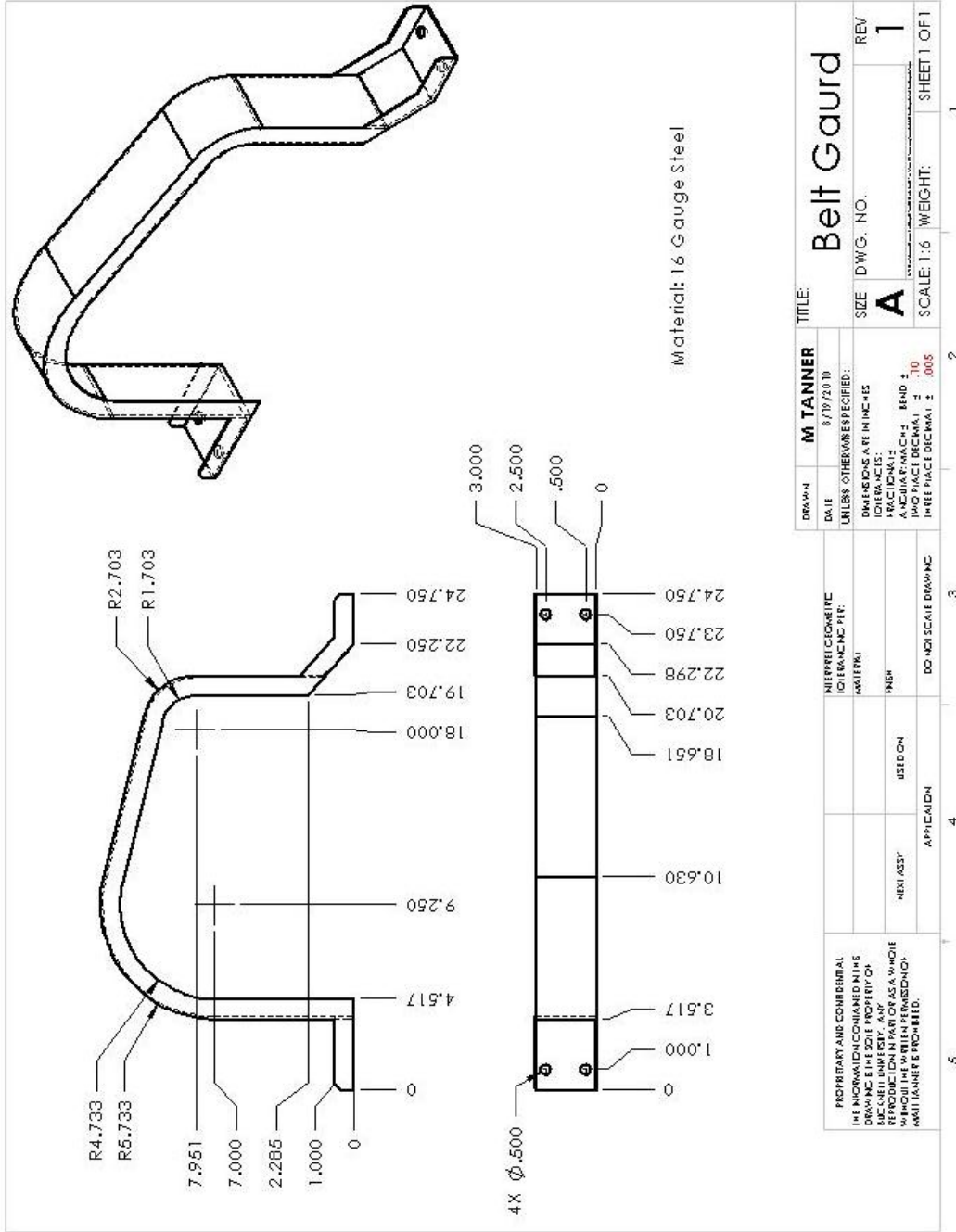


Figure H-2: Belt Guard

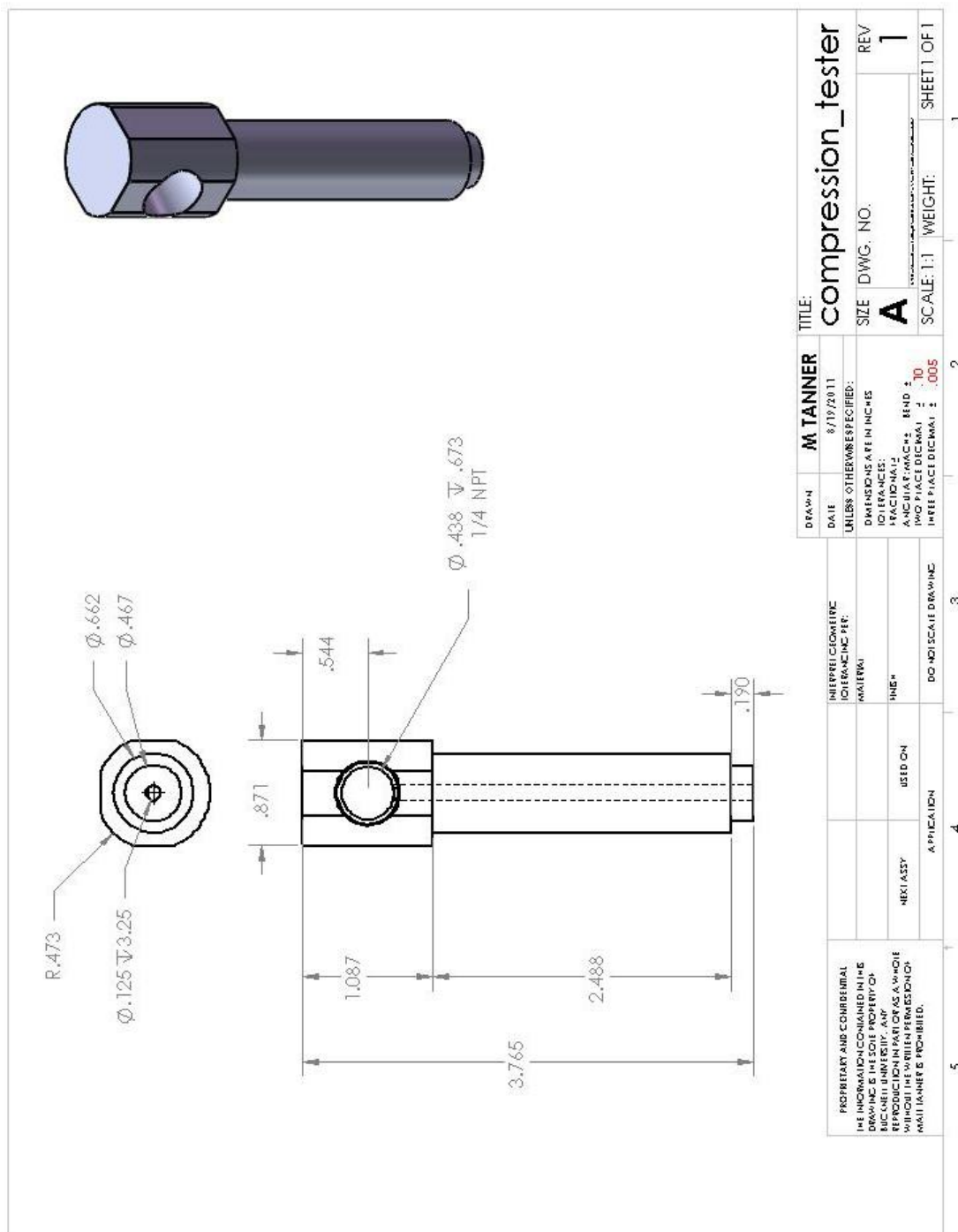


Figure H-3: Compression Tester

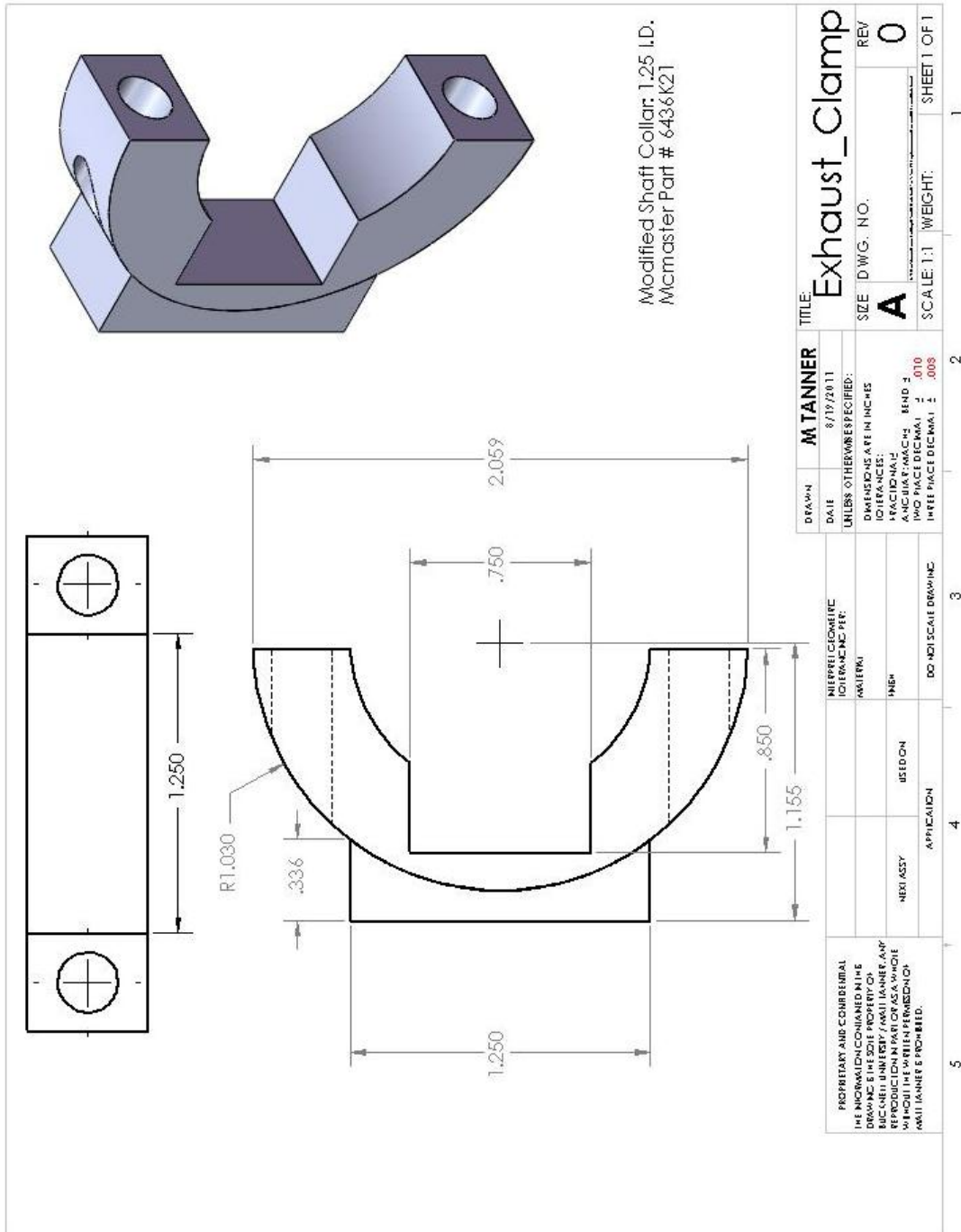


Figure H-4: Exhaust Clamp

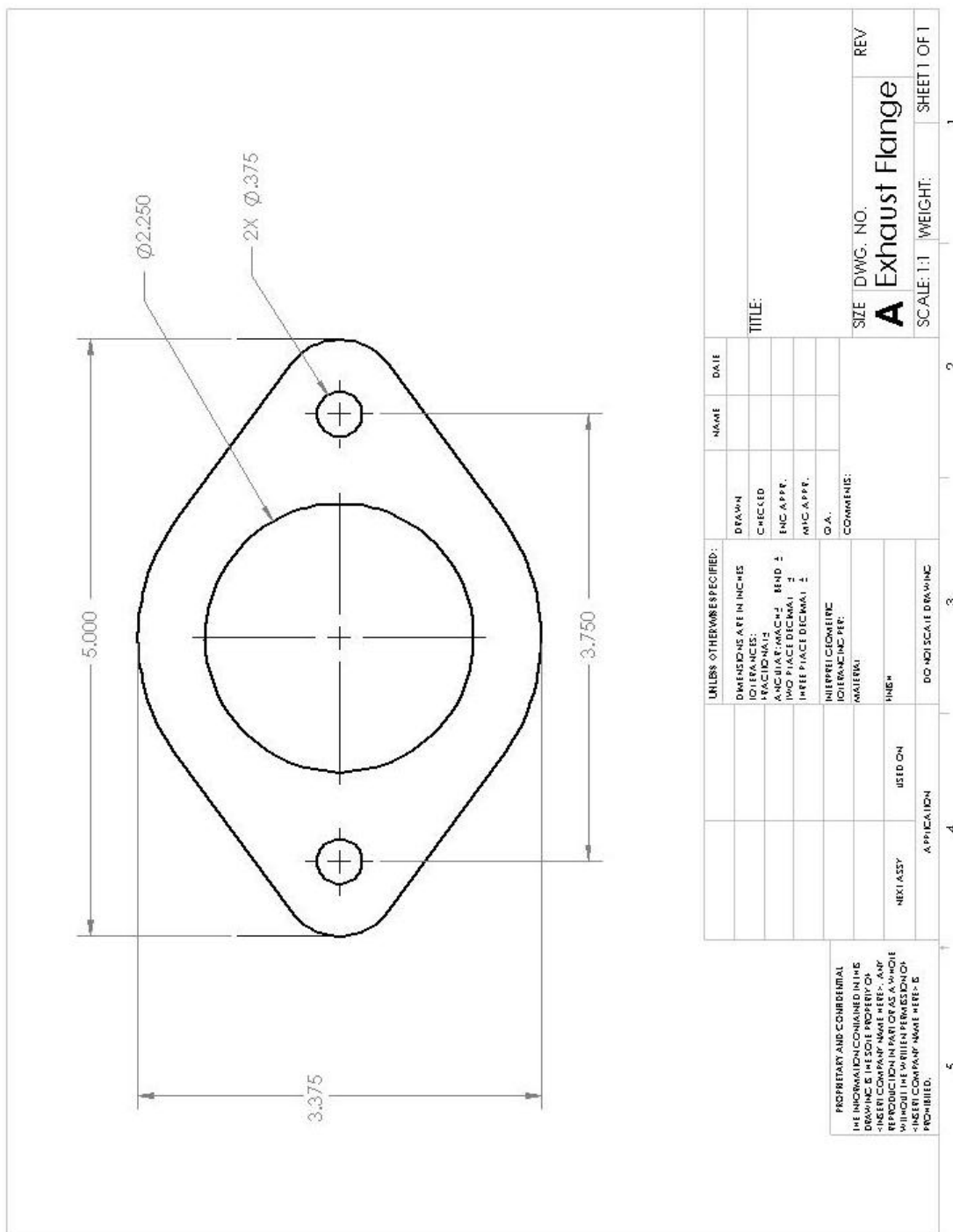


Figure H-5: Exhaust Flange

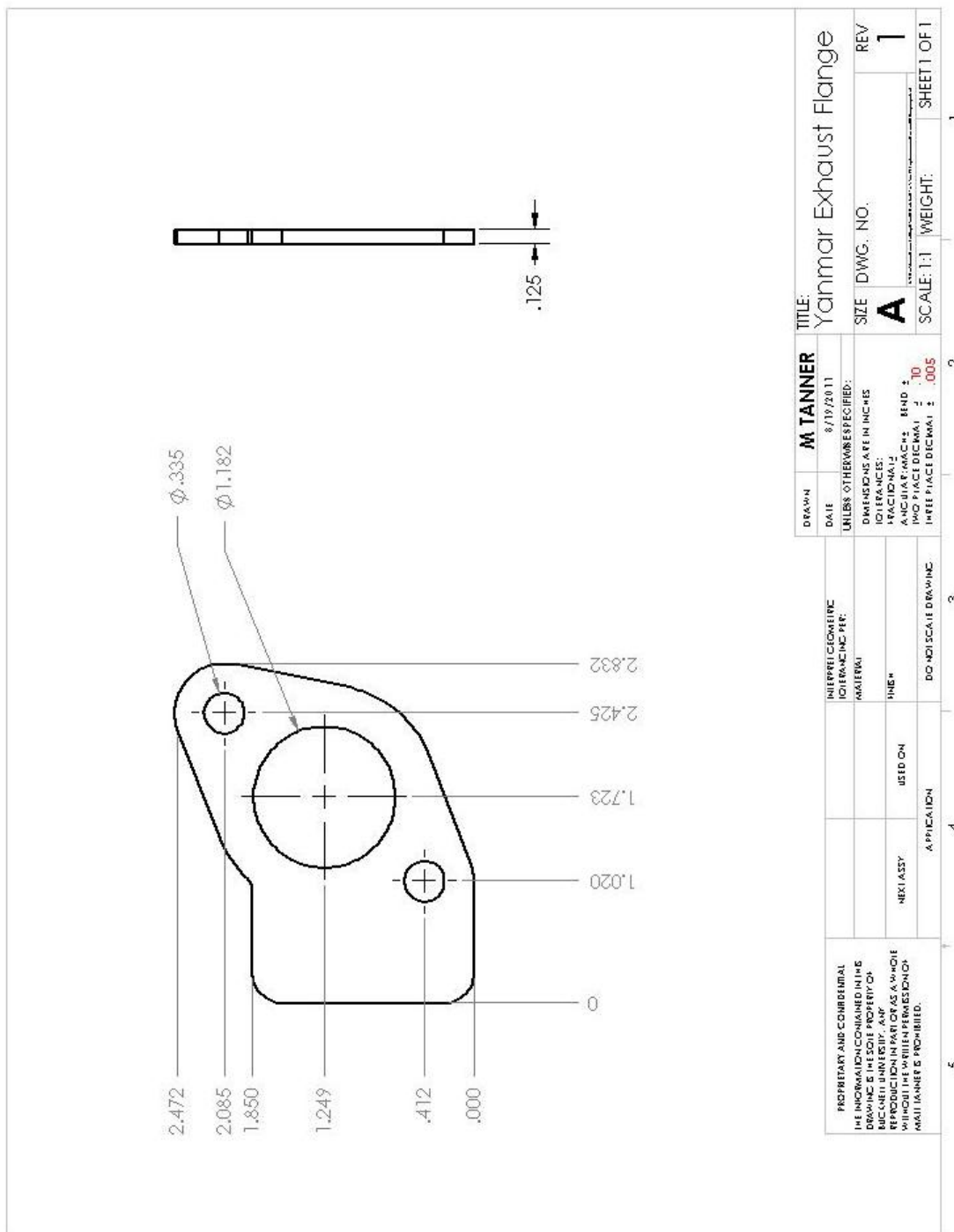


Figure H-6: Exhaust Flange Yanmar Side

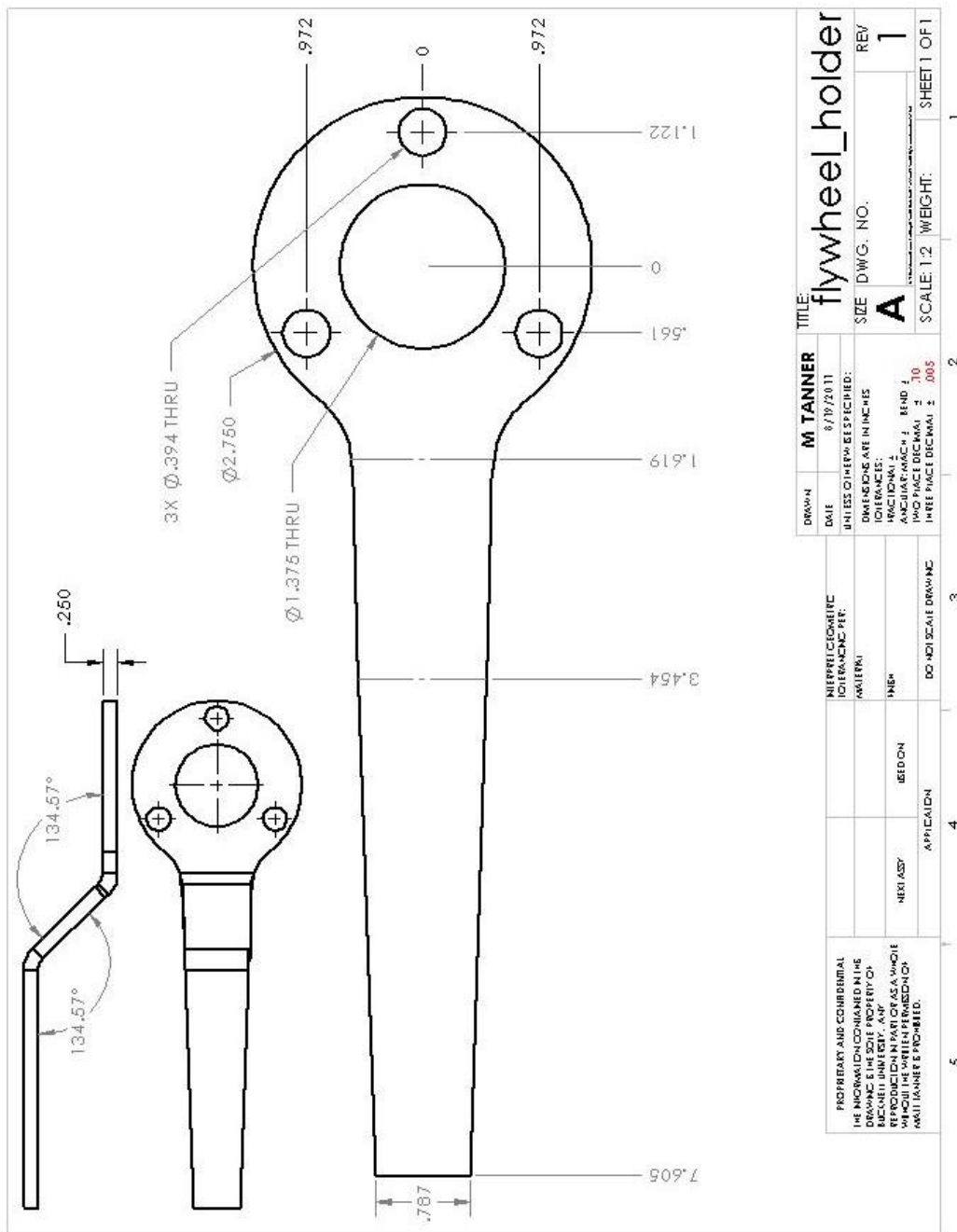


Figure H-7: Flywheel Holder

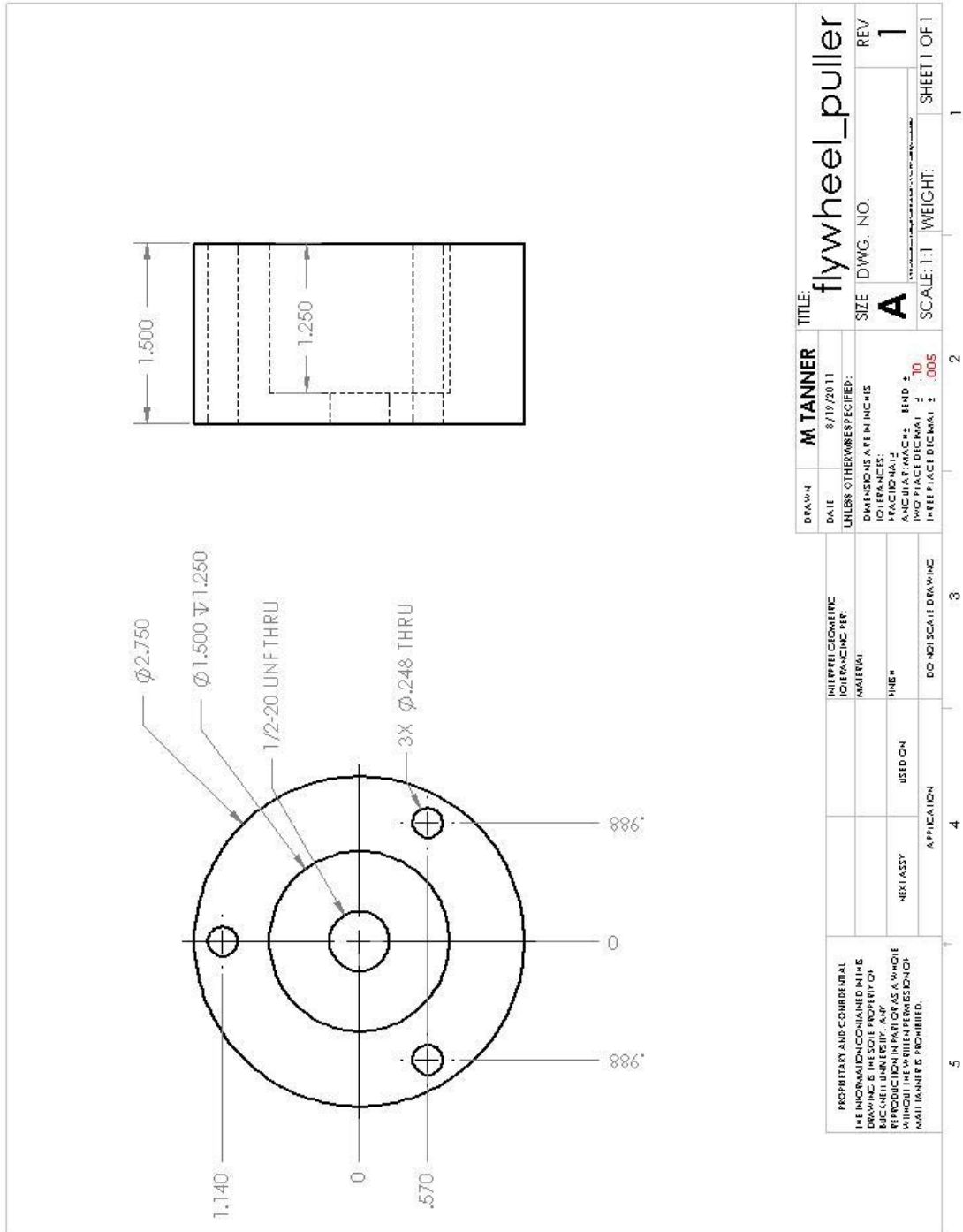


Figure H-8: Flywheel Puller

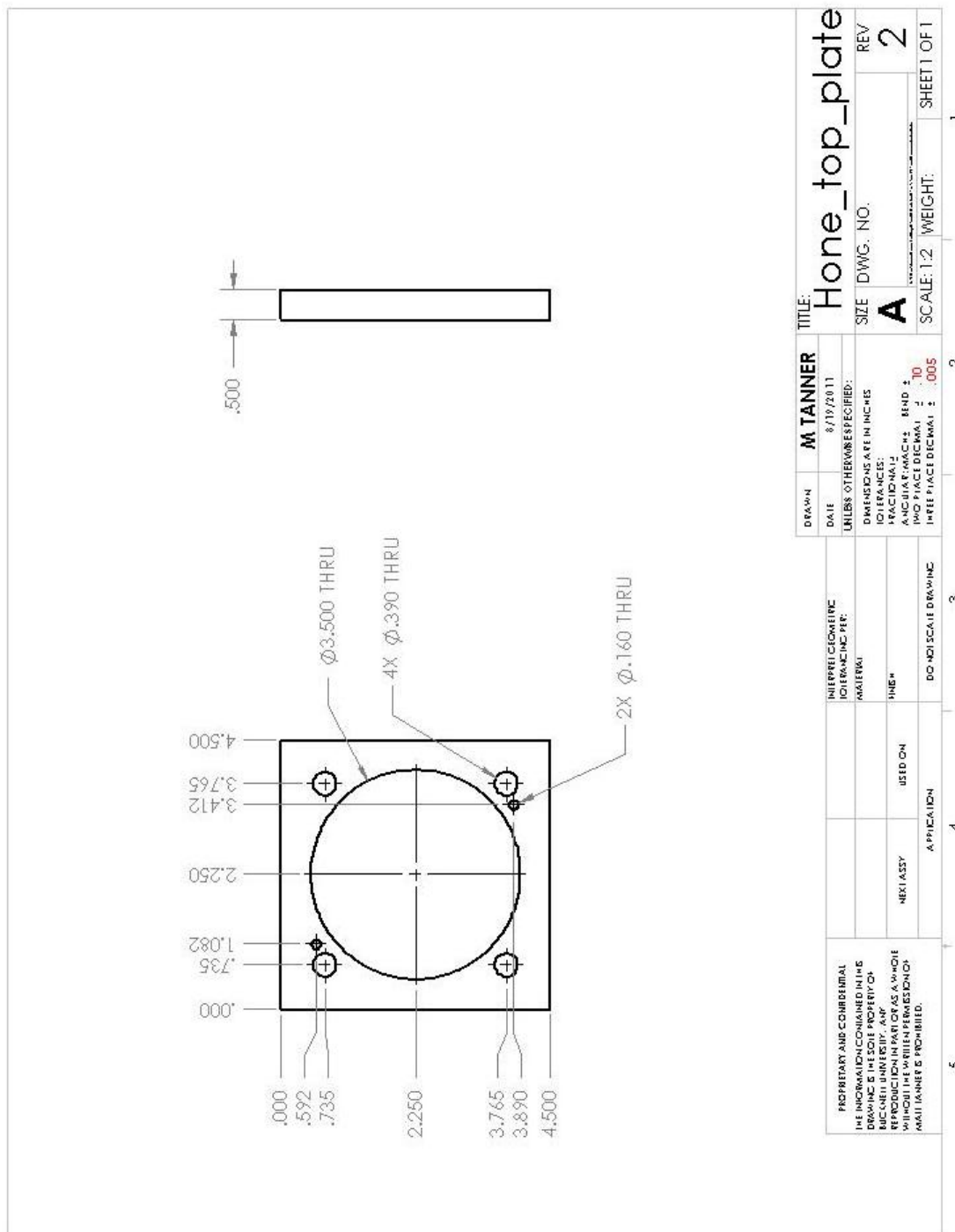


Figure H-9: Hone Top Plate

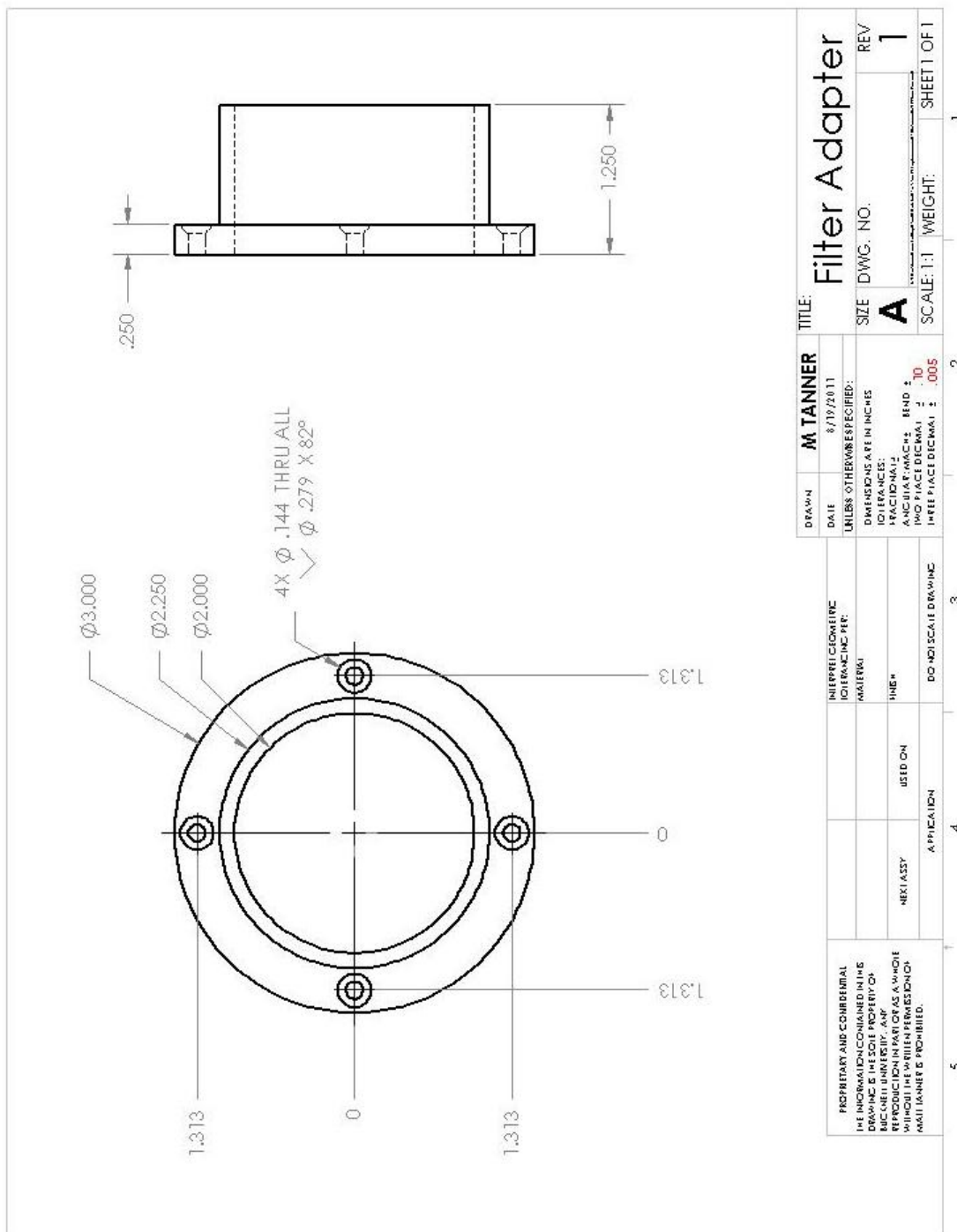


Figure H-10: Intake Filter Adapter

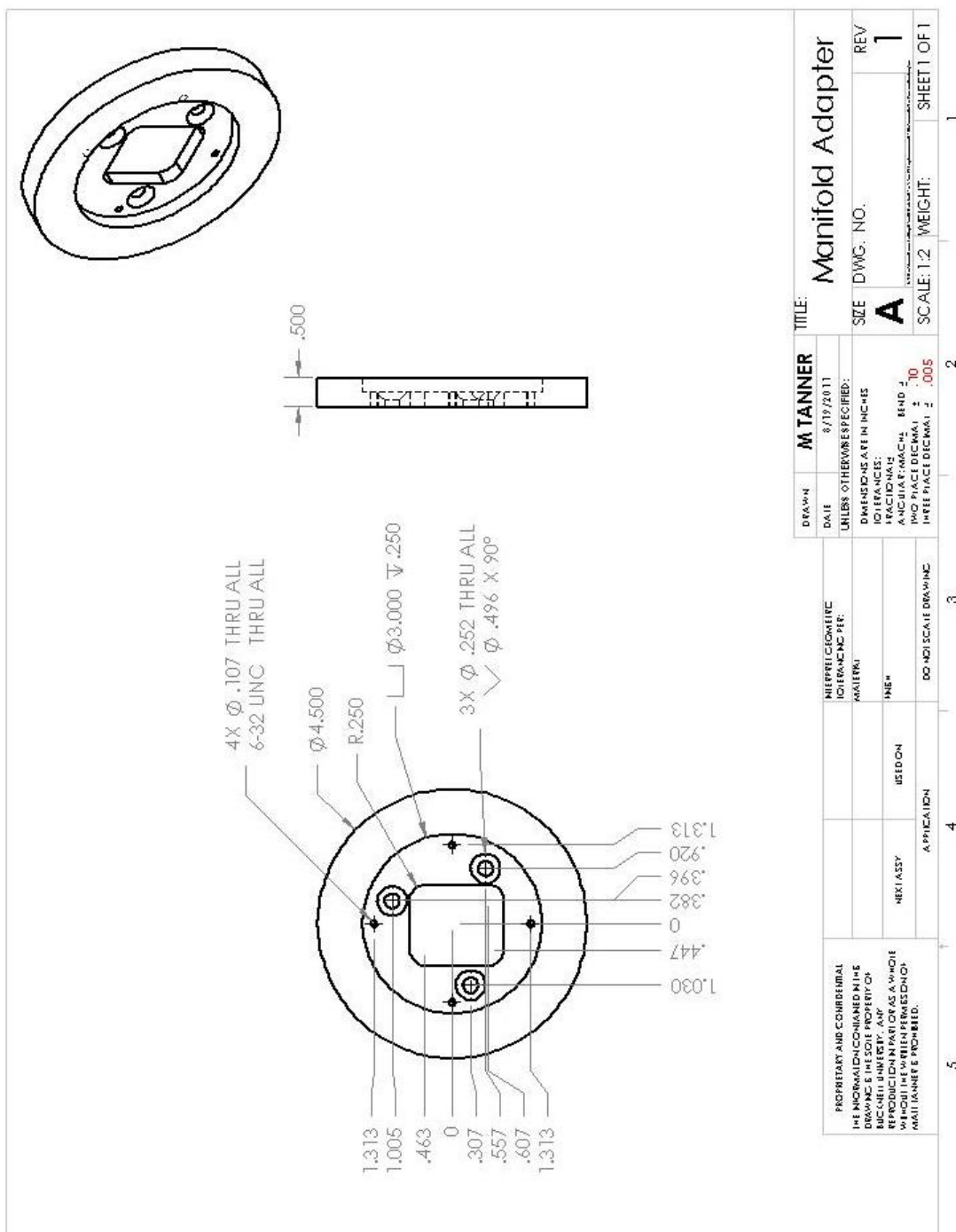


Figure H-11: Intake Manifold Adapter

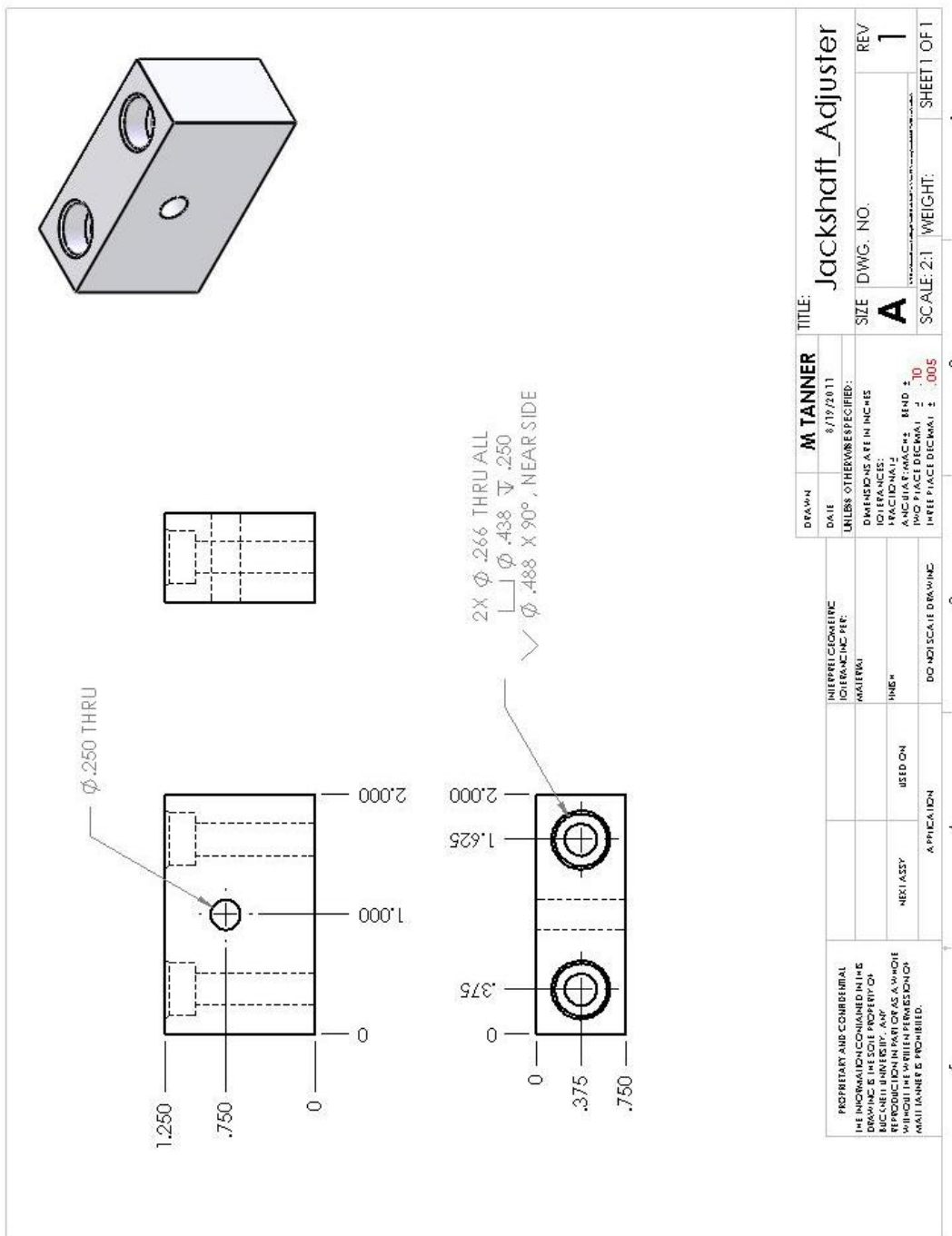


Figure H-12: Jackshaft Adjuster

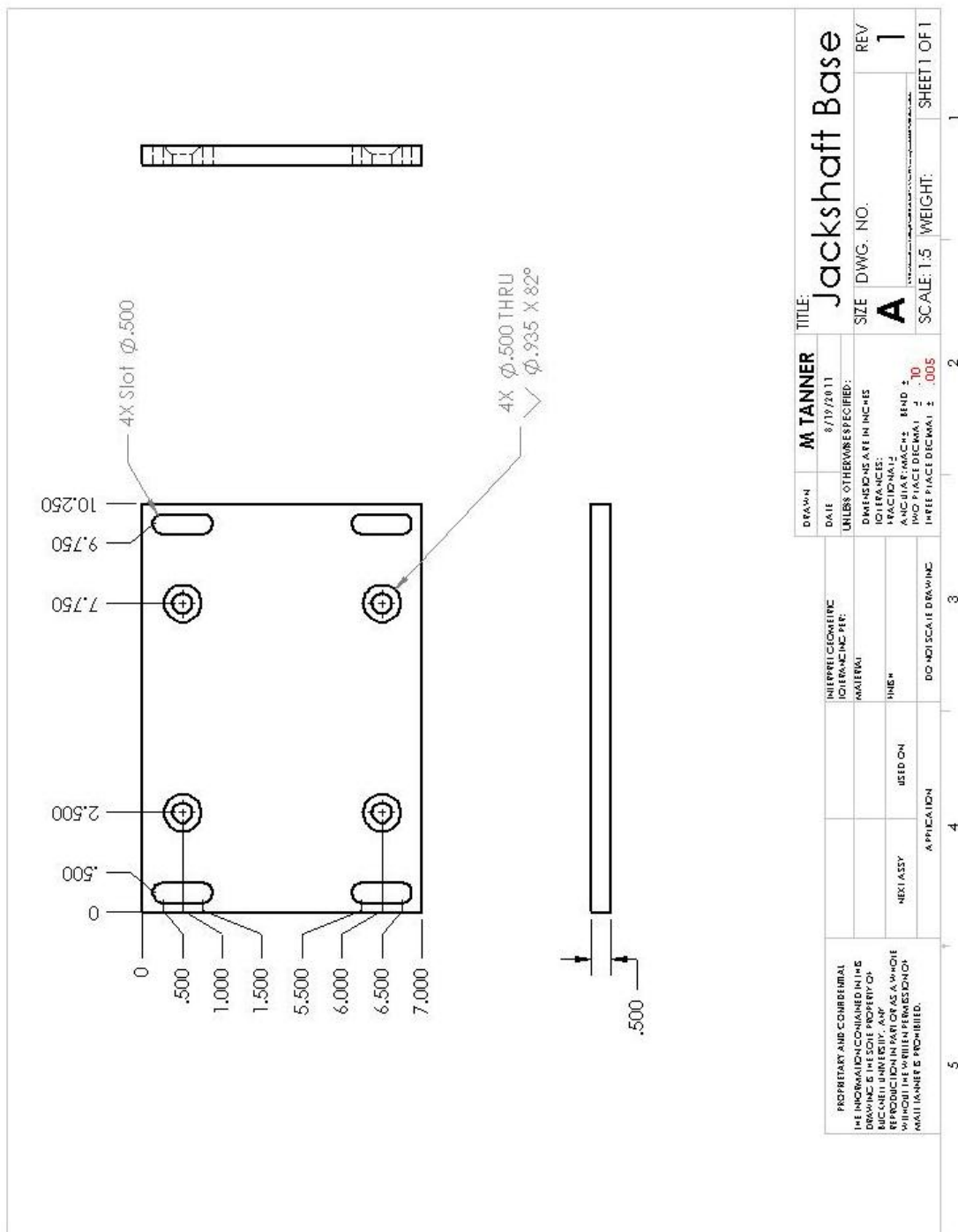


Figure H-13: Jackshaft Base Plate

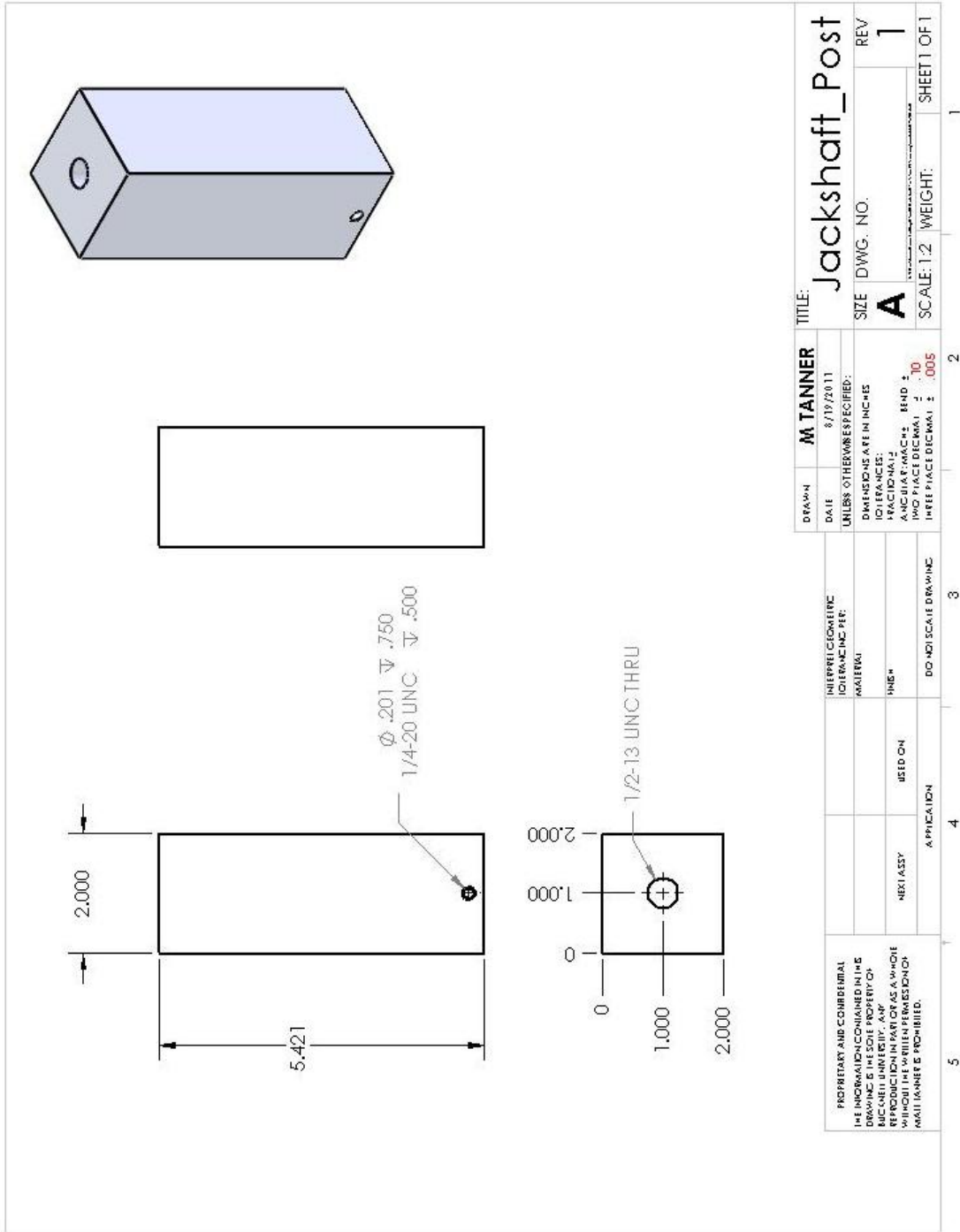


Figure H-14: Jackshaft Post

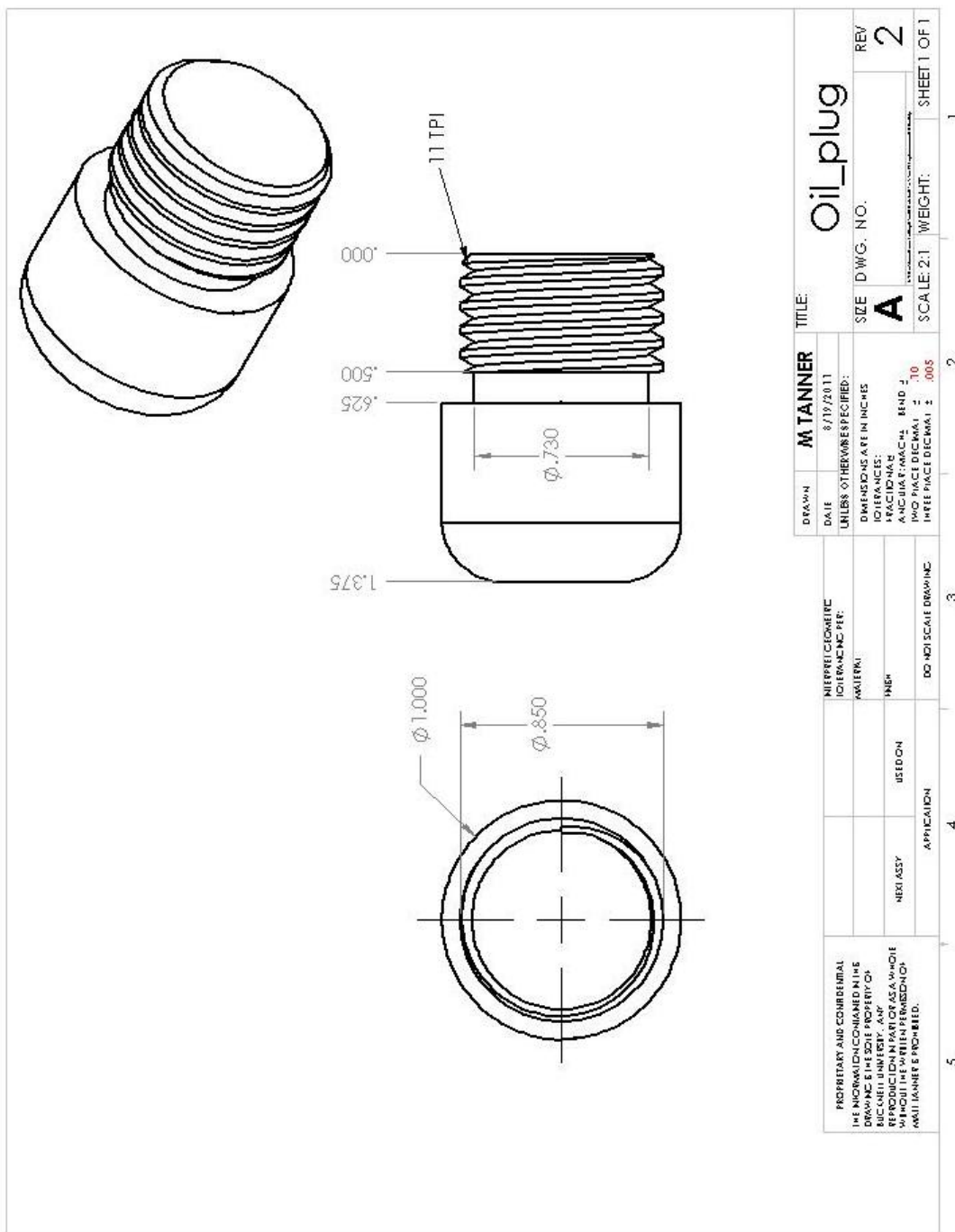


Figure H-15: Oil Plug

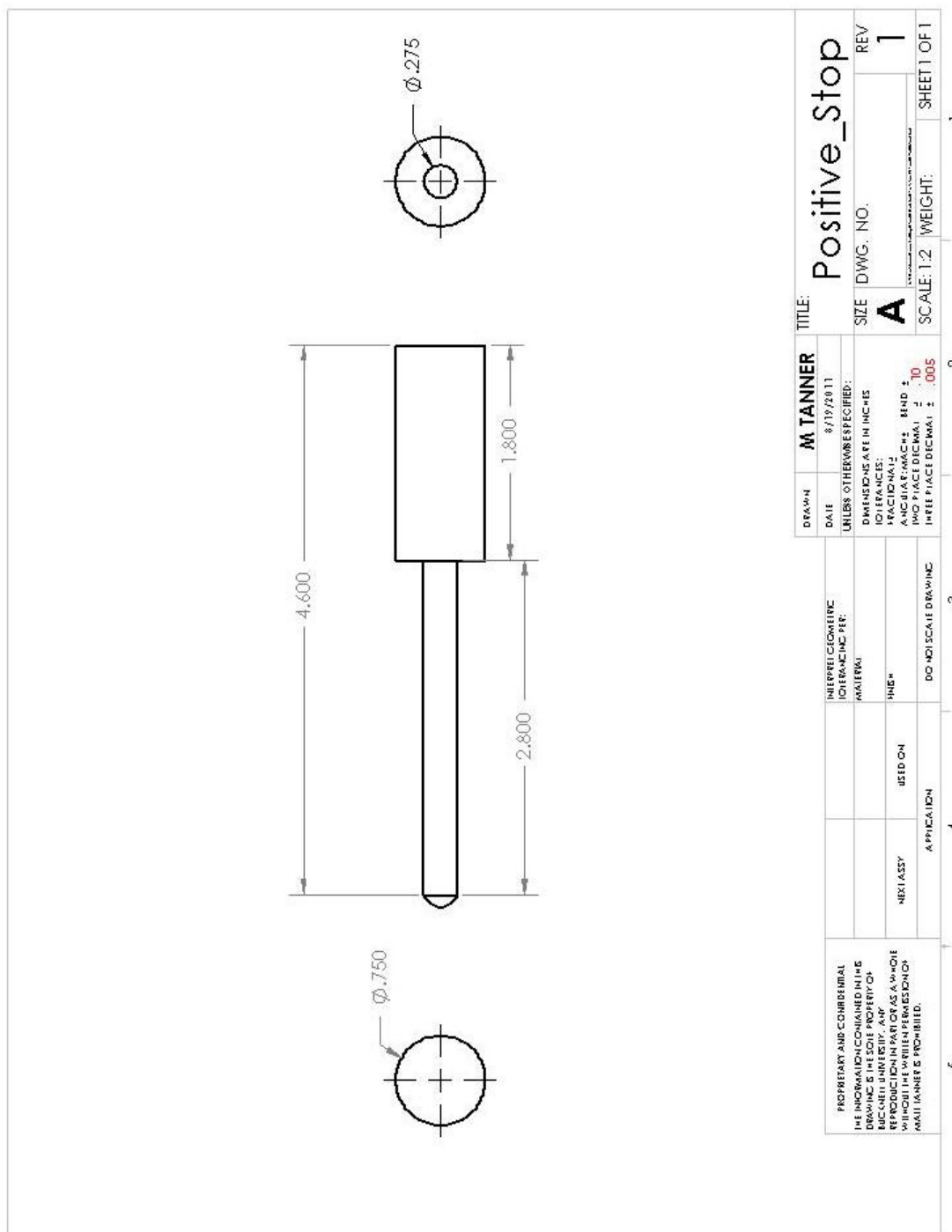


Figure H-16: Positive Piston Stop

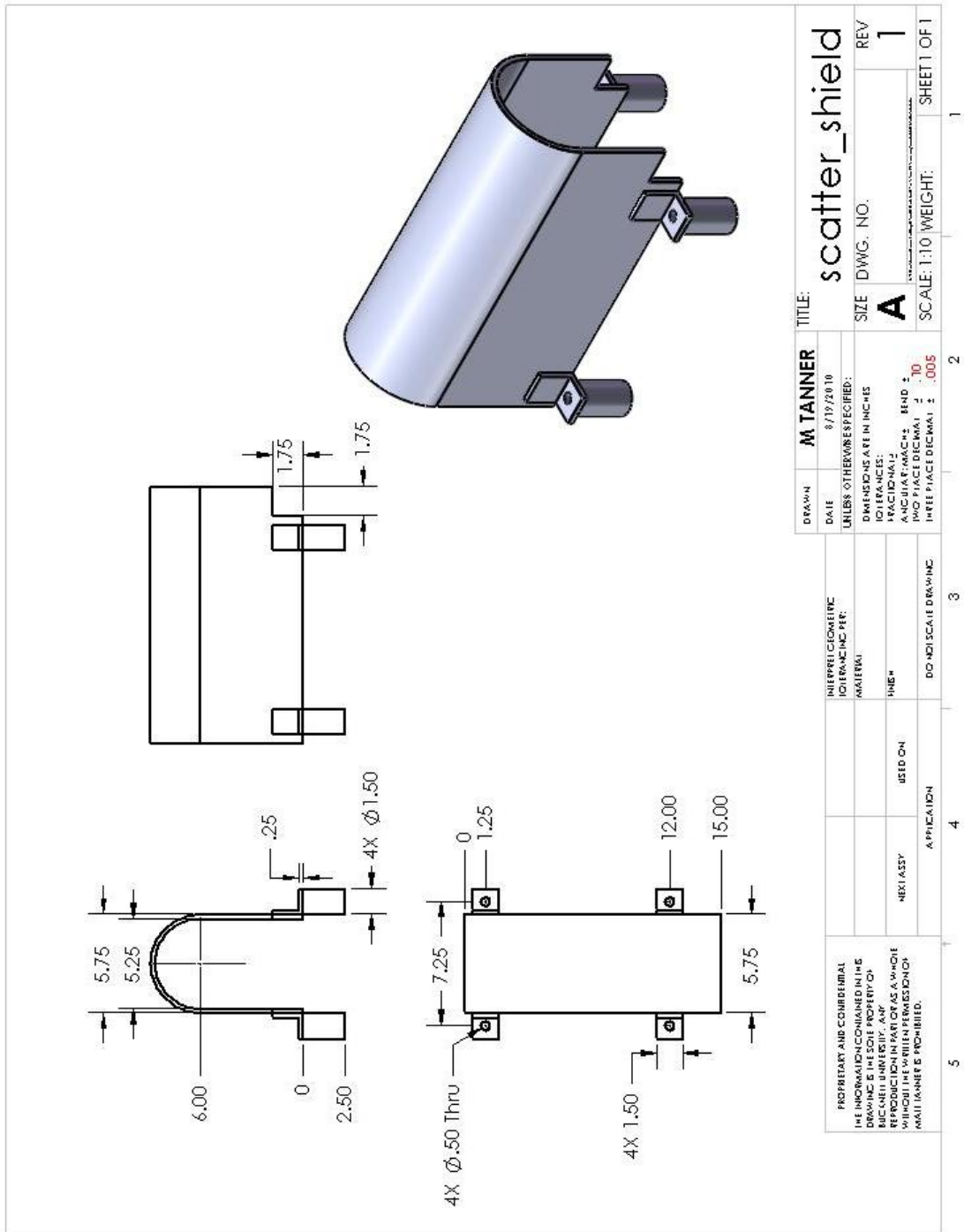


Figure H-17: Scatter Shield

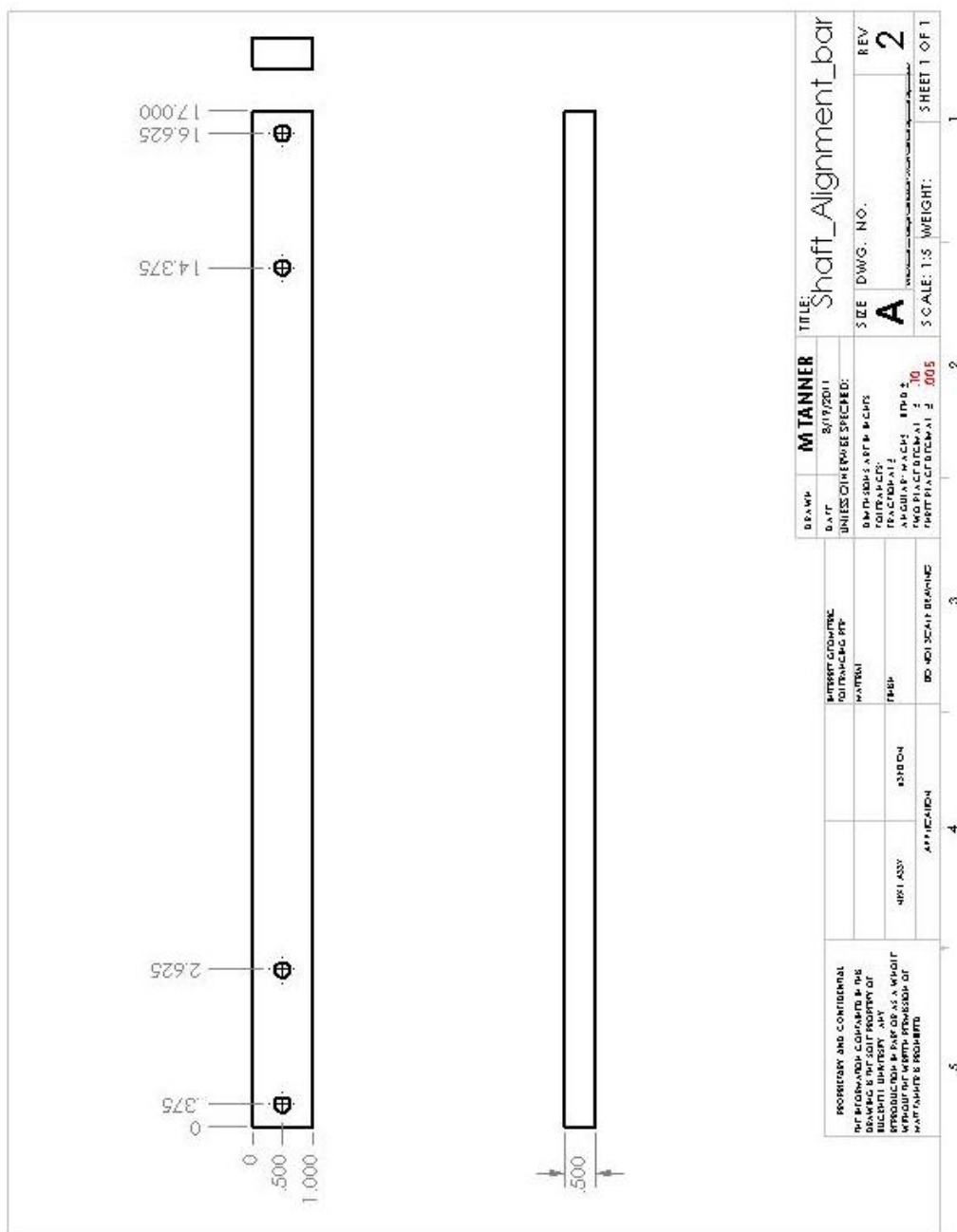


Figure H-18: Shaft Alignment Bar

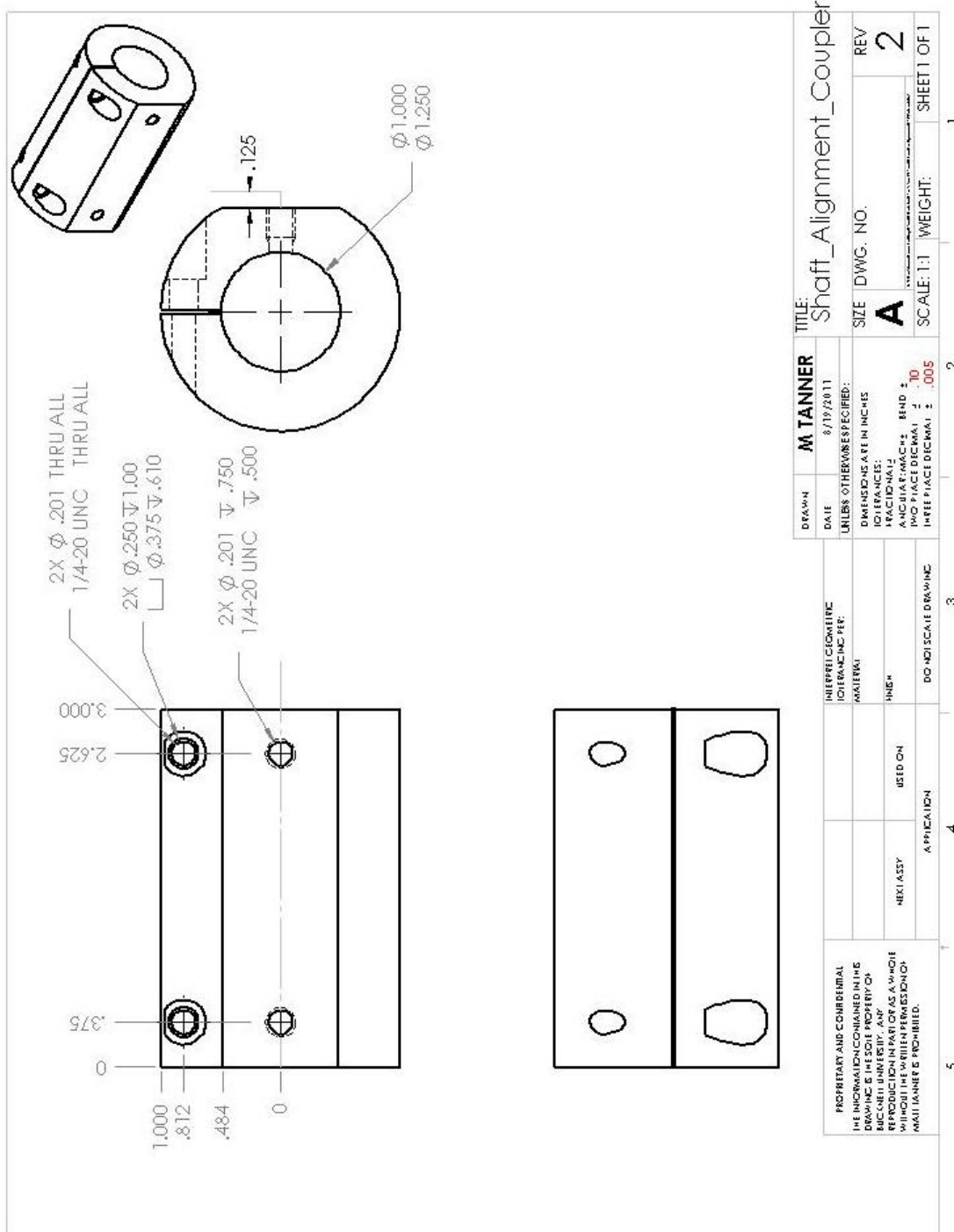


Figure H-19: Shaft Alignment Coupler

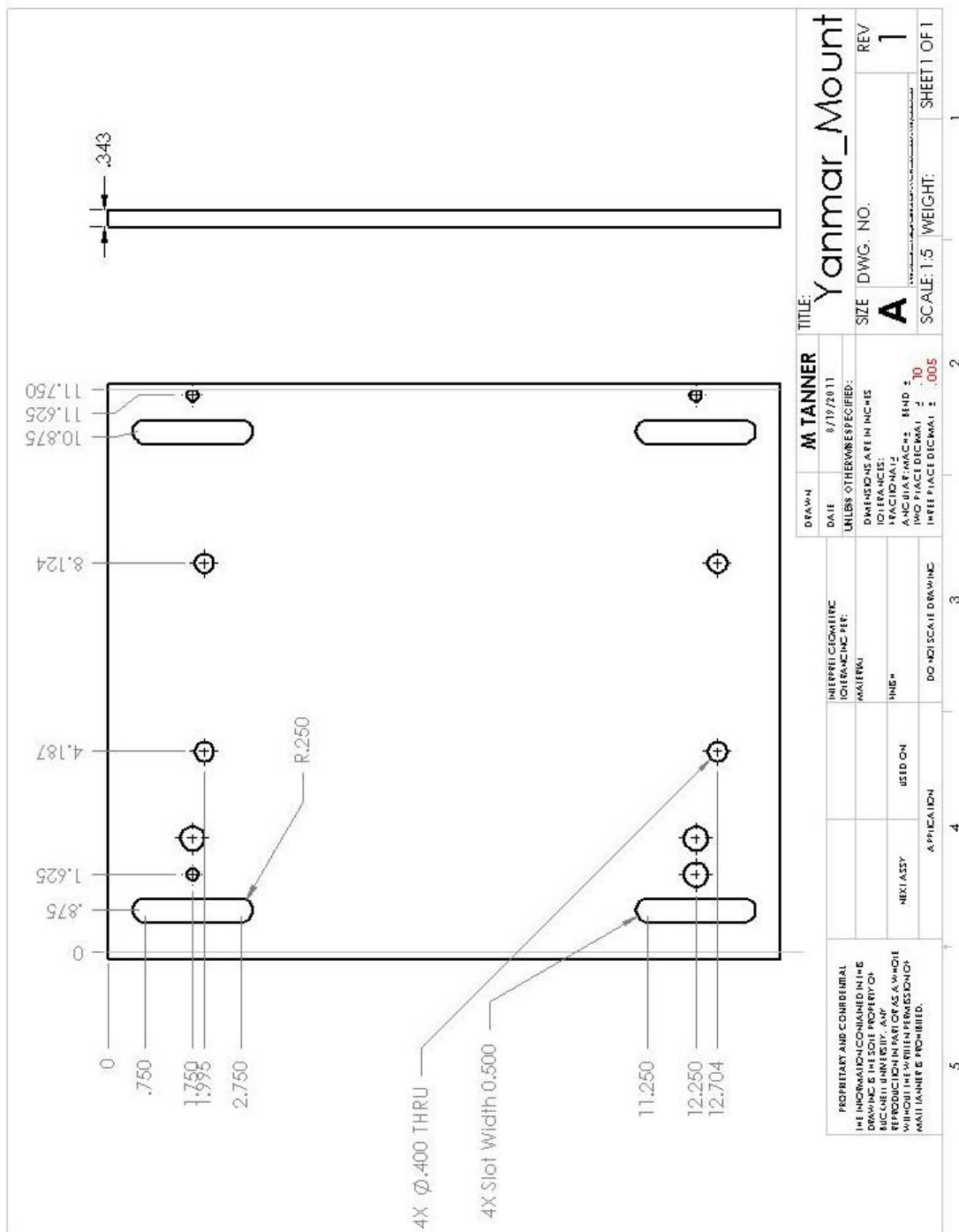


Figure H-20: Yanmar Engine Mount